

Future Avoided Cost Explorer

Hazards Technical Report



April 2020
State of Colorado

This technical report details the methodology used to develop the interactive resource *Future Avoided Costs Explorer: Colorado Hazards* (or “FACE:Hazards”). This effort was jointly led by the Department of Public Safety (Division of Homeland Security & Emergency Management), the Department of Natural Resources (Colorado Water Conservation Board), and the Department of Local Affairs (Colorado Resiliency Office). The data collection, methods and visualization tools were developed by the project consultant, Lynker Technologies LLC, and numerous technical partners listed below. Funding was provided by the Federal Emergency Management Agency (FEMA) through the Disaster Recovery 4145 Hazard Mitigation Grant Program (HMGP), as part of Colorado's Enhanced State Hazard Mitigation Plan (E-SHMP) Phase III project, with state grant match provided by the Division of Homeland Security & Emergency Management and Colorado Water Conservation Board.



The ultimate product is the public-facing interactive online resource where a general overview, results, case studies, and frequently asked questions can be found. Use the QR code here or visit: cwcb.colorado.gov/FACE



Contents

1	Introduction	1
2	Climate Scenarios.....	2
2.1	Overview	2
2.2	Technical Details of Scenario Development.....	2
2.2.1	Flood	2
2.2.2	Drought and Wildfire	4
3	Population Scenarios	7
3.1	Overview	7
3.2	Technical Details of Scenario Development.....	7
3.3	Applying the Population Scenarios	8
3.3.1	Using ICLUS Data to Track Land Use Change with Population Growth	8
3.3.2	Flood	9
3.3.3	Drought	9
3.3.4	Wildfire	10
4	Combining Scenarios and Computing Expected Annual Damages.....	11
4.1	Climate-Population Scenario Combinations	11
4.2	Computing Expected Annual Damages	11
4.3	Adjusting to 2019 US Dollars.....	12
4.4	Today’s Economy, Tomorrow’s Climate and Population	13
5	Technical Approach: Flood.....	14
5.1	Flood Technical Approach: Buildings	14
5.1.1	Overview	14
5.1.2	Data and Inputs.....	14
5.1.3	Model Approach/Methods	15
5.1.4	Model Outputs.....	18
5.1.5	Assumptions and Limitations.....	18
5.2	Flood Technical Approach: Bridges	19
5.2.1	Overview	19
5.2.2	Data and Inputs.....	19
5.2.3	Model Approach/Methods	19
5.2.4	Model Outputs.....	22



5.2.5	Assumptions and Limitations.....	22
6	Technical Approach: Drought	23
6.1	Drought Technical Approach: Crops	23
6.1.1	Overview	23
6.1.2	Data and Inputs.....	23
6.1.3	Model Approach/Methods	24
6.1.4	Assumptions and Limitations.....	26
6.2	Drought Technical Approach: Cattle	28
6.2.1	Overview	28
6.2.2	Data and Inputs.....	28
6.2.3	Model Approach/Methods	29
6.2.4	Model Outputs.....	31
6.2.5	Assumptions and Limitations.....	32
6.3	Drought Technical Approach: Skiing	33
6.3.1	Overview	33
6.3.2	Data and Inputs.....	34
6.3.3	Model Approach/Methods	36
6.3.4	Model Outputs.....	41
6.3.5	Assumptions and Limitations.....	41
6.4	Drought Technical Approach: Rafting	42
6.4.1	Overview	42
6.4.2	Data and Inputs.....	42
6.4.3	Model Approach/Methods	43
6.4.4	Model Outputs.....	46
6.4.5	Assumptions and Limitations.....	47
7	Technical Approach: Wildfire.....	48
7.1	Wildfire Technical Approach: Buildings	48
7.1.1	Overview	48
7.1.2	Data and Inputs.....	48
7.1.3	Model Approach/Methods	50
7.1.4	Model Outputs.....	57
7.1.5	Assumptions and Limitations.....	57
7.2	Wildfire Technical Approach: Suppression Costs.....	58



7.2.1	Overview	58
7.2.2	Data and Inputs.....	58
7.2.3	Model Approach/Methods	58
7.2.4	Model Outputs.....	60
7.2.5	Assumptions and Limitations.....	61
8	References	62
9	Appendix A—Climate Scenario Tables.....	68
10	Appendix B—Population Scenario Table	69
11	Appendix C—River Reach Info	70
12	Appendix D—Historic Colorado Wildfire Suppression Costs.....	73



Key Terminology

Ablation	The process by which snow or ice changes state from solid to liquor or gas through melting, evaporation or sublimation.
Acre-Foot (AF)	A unit of measurement for water volume, typically used in the agricultural industry. An Acre-Foot is defined as the amount of water required to cover an acre of land at a depth of 1 foot. An Acre-Foot is equivalent to 325,851 gallons.
Arid	Region of land or climate having little or no rain, generally characterized as, too dry or barren to support vegetation. <i>Semi-arid is characterized as dry but having slightly more rain than an arid region or climate.</i>
Asset	A physical thing like a building, farm, bridge, head of cattle, etc that has economic value to its owner. Under a variety of circumstances, the value of an asset can be impacted by external events like natural hazards.
Basin	An area of land that drains all the streams and rainfall to a common outlet such as the outflow of a reservoir or point along a stream channel.
Climate	The long term average weather conditions prevailing over an area. Estimates of climate conditions are typically developed using many years of weather observations.
Climate Change	A change in global or regional climate patterns, in particular a change apparent from the mid to late 20th century onwards and attributed largely to the increased levels of atmospheric carbon dioxide produced by the use of fossil fuels. Climate change and Global Warming are two terms that refer to the same phenomenon and its study.
Consumptive Use	That part of water withdrawn that is evaporated or transpired by plants, incorporated into products or crops, consumed by humans or livestock, or otherwise removed from the immediate water environment.
Cost	The dollar value associated with a particular condition or event. Specifically, this is the monetary estimate of historical damages or projected future damages.
Cubic feet per second (cfs)	A unit of measurement of fluid flow, in streams and rivers, for example. It is equal to volume of water one foot high and one foot wide flowing a distance of one foot in one second.
Damages	The physical and functional impairment of an asset due to an external event, like the disasters studied in this project. Damages are often quantified in terms of reduced economic output or cost associated with returning the asset to its undamaged condition.
Downscale	Reduce in size, scale or extent. For GCMs, this means using mathematical techniques to develop results for smaller geographical areas
Drought	<i>A meteorological drought</i> is defined as an extended period of below-average precipitation for a region. Drought definitions can also recognize drought as causing a water shortage to a particular human activity or environmental (e.g. water supply, agriculture, stream fisheries, forest health). <i>An agricultural drought</i> refers to situations in which soil moisture and irrigation supplies are insufficient to meet the



needs of the crops growing in the area. A *hydrologic drought* effectively reduces stream flows, reservoirs, lakes and groundwater to below-normal levels. A *socioeconomic drought* is when water shortages begin to effect people and their lives in terms of water supply, loss of hydropower production, loss of fisheries, agricultural production losses and food shortages.

Evaporation	The process of liquid water becoming water vapor, including vaporization from water surfaces, land surfaces, and snow fields, but not from leaf surfaces (see transpiration). <i>Evapotranspiration</i> is the sum of evaporation and transpiration.
Exposure	The people, livelihoods, habitats, species, infrastructure, or economic, social, or cultural assets that could be adversely affected by a stressor (Sayers <i>et al.</i> , 2016).
Expected Annual Damages	The average yearly cost of natural hazards, annualized 2035-2065. Detailed project explanation here .
Flood	An overflow of water onto lands that are used or usable by man and not normally covered by water. Floods have two essential characteristics: 1) The inundation of land is temporary and 2) the land is adjacent to and inundated by overflow from a river, or lake. <i>100 Year Flood</i> is a flood level with a 1 percent chance of being equaled or exceeded in any given year. <i>Flood Plain</i> is a strip of relatively flat and normally dry land alongside a stream, river, or lake that is covered by water during a flood. <i>Flood Stage</i> is the elevation at which overflow of the natural banks of a stream or body of water begins in the reach or area in which the elevation is measured.
Fire Suppression	An umbrella term covering a wide range of methods used by firefighters and other emergency response agencies to reduce the heat output from a fire through restriction and reduction of the flame area.
Freeboard	Freeboard is a factor of safety usually expressed in feet above a flood level for purposes of floodplain management. "Freeboard" tends to compensate for the many unknown factors that could contribute to flood heights greater than the height calculated for a selected size flood and floodway conditions, such as wave action, bridge openings, and the hydrological effect of urbanization of the watershed.
Gaging Station	A site on a stream, lake, reservoir, or other water body where observations and hydrologic data are obtained.
General Circulation Model (GCM)	Also known colloquially as Global Climate Models, GCMs are numerical models representing physical processes in the atmosphere, ocean, cryosphere and land surface. GCMs are used to provide globally- and regionally-averaged estimates of the climate response to increased greenhouse gas emissions. (IPCC)
Hazard (analysis)	An assessment of the probability and severity of flood, drought, and wildfire stressors.
Hazard (natural)	Historical or future flood, drought, and wildfire events that lead to adverse consequences for social, economic, and or natural systems.
Headwater(s)	(1) the source and upper reaches of a stream; also the upper reaches of a reservoir. (2) the water upstream from a structure or point on a stream. (3) the small streams



that come together to form a river. Also may be thought of as any and all parts of a river basin except the mainstem of the river and key tributaries.

Impacts	The consequences or effects of a hazard on the environment, economy, and human health.
Infrastructure	The basic physical and organizational structures and facilities (e.g. buildings, roads, power supplies) needed for the operation of a society or enterprise. <i>Critical Infrastructure</i> is a terms used by governments to describe assets that are essential for the function of society and the economy (i.e. hospitals, power plants, emergency response facilities). <i>Grey Infrastructure</i> refers to the human-engineered infrastructure for water resources such as water and wastewater treatments plants, pipelines, and reservoirs.
Inundation	When water covers an area of the land that is not typically covered. This can be caused by natural hazards, or by manmade structures as in the case of certain types of irrigated agriculture
Irrigation	The controlled application of water for agricultural purposes through manmade systems to supply water requirements not satisfied by rainfall.
Livestock water use	Water used for livestock watering, feed lots, dairy operations, fish farming, and other on-farm needs.
Losses	Impacts that refer to a complete loss of something that cannot be recovered (e.g. human and animal life).
Meteorological	Relating to the branch of science concerned with the processes and phenomena of the atmosphere, especially as a means of observing and forecasting the weather.
Montane	Zone of semi-arid foothills to low mountain areas with ponderosa pine intermixed with grasses and shrubs. Taller and more densely spaced conifers can often be found on north-facing slopes.
Projection	An estimate or forecast of a future situation or trend based on a study of present ones.
Peak flow	The maximum instantaneous discharge of a stream or river at a given location during a defined time interval.
Region	An area or division having definable characteristics but not always fixed boundaries. The Colorado regions were derived by a compilation of a number of classification schemes including Climate Change in Colorado (Lukas et al., 2014), NOAA's climate divisions, watershed boundaries, EPA level III Ecoregions, the Colorado State Hazard Mitigation Plan (Colorado DPS, 2018) and Colorado Resiliency Framework.
Resiliency	The ability of social, economic and environmental systems to cope with flood, drought, and wildfire risks, limiting the significance of any associated harmful consequences should they occur, and having the capacity to adapt in a way that reduces future risks.
Risk	An assessment of where populations, infrastructure, and critical facilities are vulnerable to hazards, and to what extent injuries or damage may occur (FEMA, 2015).



Runoff	That part of the precipitation, snow melt, or irrigation water that appears in uncontrolled surface streams, rivers, drains or sewers.
Scenario	A baseline state or future projection of one or both of (a) climate conditions or (b) the human population occupancy and distribution on the environment.
Sectors	Categories of the environment and society that represent systems that may be impacted by natural hazards (e.g. infrastructure, economy, public health, agriculture, recreation & tourism, and environment).
Sensitivity	The propensity of a particular receptor/asset to experience harm as a result of a given hazard.
Snowmaking	The manmade production of snow from liquid water; usually used to cover ski slopes.
Technical Update	Abbreviated reference to the Analysis and Technical Update to the Colorado Water Plan.
Today's Economy/Today's Dollars	An estimate of the value of an asset taking account the cumulative inflation between when the value was measured and present day.
Transpiration	The process by which water that is absorbed by plants, usually through the roots, is evaporated into the atmosphere from the plan surface, such as leaf pores. See evapotranspiration.
Vulnerability	The propensity or predisposition of a given receptor (or group of receptors) to be adversely affected by a hazard. Vulnerability encompasses a variety of concepts and elements including sensitivity to harm, exposure, and value (the value society places on the harm caused).
Watershed	The land area that drains water to a particular stream, river, or lake. Watersheds are typically land features that can be identified by tracing a line along the highest elevations between two areas on a map, often a ridge. Large watersheds can contains thousands of smaller watersheds (eg, the Mississippi River watershed spans most of the central continental United States).
Water Plan	Abbreviated reference to the Colorado Water Plan (also referred to as the Colorado Water Plan).
Wildfire	A large destructive fire that spreads quickly over woodland or brush, often in rural or less-developed areas.



1 Introduction

As a semi-arid, headwater state with terrain ranging from the High Plains to Rocky Mountains, **Colorado is exposed to major economic impacts from floods, droughts, and wildfires.** Recent events such as the 2013 flood, the 2002 drought, and 2012 wildfire season are examples of the physical magnitude and economic damages such hazards can exact. These extreme events are becoming more severe and potentially more frequent as global climate dynamics change regional patterns (Gonzalez et al., 2018).

Researchers expect floods to increase in severity, droughts to deepen and become more spatially expansive, and wildfire seasons to become longer with more acres burned in a warming climate (Wehner, Arnold, Knutson, Kunkel, & LeGrande, 2017). In addition, Colorado's growing population is projected to reach between 7.7 and 9.3 million by 2050 (CWCB, 2019 2(2)). With more residents comes greater natural hazard exposure if floodplain margins become developed, agricultural land shrinks, and the number of people in the wildland urban interface increases.

The first step to understanding and preparing for these events is to assess the possible risks—both now and in the future. This is done by quantifying the difference in economic costs between historic relationships and modeled future scenarios. Tasked by the Colorado Department of Public Safety to perform such an analysis, the objective of this project is to **estimate the expected costs of floods, droughts, and wildfires to a selection of economic sectors under historic and future climate and population scenarios.**

These sectors varied by the hazard being examined. For flooding, we evaluated impacts to **buildings** and **bridges**. For drought, we examined agricultural—**crops** and **cattle**—and outdoor recreation—**skiing** and **rafting**—impacts. For wildfire, we again analyzed **buildings** and also computed the cost of **suppression**, which is the amount the state spends to fight and extinguish ongoing fires. In total, we analyzed eight sectors, all of which have experienced observed economic damages in the tens of millions to billions of dollars due to natural hazards.

While we did not quantify the following items as part of this project, we recognize that climate change will have serious impacts beyond economic costs, including injury and loss of life, harm to mental health and wellness, and significant adverse effects on Colorado's ecosystems and biodiversity.

In this document, we first outline how we developed and applied the climate (Sect. 2) and population scenarios (Sect. 3) in our analysis. After that, we provide information on how we combined the scenarios and quantified expected annual damages (i.e., economic cost) for the various sectors (Sect. 4). The remaining pages are dedicated to detailed descriptions of the input data and methodologic approaches for each hazard and the related sectors (Sects. 5, 6, and 7).



2 Climate Scenarios

2.1 Overview

A key goal of this project is estimating the *current* and *future* costs of flood, drought and wildfire for the state of Colorado. As such, each hazard considers three climate scenarios, as shown in Figure 2-1.: one current scenario, and two realizations of climate change in 2050.

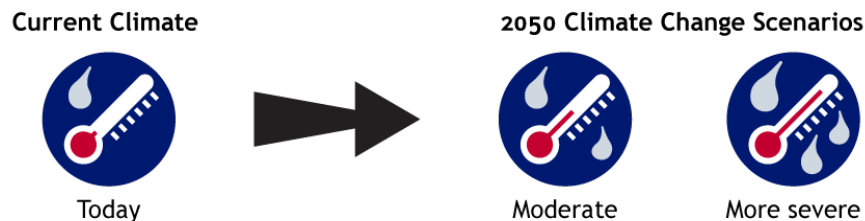


Figure 2-1. Conceptual diagram showing current climate (left) and our two 2050 climate change scenarios, Moderate and More Severe.

To develop these scenarios, we used historical meteorological data sets, as well as climate-adjusted meteorological data. Following the approach developed for the 2015 Colorado Water Plan, the two future projections (i.e., Moderate and More Severe) are representative of two potential 2050 conditions that differ in their relative severity in the context of a large ensemble of projected future conditions. For drought and wildfire, our climate scenarios are identical to the two scenarios considered in the 2015 Colorado Water Plan. While the technical details of scenario development are documented by Harding (2015) and the 2019 Analysis and Technical Update to the Colorado Water Plan Volume 2, Section 14 (CWCB, 2019 2(14)), we summarize the development below.

Due to inherent differences in the physical processes driving the three hazards, our approach to flood hazard modeling employed a different climate scenario development approach, while still using the Moderate and More Severe nomenclature. Fundamentally, the climate scenarios with heightened drought or wildfire risk may not be those with heightened flood risk. The scenarios driving our flood models are based on ensembles extracted from downscaled hydrology data representing two different warming scenarios (Reclamation, 2014).

2.2 Technical Details of Scenario Development

In this project, climate change is generally enacted as a scalar adjustment applied to historic observations and model outputs. Below, we provide brief information on how we developed and applied the climate scenarios. The hazard-specific discussions contain further details on how climate scenarios were applied to the specific sectors. For tabularized info on the climate change scenarios, please see Appendix A—Climate Scenario Tables.

2.2.1 Flood

To calculate future damages due to Moderate climate change, we followed the methods described by Wobus, Gutmann, et al. (2017), using downscaled hydrologic projections

(Reclamation, 2014) to estimate the change in frequency of flood events that have an average 100-year recurrence interval in today’s climate.¹ From the Reclamation (2014) dataset, we extracted annual maximum flow projections from approximately 1600 river reaches throughout the state of Colorado over the time period of 2000-2100. These projections are available from 58 different downscaled climate model runs from the Coupled Model Intercomparison Project (CMIP) Phase 5, commonly known as CMIP5 (Taylor, Stouffer, & Meehl, 2012). From these projections, we selected an ensemble of models that represents approximately 2°C (3.6°F) of summer warming in Colorado by 2050 relative to present day for our “Moderate” future scenario.

From this full suite of downscaled hydrology outputs, we constructed an ensemble annual maximum flow time series for the baseline at each river reach and used a generalized extreme value fit to this ensemble to estimate the magnitude of the 100-year flood. We then developed a new annual maximum time series from the future ensemble and estimated the frequency of flows exceeding the baseline 100-year event in the future (Figure 2-2).

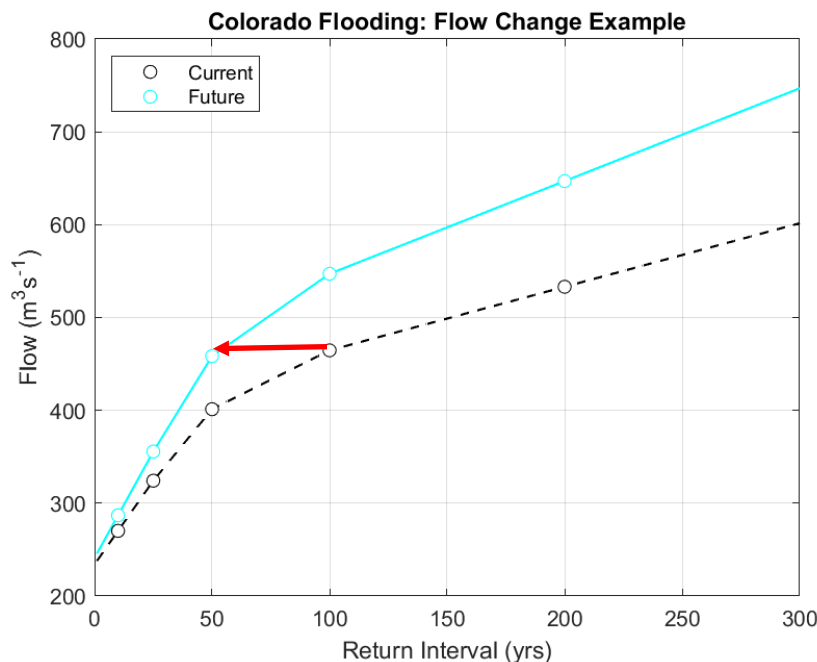


Figure 2-2. Example of current (black) and future (blue) magnitude frequency curves for a single modeled stream reach. In this example, the baseline 100-year (1% probability) event of ~450 m³s⁻¹ becomes an approximately 50-year (2% annual probability) event in the future, as illustrated by the red arrow.

Basic physical principles dictate that a warmer atmosphere can hold more water; this is widely recognized to result in an increase in potential precipitation of 7% per 1°C. This increase in rainfall potential is referred to as “Clausius-Clapeyron scaling,” and background on this topic is described in detail in Mahoney et al. (2018). For the More Severe climate scenario, we assumed

¹ Throughout this report, we use recurrence interval (years) and annual exceedance probability (percent) interchangeably. In this context, a 100-year flood has a 1% annual exceedance probability (i.e., it has a 1 in 100 chance of occurring in a given year).

that summertime temperatures in Colorado increase by approximately 3°C (5.4°F) in 2050, at the upper end of projections from a 52-model ensemble comparing the 30 years centered on 2019 to the 30 years centered on 2050. We used the same baseline magnitude-frequency curve for each river reach as in the Moderate climate change scenario described above using the downscaled hydrology data. We then assumed that each flood event increases in magnitude according to the Clausius-Clapeyron relationship (i.e., 7% per 1°C of warming). We thus shifted the flood magnitude-frequency curve upwards by 21% and calculated the change in frequency of the 100-year event based on this shift.

The future climate projections generate changes in the frequency of flooding of all magnitudes. For example, in the result shown in Figure 2-2, the data for that site indicates an approximate doubling in the frequency of the 100-year event for the climate scenario shown. As summarized in Section 5, we aggregated all of the data for each county to calculate an average change factor for that county. This change in the frequency of flooding translates directly into a change in damages from flood hazards: if all damaging flood events become twice as frequent in the future, so too do the economic costs of flooding.

2.2.2 Drought and Wildfire

For drought and wildfire, we use hydrologic projections developed for Colorado River Water Availability Study, Phase 2 (CRWAS-II) (Harding, 2015). As a first step, we accessed an ensemble of hydrologic projections for the United States from the same dataset as the flood hazard (Reclamation, 2014). These projections were generated by the Variable Infiltration Capacity (VIC) hydrologic model (Liang, Lettenmaier, Wood, & Burges, 1994) forced with climate projections from CMIP Phases 3 and 5 (Meehl et al., 2007; Taylor et al., 2012). Each projection represents a realization of how climate change may alter key elements of the hydrologic cycle. The ensemble (i.e., the total set of projections considered) comprises 209 hydrologic projections: 112 from CMIP3 and 97 from CMIP5. To note, while using the same dataset as flood, the final ensemble for drought and wildfire is different.

Following CRWAS-II (Harding, 2015), we categorize hydrologic projections according to the balance between water supply and demand simulated for the state of Colorado. Specifically, we calculate statewide average runoff and consumptive irrigation requirement (CIR, the depth of water required to satisfy the gap between potential and actual evapotranspiration) anomalies between a baseline (1970 – 1999) and future period (2035-2064) for each hydrologic projection. When plotted on a range-normalized axis, the relationship between runoff and CIR anomalies emerging from the ensemble of hydrologic projections is approximately linear and represents a gradient of water supply stress conditions (Figure 2-3., blue points). When runoff is high, CIR is low, and the system is minimally stressed (upper right quadrant of Figure 2-3.). Conversely, when runoff is low, CIR is high, and the system is maximally stressed (lower left quadrant of Figure 2-3.).



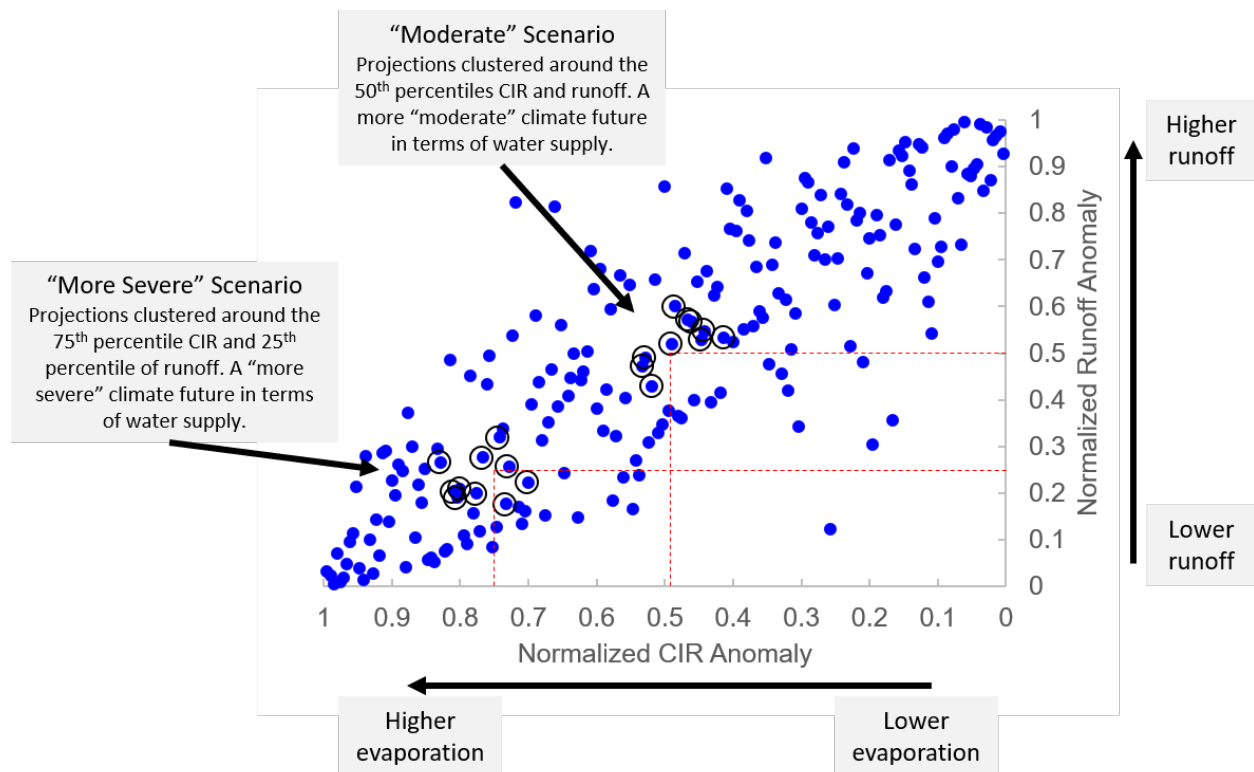


Figure 2-3. A linear relationship emerges between state-averaged normalized consumptive irrigation requirement (CIR) and normalized runoff anomalies in the 209 hydrologic projections (blue points). Two clusters of 10 projections (black circles) are identified surrounding key percentiles of the CIR/runoff domain. Our climate scenarios are based on the climate projections forcing either cluster of hydrologic projections.

Our climate scenarios were developed from clusters of hydrologic projections in the CIR/runoff space (Figure 2-3.). We identified two clusters of projections, each associated with one of our climate scenarios, as identified by black circles in Figure 2-3.. The Moderate cluster is derived from the 10 projections nearest to the 50th percentile of normalized runoff anomaly and 50th percentile of normalized CIR anomaly. The More Severe cluster is derived from the 10 projections nearest to the 25th percentile of normalized runoff anomaly and 75th percentile of normalized CIR anomaly. From these clusters, we developed monthly temperature offsets and precipitation change factors that represent the average difference between 2050 climate and current climate.

We then applied these monthly temperature offsets and precipitation change factors to historical gridded meteorological data products to create climate-adjusted datasets for each 2050 scenario. Statewide annual average temperature offsets projected by the Moderate and More Severe scenarios are +2.1°C and +2.3°C, respectively for drought. For the wildfire model, the baseline period was 1988 to 2017 to be consistent with previous modeling efforts by the Colorado State Forest Service (CSFS) (see Section 7.1.3.5 for more details). As a result, statewide annual average temperature offsets projected by the Moderate and More Severe scenarios for wildfire are slightly lower at +1.5°C and +1.7°C, respectively. In all cases, temperature offsets are greater in summer and autumn months than winter and spring months. Statewide average annual precipitation change factors for the Moderate and More

Severe scenarios are +5% and -1% respectively. Both scenarios project precipitation declines during spring and summer months, with slight increases during winter months. Overall, both scenarios simulate year-round warming by 2050, however the directionality and magnitude of precipitation changes are contrasting between scenarios.



3 Population Scenarios

3.1 Overview

We use population scenarios in line with 2050 projections from the Analysis and Technical Update to the Colorado Water Plan, herein “Technical Update”. We consider current population and three future population scenarios in 2050: Low Growth, Medium Growth and High Growth (Figure 3-1).

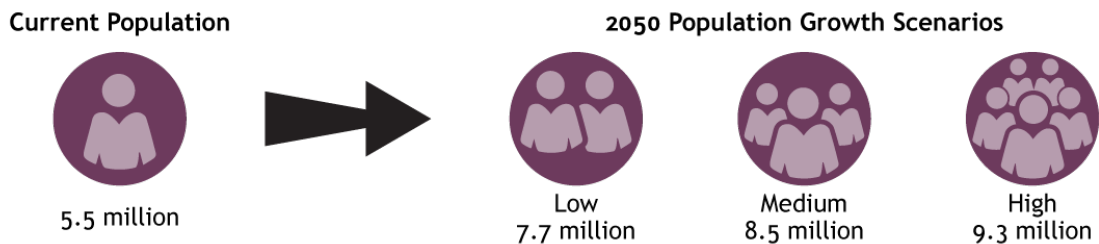


Figure 3-1. Population scenarios used in this project.

The Medium Growth scenario matches the state’s official projection for 2050. The Low Growth and High Growth population scenarios represent the 10th and 90th percentile of plausible population projections, respectively. The following section details the selected scenarios, but further information on future population projections can be found in the Technical Update (CWCB, 2019 2(2)). For tabularized info on the population growth scenarios, please see Appendix B—Population Scenario Table.

3.2 Technical Details of Scenario Development

The Colorado Water Plan developed five narrative planning scenarios that could be used for identifying future water needs around the state in 2050. The 2019 Technical Update translated these narrative scenarios into quantitative population data. In the context of that report, each scenario represents a combination of both climate and population change. For this project, we adjusted climate and population independently, and combined those adjustments to develop a complete permutation set. That is, we consider only climate change, only population growth, and all combinations thereof. Thus, while we use the population projections from the Technical Update, we use a different naming convention to avoid confusion with the hybrid climate-population scenarios. Details are as follows:

- **Low Growth:** Identified in the Technical Update as “Weak Economy,” this scenario assumes an economic slowdown and a reduction of migration to Colorado relative to historical rates.
- **Medium Growth:** The “Business as Usual” scenario from the Technical Update assumes ‘median’ or Colorado State Demography Office’s standard population growth projection.
- **High Growth:** The “Hot Growth” scenario from the Technical Update assumes a booming economy and high rates of migration to Colorado relative to the other scenarios.

3.3 Applying the Population Scenarios

The population scenarios on their own only provide information about magnitude of change in the number of Colorado residents by 2050. For each sector, we used available literature, published relationships, and ancillary data in order to convert the population increase into a meaningful change in hazard exposure. In general, we followed two approaches: 1) spatially explicit changes in land use calculated from gridded data products and 2) scaling participation rates from the number of new Colorado residents. We provide brief information below for each hazard, with **further details provided in the sector technical approach sections**.

3.3.1 Using ICLUS Data to Track Land Use Change with Population Growth

For hazard/sector combinations where spatially explicit future land use was required, we matched land use projections from the US Environmental Protection Agency’s Integrated Climate and Land-Use Scenario (ICLUS) Version 2 project (U.S. Environmental Protection Agency, 2017) to associated changes in county-level population from the growth scenarios.

ICLUS is a modeling framework that produces maps on a 295 ft. (90 m) grid of current and future land use in 19 different categories (Figure 3-2). ICLUS maps show how development may look under various future scenarios. For this project we used geospatial data from ICLUS in several ways to provide information on how county-level changes in population translate into changes in exposure to flood, drought and wildfire.

Code	Group	Class Name
0	Water	Natural water
1		Reservoirs, canals
2		Wetlands
3	Protected	Recreation, conservation
4	Working/production	Timber
5		Grazing
6		Pasture
7		Cropland
8		Mining, barren land
9	Developed	Parks, golf courses
10		Exurban, low density
11		Exurban, high density
12		Suburban
13		Urban, low density
14		Urban, high density
15		Commercial
16		Industrial
17		Institutional
18		Transportation

Figure 3-2. Land use classes used in ICLUS Version 2.

The first step for each sector that uses ICLUS data was to identify current and future and land use maps. For current data, we used the ICLUS 2010 layer. For future scenarios, we matched each of the county-level population projections in the Technical Update to the population of the ICLUS scenario and year (2020–2100) that was closest to the projection. As some ICLUS areas consist of multiple counties (micro or metro areas), we summed the Colorado Water Plan county population estimates across counties before selecting the best match. We then used the selected future ICLUS scenario/year layer as a representation of the spatial distribution of land use associated with the projected population from each future scenario.

For flood and wildfire, we used ICLUS to track changes in the number and value of exposed buildings in conjunction with building replacement costs from the Federal Emergency Management Agency’s Hazus dataset (Federal Emergency Management Agency, 2015). Importantly, these data do not correspond to building value (i.e., the price you would pay to purchase it), but rather the cost of materials and labor to repair and replace a damaged structure. To connect each ICLUS land use type to a building replacement cost from Hazus, we spatially overlaid the two datasets. We then calculated the areal fraction of each land use category from the ICLUS 2010 layer within every Hazus census block. We then multiplied the resultant values by the total replacement cost of buildings within a given census block to get the area-weighted replacement cost value for every ICLUS category in that block. Next, we

averaged building replacement cost per ICLUS category in every Colorado county. We then assigned the per-category values to the ICLUS land use layer to create a new grid of building replacement costs for the current population scenario.

For the 2050 population growth scenarios, we tracked changes to the ICLUS land use pixel values and assigned a new building replacement cost whenever a given grid cell changed from one category to another. For example, if one grid cell changed from cropland in the current scenario to suburban in the future, then we would change the cropland building replacement cost to the suburban building replacement cost for that county. It is important to note that the building replacement cost for a given land use type does not change in value from current to future scenarios. Instead, all changes to building replacement costs within a county are caused by ICLUS pixels changing from one land use type to another. If the land use type does not change, then there is no change in building replacement cost. In general, population growth tended to increase the value of structures exposed to flood and wildfire as development intensifies in the 2050 scenarios.

The sections below explain in further detail how we integrated ICLUS and other datasets into our population change scenarios. More information can also be found in the text for each sector in Sections 5,6, and 7.

3.3.2 Flood

For the buildings sector, we used geospatial data from ICLUS to provide information on how county-level changes in population would lead to increased development in and near mapped floodplains. Across all counties, we assumed that local regulations will prevent development within mapped 100-year floodplains, but that future development will be unrestricted in the zone between the 100-year and 500-year floodplains. Thus, we calculated the change in building replacement cost between the 100 and 500-year floodplains for each population growth scenario. There was insufficient information on how bridge size and location would be affected by growth, so we did not apply population scenarios to these estimates.

3.3.3 Drought

The multiple drought sectors required different approaches when taking population change into account. For the crops sector, we used the associated change in irrigated acres for each population scenario from the Technical Update in order to estimate future production (CWCB, 2019 2(3)). For cattle, we scaled total pasture and grassland per county by the ICLUS-estimated change in pasture and grazing land use pixel types. For the two recreation sectors, changes in population were used to increase the total baseline and annual user days based on historic rates of Colorado residents participating in rafting and skiing. Increasing user days had the effect of producing larger swings between drought and non-drought years. In other words, the good years, with long ski and rafting seasons, became better and the bad years, with short ski and rafting seasons, became worse relative to the new baseline.



3.3.4 Wildfire

We used ICLUS for the two wildfire sectors through two primary pathways: changes in building replacement cost and change in the number of buildings. For the buildings sector, we calculated new building replacement costs as we did above based on changes to ICLUS land use types. We also used various ICLUS land use types to mask heavily urban areas from potential wildfire hazards, as was done in the Colorado Wildfire Risk Assessment (CO-WRA) 2017 Update (Colorado State Forest Service, 2018). For the suppression sector, we created a baseline count of the number of buildings per land use type based on ICLUS data and Microsoft's building footprint database (Microsoft, 2018). Similar to how we calculated changes in building replacement costs, we updated building counts for the population growth scenarios based on changes in ICLUS land use type.



4 Combining Scenarios and Computing Expected Annual Damages

4.1 Climate-Population Scenario Combinations

We analyzed the three climate and four population scenarios both independently as well as in all possible arrangements, giving a total of twelve unique climate-population combinations (Figure 4-1.). The following section defines expected annual damages (i.e., the economic cost given for each hazard sector climate-population scenario combination) and how we calculated them for each hazard. These are the results presented in the online interactive visualization dashboards.

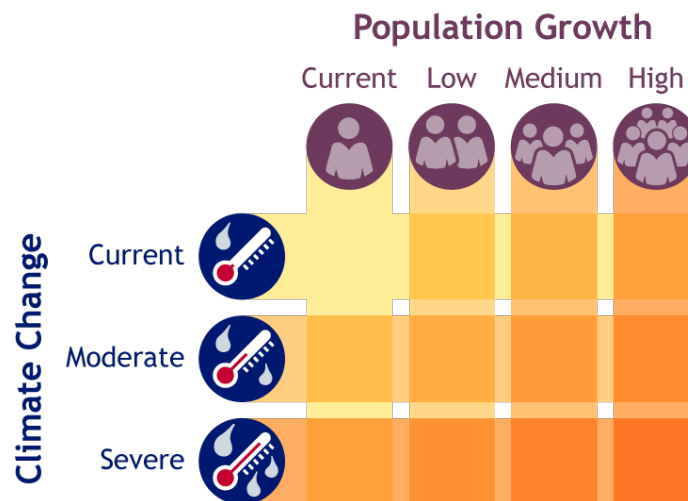


Figure 4-1. Scenario matrix showing the possible combinations of the three climate scenarios and four population scenarios.

4.2 Computing Expected Annual Damages

Results in the online interactive visualization tool are displayed as **expected annual damages**, which are a function of the hazard magnitude, probability, and exposed assets. Often climate change impacts are presented as the damage caused by a single event with an associated probability. For example, flood damages are typically given in reference to the 100-year event, which has a 1% annual probability of occurring. Thus, if total damages for the 100-year event were estimated at \$1,000,000, the expected annual damage from events of that size would be \$10,000 (1% of \$1,000,000). While useful, this approach overlooks the economic impact of hazards of lower and higher probabilities. In this sense, a 500-year flood event would be rare, but it still contributes to expected annual damages as a function of the magnitude of the damage it inflicts and its probability of occurring (0.2%).

In order to take all relevant, calculable damages into account, we treat expected annual damages as an integration of hazard magnitudes and probabilities:

$$EAD = \int D dAEP$$

where EAD is expected annual damages (US dollars), D is damages (US dollars), and AEP is the annual exceedance probability. Performing this integration allows to compute the area under the damage-probability curve (Figure 4-2.) and make a more complete estimate of expected annual damages. One item to keep in mind is that this does not mean that each year will produce the same damages from natural hazards. Rather, some years will have high damages, while others will have minimal damages, but overall there is an average monetary impact one should expect to incur over time.

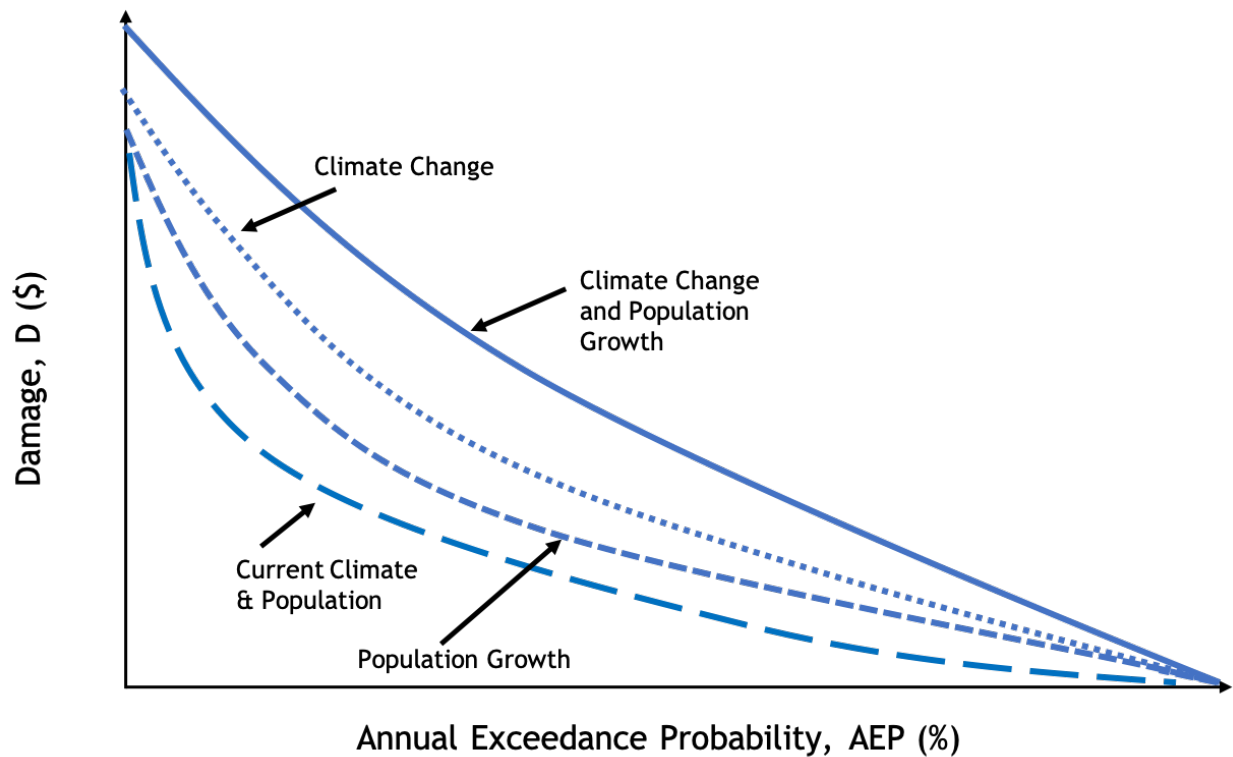


Figure 4-2. A conceptual figure showing hazard damage decreasing as its probability increase. In this project, expected annual damages are treated as an integration of the hazard damage magnitudes and their associated probabilities. In a hypothetical scenario, the area under the dashed blue curve is smaller relative to the area under the dotted blue curve, showing conceptually how hazard damages and probability, as well as the resultant expected annual damages, are affected by climate change.

Additionally, we perform these calculations for the current climate and population scenario along with all combinations of future climate change and population growth scenarios (Figure 4-2.). We expect, in general, that: climate change will increase the frequency and intensity of flood, drought, and wildfire; population growth will increase hazard exposure; and the two combined will lead to greater expected annual damages.

4.3 Adjusting to 2019 US Dollars

The economic data used in this project were sourced from various reports and databases covering a range of years. To give all expected annual damages a common frame of reference, we adjusted the final value based from the source year of the economic data to 2019 US dollars using the Consumer Price Index (CPI) from the US Bureau of Labor statistics:

$$EAD_{final} = EAD_i \frac{CPI_{2019}}{CPI_i}$$

where EAD_{final} is the value displayed in the online visualizations (2019 US dollars), EAD_i is the value calculated in dollars from year i , CPI_{2019} is the 2019 CPI, and CPI_i is the CPI from year i .

4.4 Today's Economy, Tomorrow's Climate and Population

Our approach considers how 2050 climate and population projections may affect Colorado's economy given current conditions. We do not project changing economic parameters, such as supply, demand, prices, or technology, out to 2050.

Critically, our analyses do not consider how asset prices (e.g., housing replacement values, crop prices, lift ticket costs, etc.) may change in the future. Instead, we assume that current asset prices remain constant (today's economy, tomorrow's climate and population). We operate under this assumption for two reasons. First, it is difficult to project price changes over decadal timescales. Macroeconomic forces controlling prices are stochastic and extremely difficult to predict. For example, commodity prices are subject to supply/demand, domestic governance, international relations, and other factors. Second, by holding asset prices constant, we can isolate the effects of climate change and population growth on hazard impacts.

Additionally, this analysis does not apply discount rates when calculating 2050 expected annual damages. Our analyses also do not include an assessment of the level and timing of expenses associated with adaptive or mitigation measures. Rather, our methods are aimed at assessing potential impacts of flood, drought, and wildfire assuming no adaptive or mitigative efforts are taken. Should future work look to more directly address the efficacy of adaptation and mitigation, then discounting would be particularly relevant for evaluating the balance between costs and benefits of those actions.

5 Technical Approach: Flood

5.1 Flood Technical Approach: Buildings

5.1.1 Overview

Although flood damage can affect many different parts of the Colorado economy, we focused our flood damages analysis on losses to buildings and bridges, as these have historically been two of the largest sources of monetary damages from flooding. Below, we summarize the methods used for tabulating building losses in the baseline and future scenarios. The outputs of this analysis are changes in expected annual damages to buildings due to flooding.

5.1.2 Data and Inputs

We extracted baseline building damages by county from the planning-level loss estimates described in the Colorado Flood Hazard Mitigation Plan (FHMP; CWCB, 2013). Those planning-level estimates were derived using a modeled 100-year floodplain for the entire state, combined with data from the national building stock inventory at a census block level. Flood depths for the modeled 100-year event were combined with depth-damage functions and building stock values to calculate baseline loss estimates by county under current conditions.

5.1.2.1 Statewide Hazus-MH Inferred 100-year Floodplain and Census Data

The FHMP baseline loss values used an inferred 100-year floodplain from Hazus-MH that characterizes exposure across the entire state. The Hazus-MH software uses USGS gage data along with available digital elevation models (DEMs) to develop statewide flood polygons and depth grids for the 100-year floodplain. These depth grids are then combined with census-level data on building stock inventories and depth-damage functions within Hazus-MH software to calculate building and content losses from the 100-year flood statewide. Further details on the Hazus-MH derived floodplain can be found in the Flood Hazard Mitigation Plan (CWCB, 2013).

5.1.2.2 RiskMAP depth grids for 10 through 500-year events

The state of Colorado does not consistently have floodplains mapped at multiple recurrence intervals (i.e. 5, 10, 25, 50 and 500-year flood). However, there are seven counties in Colorado in which there are detailed RiskMAP studies that delineate the depth and extent of 10-year through 500-year recurrence interval floodplains on the major rivers passing through them: Boulder, Jefferson, Larimer, Logan, Morgan, Sedgwick and Washington. We used the depth grids from these counties to estimate the ratio between expected annual damages (from all flood events) and the damages expected from just 100-year events as compiled in the FHMP.

5.1.2.3 Building footprints attributed with replacement cost and first floor elevation

We used the Microsoft building footprint dataset (Microsoft, 2018), attributed with replacement costs and first floor elevation from census block data, to feed into calculations of expected annual damage for multi-recurrence interval floodplains.



5.1.2.4 *Climate Data and Scenarios*

We used downscaled hydrologic projections from a joint project between US Bureau of Reclamation, the National Center for Atmospheric Research (NCAR), the US Army Corps of Engineers, and others (Reclamation, 2014) to estimate the change in frequency of historical 100-year flood events by mid-century. These data were available as annual maximum flow time series at approximately 1600 unique river reaches across the State of Colorado.

5.1.2.5 *Future Land Use Data for the Population Scenarios*

The ICLUS data discretizes current and future land uses into 19 unique categories on a ~300 ft (90 m) grid (U.S. Environmental Protection Agency, 2017). As summarized in Sections 3.3.1 and 3.3.2, we used the ICLUS data to calculate the change in building value between the 100 and 500-year floodplains for each population growth scenario, and compared this to the total change in building value per county to estimate what fraction of new building value occurs within flood hazard zones in each county. We used these data to calculate a state-wide scalar to adjust the total population change in each county to reflect changes in building exposure to flooding under each climate change scenario.

5.1.3 Model Approach/Methods

5.1.3.1 *Translating Hazus-MH damages to Baseline Expected Annual Damages*

The results from the FHMP provide a planning-level summary of the total building loss that would be estimated to result from a 100-year event, by county. Since these events have a 1% probability of occurring in any given year, the expected damages from these events alone, in any given year, is 1% of this value. However, previous work has shown that the expected annual damages from a full range of potential flood events is substantially larger than the expected damages from the 100-year event alone (e.g., C. Wobus et al., 2019).

Because the state of Colorado does not consistently have floodplains mapped at multiple recurrence intervals, we used the seven counties where we did have multi-recurrence interval flood mapping, along with building footprints within those counties, to calculate the ratio of EAD to expected damages from 100-year events alone. To do this, we overlaid building footprints onto RiskMAP depth grids for those counties where data were available, and we assigned a flood depth to each building footprint for each recurrence interval. We then used the depth-damage functions compiled in Hazus to estimate the dollar damages to each property for each recurrence interval. We aggregated these damages up to the county level for all recurrence interval events and compared the expected annual damage to the damages from 100-year events alone for each county. From this analysis, we found that the EAD from all events is on average a factor of 2.5 higher than the expected value of 100-year damages alone. In other words, on average the baseline EAD can be derived by multiplying the total estimated losses from 100-year events, as described in the FHMP, by 0.025 (1% probability of a 100-year event times a factor of 2.5 to translate from 100-year expected damages to total EAD).

5.1.3.2 Applying the Climate Change Scenarios

The majority of damaging flood events in Colorado occur between spring and fall (CWCB, 2013), so we used projected summertime temperatures to scale our flood damage projections. The average summertime temperature increase in Colorado is projected to be between approximately 1-3°C by 2050, depending on the emissions scenario. As detailed in Sect. 2.2.1, we selected an ensemble of model outputs representing approximately 2°C of summertime (May-September) warming by 2050 as our “moderate” scenario. We then extracted the annual maximum flow time series from this ensemble for each modeled river reach across the state, for a baseline period centered on 2019 (2009-2028) and a future period centered on 2050 (2040-2059). The choice of 2019 as our baseline means that this ensemble already includes some climate warming compared to the late 20th century; however, this choice was made to avoid artifacts in the downscaled hydrology data, as described in Wobus et al. (2017).

We used the baseline and future ensembles to calculate the parameters of an extreme value distribution, from which we calculated the 10-year through 200-year flow events in the baseline period, and the corresponding return period for each of those flow events in the future period (Figure 5-1.). The output from this analysis is a change factor on the frequency of the current 100-year event for each river reach in the state. We then calculated a flow-weighted average change factor for each county to estimate the change in the future probability of the current 100-year event. We assumed that the future ratio of EAD to expected 100-year damages remains the same (e.g., EAD is 2.5 times the expected 100-year damage).

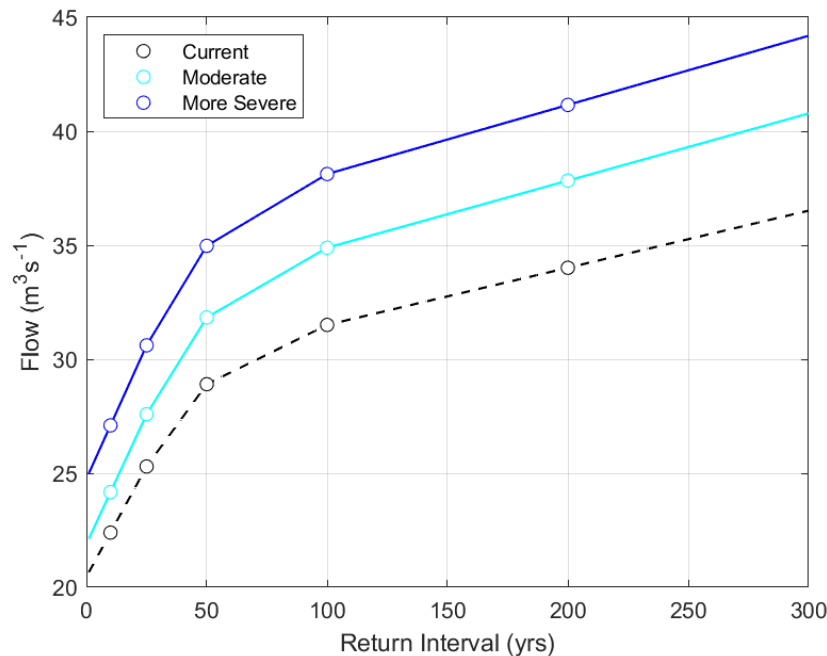


Figure 5-1. Example of changes in flow magnitude (vertical shifts in flow/RI curve) being translated to changes in flow frequency (e.g., horizontal shifts in flow/RI curve: in this example baseline 100 year event becomes ~45 year event under the moderate climate scenario and ~30 year event under the more severe scenario).

The benefit of the Reclamation (2014) dataset is that this product summarizes data from climate modeling output that is run through a hydrologic model. Thus, it includes, in a simplified way, both the spatial variability in projected changes in rainfall, as well as the relevant hydrologic processes that drive inland flooding (e.g., evapotranspiration, soil moisture, snowpack, and other land surface processes). However, this data product also requires multiple simplifying assumptions regarding atmospheric processes, as the data driving this model are ultimately compiled only at a global climate model grid cell resolution (Reclamation, 2014). Thus, while these outputs account for the land surface processes that create flooding, they are likely to under-represent the atmospheric processes that drive extreme precipitation.

A simpler approach is to assume that all of the extreme events that cause flooding will change in proportion to the increase in rainfall potential created by increased moisture holding capacity of the atmosphere. This increase in rainfall potential is referred to as “Clausius-Clapeyron scaling,” and results in an increase in precipitation of 7% per 1°C. Mahoney et al. (2018) present a summary of the recent literature regarding the scaling of extreme precipitation according to the Clausius-Clapeyron relationship. As a check on the USBR-derived results, we assumed that every event on each magnitude-frequency curve increases in proportion to Clausius-Clapeyron scaling for a 2°C warmer atmosphere (i.e., each event increases in magnitude by 14%) and re-calculated the change in frequency of the 100-year event that results. These events were also aggregated by county using a flow-weighted averaging approach and compared to the state-wide results from the USBR analysis. At a state-wide scale, the USBR and Clausius-Clapeyron derived climate change scenarios generated very similar results, lending support to the use of the simpler Clausius-Clapeyron scaling for the More Severe scenario, as described below.

The More Severe climate scenario followed the Clausius-Clapeyron approach described above; specifically, we constructed a baseline magnitude-frequency curve for each river reach in the state using the downscaled hydrology data, we applied a change factor to the magnitude of each event, and we calculated the change in frequency of the 100-year event based on these calculations. The main difference in this approach is that we assumed a higher degree of summertime warming – 3°C rather than 2°C – and applied Clausius-Clapeyron scaling of 7% per degree to this higher warming amount, resulting in an increase of 21% for all return interval events.

5.1.3.3 Applying the Population Scenarios

In order to account for population change, we used the ICLUS (Sect. 3.3.1) change in land use for the Low, Medium, and High Growth scenarios. In this context, ICLUS allowed us to calculate how changes in floodplain development might influence flood risk in the future. For the future population scenarios, we assumed that growth remains restricted within all 100-year floodplains across the state, so that no future development occurs in these floodplains unless it is designed to withstand a 100-year flood event. We thus focused on future development between the 100-year and 500-year floodplain boundaries and its influence on future flood risk. To do this, we overlaid ICLUS land use data with mapped floodplains throughout the state to represent the fraction of the development in each county that occurs inside versus outside of



flood hazard zones. We then selected 100-year and 500-year floodplain maps from each watershed in the state where both sets of maps were available. We overlaid these maps with the gridded building replacement cost data described in Sect. 3.3.1 to calculate the fractional change in the total value of buildings within the 100 and 500-year floodplains between the current and each future population scenario.

5.1.4 Model Outputs

The ultimate product created by the steps outlined in this document is a per-county expected annual damage for each combination of the three climate and four population scenarios (i.e., each county has 12 unique expected annual damage values). These are the data that can be found in the interactive online visualization tool.

5.1.5 Assumptions and Limitations

We developed our flood modeling approach to leverage available datasets across the state, while also expanding on the previous flood hazard work that was focused on risks around 100-year floodplains (CWCB, 2013). Both the baseline analysis described in CWCB (2013) and the methods we used to extend these analyses introduce some limitations into the analysis, as summarized below.

- The county-scale damages from 100-year floods as described in the state Flood Hazard Mitigation Plan are based on a generalized flow model, intersecting with buildings at a census block level. The limitations introduced from this analysis are described more fully in CWCB (2013).
- There are only seven locations in the state where we were able to gather depth grids from multi-return interval events. We used those seven locations to overlay flood depths with building footprints and calculate EAD from a full range of floods in order to arrive at an average factor of 2.5 relating EAD to 100-year damages. However, there is likely to be considerable uncertainty around this scalar due to the small sample size.
- The projected changes in flood damages under future climate change scenarios do not account for local-scale adaptations that could potentially limit damages in the future.



5.2 Flood Technical Approach: Bridges

5.2.1 Overview

As a state crisscrossed by rivers, bridges represent a valuable lifeline for many Colorado residents. Recent events, such as the 2013 flood, have highlighted how sensitive this infrastructure is to damage during high flows. Once impaired, bridge repairs and replacements can be extremely expensive. During the 2013 event alone Colorado Department of Transportation (CDOT) bridge costs exceeded \$300M, with some repairs approaching \$1000 per square foot of bridge deck area. With flood magnitudes and frequencies expected to increase in a warming world, it stands to reason that bridge repair and replacement costs will rise over the coming years. In the following sections, we describe how we used available data from the 2013 flood to quantify the cost of bridge repairs due to historic and future flooding.

5.2.2 Data and Inputs

5.2.2.1 *National Bridge Inventory and Related Geospatial Data*

The National Bridge Inventory (Federal Highway Administration, 2019) includes data on the location, size, condition, and other parameters on more than 8000 bridges across Colorado. For this work, we analyzed only CDOT-owned bridges that were built over waterways (i.e., we did not include bridges over roadways and railways because they are not exposed to flood risk). We combined these bridge data with streamlines from the National Hydrography Dataset (United States Geological Survey, 2019) and roadway information from OpenStreetMap (OpenStreetMap Contributors, 2019).

5.2.2.2 *2013 Bridge Damage and Streamflow Data*

CDOT provided a list of damaged bridges and their repair costs from the 2013 flood event (Colorado Department of Transportation, 2019). We used this information in conjunction with annual exceedance probability estimates (i.e., the probability of a given flow value being exceeded in a year) on various river reaches from Table 1 in Gochis et al. (2015).

5.2.2.3 *Climate Data and Scenarios*

The bridges sector uses the same climate data and methods as described in Sects. 2.2.1 and 5.1.3.2.

5.2.3 Model Approach/Methods

The general approach for this sector was to first relate the probability of damage and cost of repair for various annual exceedance probabilities for damaged and undamaged bridges crossing river reaches with flow estimates in Gochis et al. (2015). Then, we used these relationships to estimate statewide bridge damages.

5.2.3.1 *Calculating Damage Probabilities and Repair Costs from 2013 Flood Event*

The first step was to link damaged and undamaged CDOT bridges to river reaches where annual exceedance probability estimates were available. For this step, we only included bridges that



crossed the streamline of the reach of interest (i.e., CDOT bridges that crossed nearby tributaries without flow estimates were not included). We counted bridges matching these criteria, classifying whether they were damaged or not. We then aggregated the damaged and undamaged bridge counts by annual exceedance probability to calculate the probability of damage at the 0.2%, 1%, and 4% levels. We found that the probability of damage decreased with increasing annual exceedance probabilities (Figure 5-2).

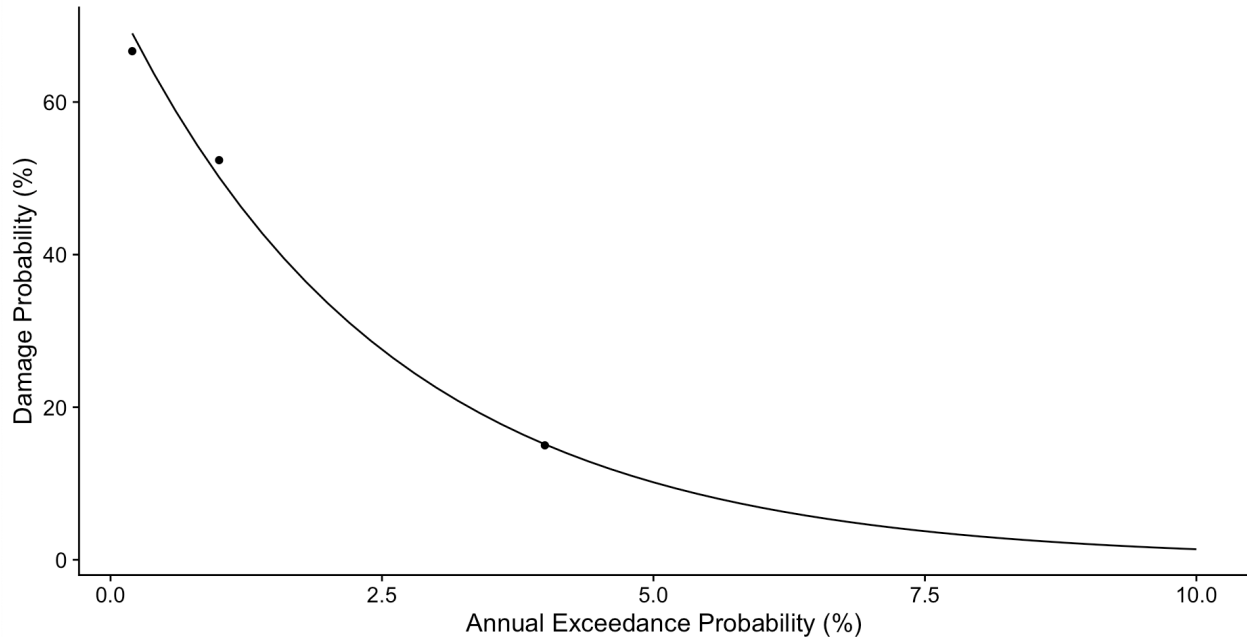


Figure 5-2. Relationship between annual exceedance probability and damage probability. Points are from CDOT observed damages and the solid curve is fit to those data with an exponential linear model.

We next calculated repair costs in terms of dollars per square foot for the damaged bridges at the three annual exceedance probability levels. For this we binned all bridge repair costs by their associated annual exceedance probability. Next, we summed the total deck area of CDOT-reported damaged bridges per annual exceedance probability bin using bridge size data from the National Bridge Inventory. We then divided the total repair cost by total bridge area for the 0.2%, 1%, and 4% annual exceedance probability bins. Similar to the damage probability curve, we found that repair costs decreased with increasing annual exceedance probability (Figure 5-; i.e., more frequent and less intense events have lower costs). We next computed a conditional repair cost as a function of the probability of damage and repair cost per annual exceedance probability level (Figure 5-3).

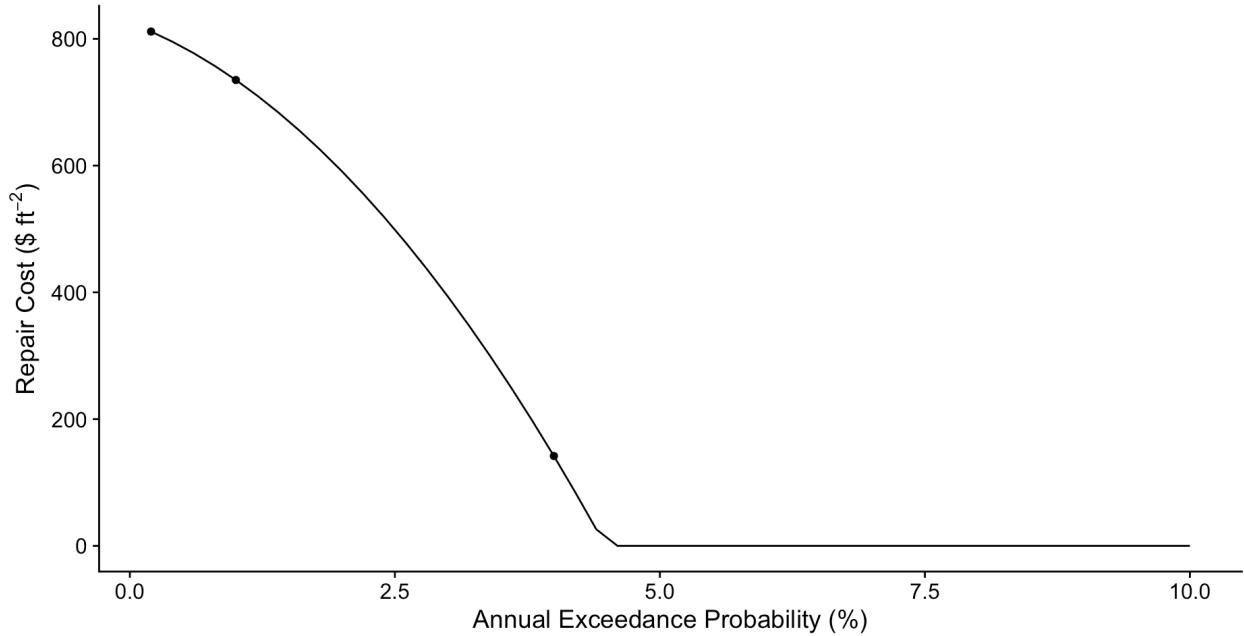


Figure 5-. Repair costs plotted against annual exceedance probability. Points are from CDOT observed damages and the solid curve is fit to those data with a 2nd-order polynomial linear model. Repair costs go to zero at annual exceedance probability = 4.6%.

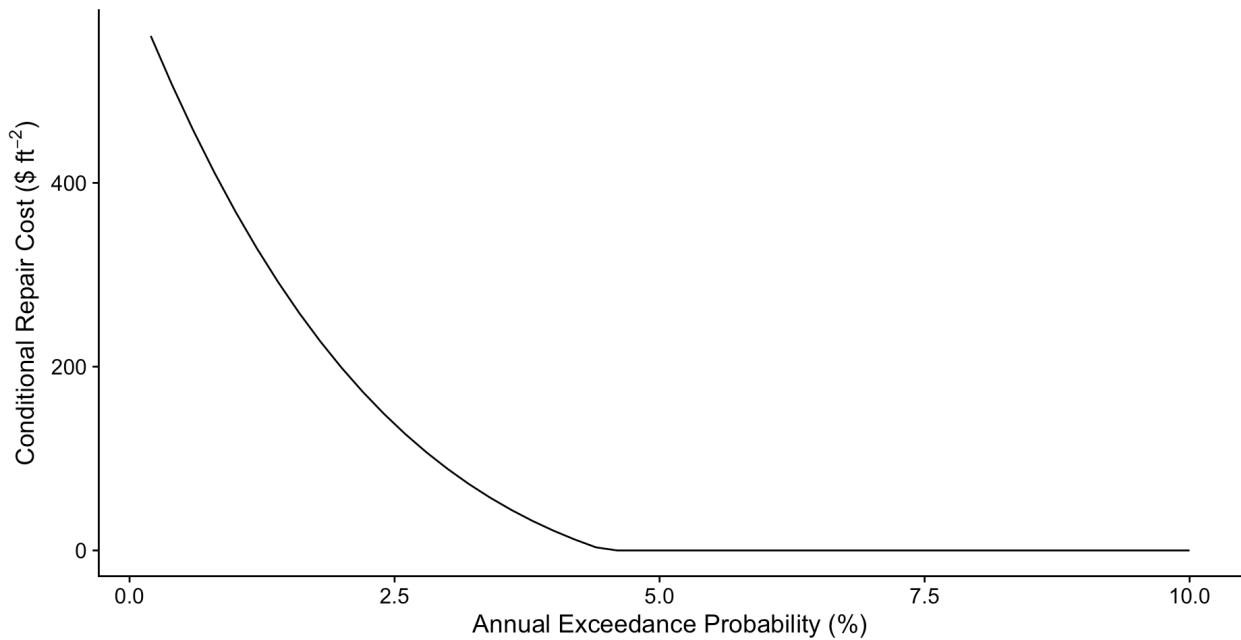


Figure 5-3. Conditional repair cost (i.e., repair cost times damage probability) plotted against annual exceedance probability.

5.2.3.2 Calculating Expected Annual Damages

We then computed the expected annual damage value for all CDOT-owned bridges over waterways in the National Bridge Inventory. Here, the expected annual damage is a function of a bridge's deck size, the annual exceedance probability, and the conditional repair cost. In this context, a high conditional repair cost has a low probability of occurring and a low conditional repair cost has a high probability. The final expected annual damage is an integration of all such

probabilities and magnitudes. To get county-level damages, we then summed the expected annual damages for all bridges within a given county.

5.2.3.3 *Accounting for Climate Change*

To account for the effect of increasing flood frequencies due to climate change, we used the approach outlined in Sect. 5.1.3.2 for the Moderate and More Severe climate scenarios. In this case, we repeated Section 5.2.3.2 with new annual exceedance probabilities. We did not perform any adjustments based on future population due to a lack of data on the relationship between population growth and changes to the number, size, and design criteria of bridges. Thus, the values given for a population scenario are equal to those for the associated climate scenario.

5.2.4 *Model Outputs*

The ultimate product created by the steps outlined in this document is a per-county expected annual damage for each combination of the three climate scenarios. These are the data that can be found in the interactive online visualization tool. In addition to this product is a series of intermediate model outputs listed below:

1. Number of damaged and undamaged bridges per reach and return period from the 2013 flood event
2. Bridge-level EADs for historic and future climate conditions

5.2.5 *Assumptions and Limitations*

- For this analysis, we were limited to the bridge damage data from CDOT during the 2013 flood event as they had complete documentation of the location of damaged bridges as well as the costs of repairs. We then extrapolated our findings to the rest of the state, but the limited CDOT data may not be representative of other locations.
- The estimation of flood annual exceedance probabilities is inherently uncertain, particularly for extreme events. Thus, our relating of damage probabilities and repair costs to annual exceedance probabilities is affected by those uncertainties.
- We could not estimate the effects of population growth because of a lack of information relating increased population to the size, location, and design criteria of bridges.



6 Technical Approach: Drought

6.1 Drought Technical Approach: Crops

6.1.1 Overview

Crop growth in Colorado is inherently water limited. As such, prolonged periods of abnormally dry conditions, or droughts, can reduce yields and production (e.g. Zipper et al., 2016). This analysis has two objectives. First, we aim to quantify the impact of historical drought on Colorado’s crop production. Second, we seek to project the impact of future droughts on Colorado’s crop production, considering climate change and population growth scenarios.

To accomplish these goals, we develop an empirical model of county-level production of major commodity crops (corn, wheat, hay, and sorghum) as a function of drought indicator metrics and meteorological data. The model is calibrated against historical data across a large geographic domain of 14 western US states.

6.1.2 Data and Inputs

6.1.2.1 Climate Data and Scenarios

For the crops sector, we use precipitation and air temperature, in addition to derived drought metrics, as predictor variables in the empirical modeling framework. These data are extracted from a historical (1949 – 2014) meteorological data product (Maurer, Wood, Adam, Lettenmaier, & Nijssen, 2002), with a 1/8° spatial resolution and daily temporal resolution. These Baseline data are then adjusted for the Moderate and More Severe scenarios as noted in Section 2.2.2.

6.1.2.2 Agricultural Data

Agricultural data are needed for model calibration and interpretation. We retrieved crop production and price data from the USDA National Agricultural Statistics Service (NASS) (U.S. Department of Agriculture, 2020). Specifically, we obtained annual county-level corn, wheat, hay and sorghum production data between 1975 and 2018 for all western US states (AZ, CA, CO, ID, KS, MT, NE, NV, OK, OR, TX, UT, WA, and WY). In this context, production is a measure of a county’s total agricultural output, measured in either bushels or tons depending on the crop.

Commodity prices typically exhibit strong inter- and intra-annual variability, responding strongly to factors influencing supply and demand in markets that can be global and local. Moreover, global commodity prices are typically insensitive to supply in Colorado. To avoid the influence of price volatility, we used 2011 commodity “base” prices (U.S. Department of Agriculture, 2020). The “base” price establishes the commodity price against which further price movements are compared. In this way, we isolate the influence of climate on agricultural production and revenue, independent of macroeconomic influences. We adjusted 2011 prices (Table 6-1.) for inflation to 2019 nominal dollars using the consumer price index (BLS, 2020).

Table 6-1. 2011 commodity base prices. Data source: USDA NASS

Commodity	Price	Unit
Corn	6.02	\$/BU
Wheat	7.44	\$/BU
Hay	159.00	\$/ton
Sorghum	10.70	\$/CWT

6.1.3 Model Approach/Methods

6.1.3.1 Annual Aridity Bins

A key predictor variable in our model is the number of months in a year assigned to each of four different aridity bins. To quantify monthly aridity, we used the self-calibrated Palmer Drought Severity Index (scPDSI) (Wells, Goddard, & Hayes, 2004). This is a relative measure of aridity derived from monthly average temperature and precipitation data. Negative values of scPDSI indicate drier than normal conditions, whereas positive values indicate wetter than normal conditions.

We calculated monthly scPDSI for each 1/8° grid cell of the meteorological data product (1949 – 2014) using the “scPDSI” package (Zhong, Chen, Wang, & Lai, 2018) for the R scripting language (R Core Team, 2019). For future climate scenarios, we calculated scPDSI from climate-adjusted temperature and precipitation data, after a spin up period over one iteration of the historical data (1949 – 2014). The spin up period is necessary to establish “normal” climatic conditions, because scPDSI is a relative measure of aridity. We aggregated data to the county-scale by taking the mean scPDSI of all 1/8° grid cells located within a county.

We categorized monthly scPDSI values into several aridity bins (Table 6-2.). That is, for each county and year, we enumerated the number of months in each scPDSI bin. For example, during a particularly dry year, a county might record 4 months in bin 1 (very dry conditions), 6 months in bin 2 (dry conditions), and 2 months in bin 3 (wet conditions), and no months in bin 4 (very wet conditions). Annual bin counts were used as predictor variables in our empirical model of crop production.

Table 6-2. Aridity bins based on monthly scPDSI.

Aridity bin	scPDSI range	Description
1	scPDSI < -3	Very dry
2	-3 < scPDSI < -1	Dry
3	1 < scPDSI < 3	Wet
4	3 < scPDSI	Very wet

6.1.3.2 Fixed effects model of crop production

We used an empirical model to estimate the impact of drought and meteorological conditions on annual crop production. The spatial domain of the model includes all counties of western US

states, and the temporal domain spans from 1975–2018. The model is formally considered a two-way fixed effects model (Equation 6-1).

$$\ln(Y_{it}^j) = \sum_{k=1}^4 \beta_k \text{Bin}_{it}^k + \beta_X X_{it} + \alpha_i + \gamma_t + \epsilon_{it}^j$$

Equation 6-1

Where Y_{it}^j is the production of commodity j in county i in year t . Bin_{it}^k denotes the number of months within the k th aridity bin (Table 6-2.) in county i during year t . X_{it} is a vector of average temperature, total precipitation, average temperature squared, and total precipitation squared in county i during year t . A spatial fixed effects parameter, α_i , controls for temporally invariant differences between counties affecting crop production (e.g. soil quality and the size of the agricultural industry). While irrigation was not explicitly accounted for in this model, its effect on crop production is implicitly captured by spatial fixed effects parameter. Additionally, a temporal fixed effects parameter, γ_t , accounts for spatially homogenous year-to-year differences affecting crop production (e.g. macro-economic trends). Model coefficients β_k and β_X describe the effects of aridity bins and meteorological conditions on crop production respectively. By computing log production, model coefficients are interpreted as the proportional change in production from a unit change in the respective response variable. Model parameters were estimated with the “plm” package (Croissant & Millo, 2008) in R, a set of functions for linear modeling with panel data.

6.1.3.3 Estimating revenue anomalies

To estimate the impact of drought conditions on crop revenue, we multiplied annual production anomalies by adjusted base unit commodity prices. The first step in this process is to estimate the annual effects of drought on crop production in each of Colorado’s counties. Annual effects quantify the proportional change in production due to drought conditions. For example, an annual effect of -0.1 on sorghum production in county i during year t would suggest that climatic conditions caused annual sorghum production to be 10% lower than normal. Annual effects are estimated by evaluating Equation 6-1 with intercept terms set to zero, leaving only the proportional influence of the climatic predictor variables on production.

Next, we estimated production anomalies by multiplying annual effects for crop j in county i by the baseline production rates. Baseline production rates were set equal to the mean annual commodity production rates in a county from 1990–2018, which was evaluated directly from NASS data. Finally, we estimated revenue anomalies by multiplying production anomalies by base unit commodity prices.

6.1.3.4 Accounting for population growth

Urbanization is likely to decrease the amount of agricultural acreage in rotation, in part because water resources will be transferred away from agricultural producers to meet the domestic needs of new residents and the footprint of urban areas will encroach on current agricultural lands. We account for this concept by using 2050 projections of irrigated land changes for three population growth scenarios in the Technical Update (CWCB, 2019 2(3)). We assume



production decreases proportionally with acreage reductions, thereby causing a uniform decrease in crop production from historical baseline levels.

The 2019 Technical Update presented year 2050 projections for urbanization of irrigated acreage for five economic planning scenarios (CWCB, 2019 2(3)). We disaggregated basin-scale projected changes in irrigated acreage to the county-level for three future growth scenarios: “weak economy”, “business as usual”, and “hot growth”. These scenarios map directly to the Low, Medium, and High Growth population scenarios used in this project. Because the Technical Update does not project changes in non-irrigated acreage, we assumed that percent reductions in total acreage will be equal to percent reductions in irrigated acreage.

Additionally, population growth in Colorado is likely to increase demand for locally grown crops as consumer preferences are becoming more geared to local choices. While this is an important consideration for the future of agricultural production in Colorado, we did not account for this in our models. Also, our models did not account for future changes in technology that change increase crop yields (e.g. genetic modifications, harvesting or planting technology, etc.). Rather, our models assume that today’s agricultural technologies remain static into the future (2050).

6.1.3.5 Model Outputs

Model outputs have an annual timestep and county-scale spatial resolution. Our model directly calculates the annual effect of climate conditions on crop production, as explained above. From this, we approximate annual production and revenue anomalies. Outputs are generated for all arrangements of climate and population change scenarios (Figure 4-1.). County-level annual revenue anomalies are synthesized in terms of expected annual damages, which describe the likely impacts of the average drought condition on a county’s crop production. Expected annual damage integrates revenue losses across all drought events and is therefore a probabilistic index of drought risk.

6.1.4 Assumptions and Limitations

- The model does not consider changes in agricultural technology. For example, engineering advancements may develop drought resistant crop strains or advances in irrigation efficiency that can improve crop yields during drought years. The model assumes today’s technology, under tomorrows climate and population.
- The model does not account for potential changes in crop production due to carbon dioxide fertilization. The empirical nature of our model is not suited to capture biophysical dynamics such as carbon fertilization. This assumption may result in over projections of negative production anomalies due to drought by 2050.
- The model does not account for changing crop demand. As Colorado’s population grows, it is likely that in-state crop demand will also grow. While important, this is not considered by our model, which is focused on production.
- We assume that future changes in non-irrigated acreage are equal to changes in irrigated acreage due to population growth. Changes in irrigated acreage are likely to be larger than non-irrigated acreage because some land will be taken out of rotation simply



from the acquisition of water rights for other uses. This is sometimes called “buy and dry”.

- The model does not differentiate between irrigated and non-irrigated crop production. This is due to the paucity of irrigation-specific historical crop production data. However, because the model is trained on historical crop production data, the effects of irrigation are implicitly captured in the spatial- and temporal-fixed effect parameters.



6.2 Drought Technical Approach: Cattle

6.2.1 Overview

Contributing \$4.0B in annual revenue (U.S. Department of Agriculture, 2020), the cattle industry is critically important to Colorado's economy and the makeup of rural communities. At nearly \$2B annually, feed costs for the state's 2.85M cattle comprise a large percentage of industry costs (U.S. Department of Agriculture, 2020). Therefore, any event that raises feed costs will inherently have a negative effect Colorado's cattle industry.

As a semi-arid state, Colorado is uniquely exposed to the threats of drought, with two severe, spatially extensive droughts occurring in the past 20 years alone. In both cases, the onset of drought corresponded with a sharp increase in feed costs. According to data from the United States Department of Agriculture's (USDA) Economic Research Service (ERS), feed costs increased by \$165M from 2001 to 2002 and by \$408M from 2010 to 2011 (U.S. Department of Agriculture, 2019). Although such increases can occur for market-related reasons and macroeconomic trends, they are mostly ascribable to increased demand and reduced production during drought (e.g., Countryman, Paarlberg, & Lee, 2016)

In this context, increased feed costs are a direct, first-order impact of drought, an effect that is magnified when drought is spatially extensive and commodity prices are elevated. In Colorado, purchasing extra feed to account for reduced range and pasture productivity is an integral component of drought adaptation decision-making (Rojas-Downing, Nejadhashemi, Harrigan, & Woznicki, 2017) as the majority of ranches are dryland operations. Without irrigation capabilities, one key question when drought strikes is: "How much extra feed do I need to purchase for my herd?" Although many ranchers will sell or move cattle during drought, increased feed costs are often their largest expense.

For the cattle sector, we use a combination of land cover data, remote sensing observations, drought severity metrics, and population growth data to estimate increased feed costs due to drought across Colorado.

6.2.2 Data and Inputs

6.2.2.1 Land Cover Data

In our analysis, we focused only on areas in Colorado classified as either pasture or grassland by the National Land Cover Dataset (NLCD; Yang et al., 2018). The NLCD maps land cover across the United States at a 98.4 ft. (30 m) spatial resolution in 20 unique categories. In this work, we selected grid cells with a value of 71 (grassland) or 81 (pasture). These were further filtered to only areas below an average elevation of 10,830 ft. (3300 m) to remove alpine meadows from the analysis.

Additional land cover data for the population growth scenarios were derived from the EPA's ICLUS dataset (Sect. 3.3.1). Specifically, we focused on changes to grazing (ICLUS code 5) and pasture (ICLUS code 6) area per county for Low, Medium, and High Growth.

6.2.2.2 Satellite Remote Sensing

For this work, we used data from the Moderate Resolution Imaging Spectroradiometer (MODIS), a sensor mounted to NASA's Terra and Aqua satellites, to evaluate how pasture and grassland vegetation responds to drought in our study area. In this context, the normalized difference vegetation index (NDVI) is a useful proxy for vegetation greenness and productivity. Specifically, we utilized the MODIS MCD43A4_NDVI product in Google Earth Engine (GEE; Gorelick et al., 2017). It is produced as a 16-day average on a 1640 ft. (500 m) grid spacing using the following equation:

$$NDVI = \frac{NIR - Red}{NIR + Red}$$

Where NDVI is a dimensionless value between -1 and 1 (1 = maximum greenness/productivity), and NIR and Red are the reflectance values in the near infrared and red wavelengths, respectively. For the MCD43A4_NDVI product, NIR corresponds to MODIS band 2 (841–876 nm) and Red corresponds to band 1 (620–670 nm). We took the annual maximum NDVI value for each pixel to create an annual composite could be used to estimate productivity.

6.2.2.3 Climate Data and Scenarios

In order to extend the productivity analysis back in time before the MODIS satellite record (pre-2000) and into future climate scenarios, we accessed high-resolution climate data from which we could compute an scPDSI time series. For details on these data and methods, please see Sects. 6.1.2.1 and 6.1.3.1.

6.2.2.4 Agricultural Data

Typical cattle forage has a lower energy content than most feed grains, making it necessary to relate the caloric content per mass of forage to the same for corn, the most commonly used feed grain. For this, we used Table 4 from *Nutrition and Feeding of the Cow-Calf Herd: Essential Nutrients, Feed Classification and Nutrient Content of Feeds* (Hall, Seay, & Baker, 2009). We also required information on the cost per unit of corn to compute feed cost anomalies during drought. We used the 2019 average per-bushel price of corn from the USDA. As a feed grain, a bushel of corn weighs 56 lbs. (25.6 kg) with a 2019 average price of \$3.75 (U.S. Department of Agriculture, 2020). Supplementary information on Colorado's cattle industry came from the USDA's NASS.

6.2.3 Model Approach/Methods

6.2.3.1 County-level scPDSI

We aggregated grid-cell scPDSI (Sect. 6.1.3.1) values to the county level to get a monthly average scPDSI for each county. For this sector, we also averaged the county-level scPDSI values from April–October to isolate scPDSI during the growing season.



6.2.3.2 Calculating Land Surface Productivity with Remote Sensing and Climate Data

From 2000–2014, we computed the maximum annual NDVI for each MODIS grid cell in Colorado using GEE. Next, we masked these values to include only those corresponding to pasture and grassland cells from the NLCD. Then we took a county-level average of all cells matching these criteria to create an annual time series of county-averaged maximum NDVI across Colorado.

We next joined the NDVI data to county-level growing season scPDSI from 2000–2014. For each county, we then created a linear regression model that would estimate NDVI based on scPDSI:

$$NDVI_{est} = \beta + \alpha scPDSI$$

where $NDVI_{est}$ is the NDVI value estimated by the model, β is the y-intercept, α is the slope of the relationship, and $scPDSI$ is the county-level growing season scPDSI. In essence, this model relates vegetation greenness (NDVI) to drought severity (scPDSI), which allows us to compute past and future productivity as a function of our previously calculated scPDSI values at the county level across Colorado. On average, scPDSI explained 39.4% of the variance in NDVI, with 75.5% of counties expressing statistically significant relationships (at the 95% level) between the two variables.

6.2.3.3 Calculating Baseline Land Surface Productivity and Anomalies

We then applied the linear model from the previous section to the historic scPDSI time series for each county to get estimated values of annual maximum NDVI from 1949–2014. In order to convert these values to land surface productivity, we used the equation from Thoma et al. (2002):

$$LBM = -2739 + 25.0NDVI_{est}$$

where LBM is live biomass (kg ha^{-1}). This gave us a time series for each county of 66 annual productivity estimates, the average of which we considered to be baseline productivity (\overline{LBM}). We then calculated the annual productivity anomaly as the difference between \overline{LBM} and the estimated LBM for that year. If the productivity anomaly were negative (i.e., LBM is less than the \overline{LBM}), then we assumed extra feed would need to be purchased.

6.2.3.4 Estimating Historic Feed Costs from Reduced Productivity

Once we had our annual time series of productivity anomalies, we needed to estimate the cost of extra feed purchases. First, we converted the productivity anomaly in kg ha^{-1} to a total amount of biomass (kg) by multiplying the anomaly by the total area of pasture and grassland (Sect. 6.2.2.1) in that county. We then multiplied the average energy ratio between pasture forage and feed corn (0.73) by the total biomass to estimate the total weight of corn that would need to be purchased to meet the energy deficit caused by drought-induced productivity losses. Finally, we divided this value by the weight per bushel of corn and multiplied the



resultant value by the 2019 average corn price per bushel to get a county-level feed cost for years where productivity was below the baseline.

6.2.3.5 Calculating Expected Annual Damages

We then used the time series of extra feed costs to calculate an expected annual damage for drought years, where the expected annual damage is a function of the probability of a given productivity anomaly occurring and its magnitude in terms in feed costs. In this context, a high feed cost value has a low probability of occurring and a low feed cost has a high probability. The final expected annual damage is an integration of all such probabilities and magnitudes (Sect. 4.2).

6.2.3.6 Accounting for Climate and Population Change

After computing expected annual damages for current climate and population levels, we followed the steps above taking both climate change and population growth into account. For climate change, we recomputed the scPDSI time series after adjusting the air temperature and precipitation by the scalars for the Moderate and More Severe climate change scenarios (Sect. 2.2.2). We next made new time series of $NDVI_{est}$ by plugging the Moderate and More Severe scPDSI values into the linear model created from the MODIS NDVI and Baseline climate data. Once we had new $NDVI_{est}$ values, we followed the steps in Sects. 6.2.3.3–6.2.3.5 to get expected annual damages for the Moderate and More Severe scenarios.

Finally, we adjusted the expected annual damages for three future population scenarios: Low, Medium, and High Growth. We did this by multiplying the NLCD pasture and grassland area in each county by the relative change in ICLUS pasture and grazing land from the current to future scenarios. We recomputed baseline productivity, \overline{LBM} , taking the new land area into account under the assumption that this would represent a new normal in future scenarios (i.e., less land available for cattle, fewer cattle to feed). We then reran productivity anomalies with the new land area and baseline productivity values, along with Sects. 6.2.3.4 and 6.2.3.5 to get adjusted expected annual damages for the population scenarios. In contrast to most other sectors, the reduced pasture area tended to slightly lower expected annual damages.

6.2.4 Model Outputs

The ultimate product created by the steps outlined in this document is a per-county expected annual damage for each combination of the three climate and four population scenarios (i.e., each county has 12 unique expected annual damage values). These are the data that can be found in the interactive online visualization tool. In addition to this product is a series of intermediate model outputs listed below:

1. County-level monthly scPDSI time series (1949–2014) for historic and future climatic conditions
2. Spatially continuous raster maps of annual maximum NDVI across Colorado
3. Annual time series (2000–2014) of maximum county-averaged NDVI for pasture and grassland grid cells



4. County-level time series of estimated annual maximum NDVI as a function of growing season scPDSI for historic and future climatic conditions
5. County-level time series (1949–2014) of estimated productivity and productivity anomalies for historic and future climatic conditions
6. County-level time series (1949–2014) of feed costs for historic and future climatic conditions

6.2.5 Assumptions and Limitations

- The model does not consider changes in agricultural technology. For example, engineering advancements may develop drought resistant forage strains or improved harvesting and storage techniques. The model assumes today's technology, under tomorrow's climate and population.
- The model does not account for potential changes in forage production due to carbon dioxide fertilization.
- Ranchers have many options when it comes to responding to drought. Increased feed purchasing is just one response to keep herd sizes at or near pre-drought levels.
- There is uncertainty in both our estimates of productivity from NDVI and our calculations of NDVI from scPDSI. These propagate into uncertainty in the final expected annual damages.



6.3 Drought Technical Approach: Skiing

6.3.1 Overview

According to the 2019 Colorado Statewide Comprehensive Outdoor Recreation Plan, the ski industry provides the highest level of statewide outdoor recreation spending while ranking 7th in terms of annual user days by residents (Colorado Parks and Wildlife, 2018). In this report, a user day is a single daily visit by one person (i.e., if one person skied 10 days at Colorado ski areas, they would account for 10 user days). Between winters 2006–2007 and 2015–2016, Colorado resorts averaged 12.2M user days per year. In terms of trips, those made for skiing comprised 4% of visitor volumes, while producing 13% of all expenditures (Longwoods International, 2019). Depending on the source, skiing and other snow sports add \$1.5B to \$3.8B in economic value to the state annually (Awuku-Budu & Franks, 2019; Hagenstad, Burakowski, & Hill, 2018). Other studies estimate skiing and snowboarding related spending to be between \$2.5B and \$9.3B (Colorado Parks and Wildlife, 2018; Longwoods International, 2019). Although the total numbers vary, they tell the same story: the ski industry is a substantial contributor to Colorado’s recreation economy.

Looming large over the ski industry is how changes to climate will affect annual skiing visits in Colorado and, as a result, annual revenue. Previous research has documented the warming-driven threats faced by the ski industry due to its inherent temperature sensitivity (Burakowski & Magnusson, 2012; Hagenstad et al., 2018; D. Scott & McBoyle, 2007; D. Scott, McBoyle, Minogue, & Mills, 2006; Steiger, Scott, Abegg, Pons, & Aall, 2019; Cameron Wobus, Small, et al., 2017). These reports have found, in general, as air temperature increases, the amount of precipitation falling as snow declines, which tends to shorten ski seasons and reduce visitor volumes. However, snowy areas of the US have not responded equally to rising air temperatures, nor are they expected to with future warming. There is therefore a need to make a detailed analysis of how Colorado user days have responded historically to snow levels and project how they may do so in the future.

To do so requires an approach that can simulate snow accumulation and melt at Colorado ski resorts under both historic and future climatic conditions. In this sense, a snow model forced by readily available air temperature and precipitation data offers a promising path forward. However, a model cannot be used on its own, as an effective model must be validated against reliable observed data to demonstrate its accuracy. In the context of snow, this means automated *in situ* snowpack measurements from the Snowpack Telemetry (SNOTEL) network from the Natural Resources Conservation Service and remotely sensed snow cover duration data from satellite-borne sensors.

In addition to climate change, it is important to consider potential future population increases in Colorado. The state forecasts 2050 populations to be between 7.7M and 9.3M residents, a 43.5% to 74.0% increase over 2014 levels. Thus, a complete analysis of future changes to the Colorado ski industry requires an in-depth accounting of user days and their sensitivity to climate, an estimate of the ski-related expenditures tied to each user day, an evaluation of the frequency with which Colorado residents ski, and future climate and population projections. For

this work, we rely on ski resort snow simulations, satellite snow cover data, as well as various user and economic statistics to quantify the cost of reduced skier user days under historic and future drought conditions.

6.3.2 Data and Inputs

6.3.2.1 Climate Data and Scenarios

To force our snow model, we used daily air temperature and precipitation from the Maurer et al. (2002) dataset as described in Sect. 6.1.2.1. Monthly temperature offsets and precipitation change factors are then applied to historical meteorological data (Sect. 2.2.2) to approximate 2050 climate conditions.

6.3.2.2 Satellite Remote Sensing

Similar to the NDVI metric used in Sect. 6.2.2.2, we computed the annual normalized difference snow index (NDSI) from MODIS to determine whether an area of land is snow covered or not. Specifically, we utilized the MOD10A1.006 Terra snow cover product in Google Earth Engine (GEE; Gorelick et al., 2017) using the SnowCloud processing framework (Sproles, Crumley, Nolin, Mar, & Moreno, 2018). MOD10A1.006 is a daily product on a 1640 ft. (500 m) grid that calculates snow cover presence/absence using the following equation:

$$NDSI = \frac{Green - SWIR1}{Green + SWIR1}$$

Where NDSI is a dimensionless value between -1 and 1 (1 = maximum snow likelihood), and Green and SWIR1 are the reflectance values in the green and shortwave infrared wavelengths, respectively. For MOD10A1.006, Green corresponds to MODIS band 4 (545–565 nm) and SWIR1 corresponds to band 6 (1628–1652 nm). In SnowCloud, NDSI values ≥ 0.4 are indicative of snow cover, with values < 0.4 corresponding to no snow cover. For each water year (Oct. 1 to Sept. 30), we computed the snow cover duration for each MODIS grid cell in Colorado based on the number of days a pixel was identified as having snow cover.

6.3.2.3 Ski Resort Data

Colorado skier user day data are derived from Wobus et al. (2017) for the 2007–2016 seasons and from Shelesky (2016) for the 2001–2006 seasons. The latter manuscript also included per-resort user day data for the 1994–2004 ski seasons from Colorado Ski Country USA. In order to allocate the total user days into Colorado residents and non-residents, we used the reported split of 5.6M resident user days to 7.0M non-resident user days from information on the 2015 Colorado Ski Country USA economic impact report (Colorado Ski Country USA, 2015). We also used ski area shapefiles from the US Forest Service (2009) when analyzing snow cover duration (Sect. 6.3.2.2 above) at the resorts in our analysis. Published lift capacities came from Skicentral.com.

6.3.2.4 Skiing Expenditures

Depending on the data source, the total annual economic impact of the ski industry in Colorado varies by several billion dollars. In an unpublished 2015 report, Colorado Ski Country USA calculates a \$4.8B annual impact from the ski industry. The US Bureau of Economic Analysis estimates that skiing and snowboarding produce an annual impact of ~\$3B for the United States as a whole, with \$1.5B of economic impact from all snowsports in Colorado (Awuku-Budu & Franks, 2019). Similarly, a 2018 Protect Our Winters (POW) report estimates snowsports-related economic contributions in Colorado amount to \$2.6B annually (Hagenstad et al., 2018). In these widely circulated reports, economic impact includes not only direct ski visit expenditures, but all also indirect and induced effects. Many such studies rely on the IMPLAN input-output model that uses region- and industry-specific multipliers to arrive at a final impact dollar amount. The structure of these models and their multipliers are often proprietary, which limits reproducibility and a robust quantification of direct expenditures. However, Table 6-3. below provides an estimate of per-user economic impact calculated by dividing total economic impact by annual user days.

An alternative approach that limits assumptions on economic processes and indirect/induced effects is to examine direct per-user-day expenditures. Published values for such expenditures also vary, depending on the report’s source (Table 6-3.). Highlighting the inherent uncertainties of quantifying expenditures and total impact is the fact that the per-user-day expenditures from these sources are similar to those values calculated by diving total economic impact by user days as noted in the above paragraph. On the low side, the POW report indicates users spend \$159.34 per day, while, on the high side, the Statewide Comprehensive Outdoor Recreation Plan puts that figure at up to \$387.67. The *Colorado Travel Year 2018* and *The Economic Contributions of Outdoor Recreation* reports put daily expenditures within the range of the low and high values. Overall, the various reports give an average daily expenditure of \$286.73 with a standard error of ±\$40.53 in 2019 US dollars.

Table 6-3. Economic impact plus user day and equipment expenditures estimate by various sources for the ski industry.

Economic impact (10 ⁹ USD)	Expenditures per user day (USD)	Equipment expenditures (USD)	Source
4.8*	398.93†	NA	(Colorado Ski Country USA, 2015)
1.5*	124.54†	NA	(Awuku-Budu & Franks, 2019)
NA	243.00–387.67	603	(Colorado Parks and Wildlife, 2018)
2.6*	159.34	NA	(Hagenstad et al., 2018)
NA	249.00	NA	(Longwoods International, 2019)
NA	233.00–383.00	≥300.00+	(Outdoor Industry Association, 2017)

* Economic impact includes direct, indirect, and induced effects

† Computed by dividing cited economic impact by average annual skier user days (includes direct and induced impacts)

6.3.3 Model Approach/Methods

6.3.3.1 Modeling Snow Cover at Colorado Ski Resorts

We simulated snow accumulation and ablation at Colorado ski resorts with SNOW-17, a widely used model developed by the National Weather Service (Anderson, 2006). SNOW-17 is a temperature index model that is forced with daily precipitation and air temperature data, while otherwise data-intensive energy balance terms are simplified in terms of air temperature only (Hock, 2003). Before running the ski resort models, we first needed to calibrate model parameters in order to ensure we were accurately simulating the evolution of snow accumulation and melt at each site. Previous research has shown snow models exhibit spatially variable performance, meaning it is not appropriate to directly transfer model parameters from one location to another (Etchevers et al., 2004; Rutter et al., 2009). As a relatively simple model that relies on precise parameterization, this is especially true for SNOW-17.

To do this we located the nearest SNOTEL site to each resort. We then forced SNOW-17 with SNOTEL-observed daily air temperature and precipitation, and calibrated the model using a shuffled complex evolution algorithm (Duan, 1993). In this framework, the model is run a large number of times with changing parameter values in order to find the near-optimal parameter set that minimizes the root mean squared error between daily observed SNOTEL snow water equivalent (SWE, the liquid depth of water that would remain if all snow were melted) and model simulated SWE.

We then built two models at each ski resort using the calibrated parameters from the nearest optimized SNOTEL model. One model represented the base elevation and another the summit, locations chosen to bracket the range of snow conditions at a given ski resort. In order to force these models, we extracted a time series of daily air temperature and precipitation from the nearest climate data grid cell (Sect. 6.3.2.1). These time series were then adjusted for elevation using monthly lapse rates (i.e., the change in air temperature and precipitation with elevation) from Wobus et al. (2017). We then ran the base and summit models at each ski resort using the daily elevation-corrected climate data. The key output we utilized from these simulations was the season lengths as discussed below.

6.3.3.2 Relating Modeled Season Length to Observed User Days

Previous research has related ski area user days to season length due to the sensitivity of visitation rates to snow conditions (Hagenstad et al., 2018; Cameron Wobus, Small, et al., 2017). Hagenstad et al. (2018) defined the season as number of days with snow depth > 100 mm, while Wobus et al. (2017) defined it to be from the day with either 450 accumulated hours of snowmaking temperatures or 100 mm of natural SWE accumulation at the base of each resort to the day when summit SWE fell below 100 mm. For this work we defined season length based on our snow model output so we could estimate user days for both historic and future scenarios. Due to uncertainty in model output and the *a priori* season length definitions, we optimized our season length parameters based on the MODIS-derived snow cover duration data.



For each ski resort shapefile, we aggregated the MODIS-derived snow cover duration for every water year between 2001–2016. We then took a statewide average of these values to get an annual snow cover duration estimate for Colorado ski areas. We found that statewide snow cover duration explained 49% of the variance in user days (Figure 6-1.), suggesting that visitation to Colorado ski areas scales with the length of the snow season. Overall, each lost day of MODIS-derived snow cover corresponded to a loss of 27,700 user days.

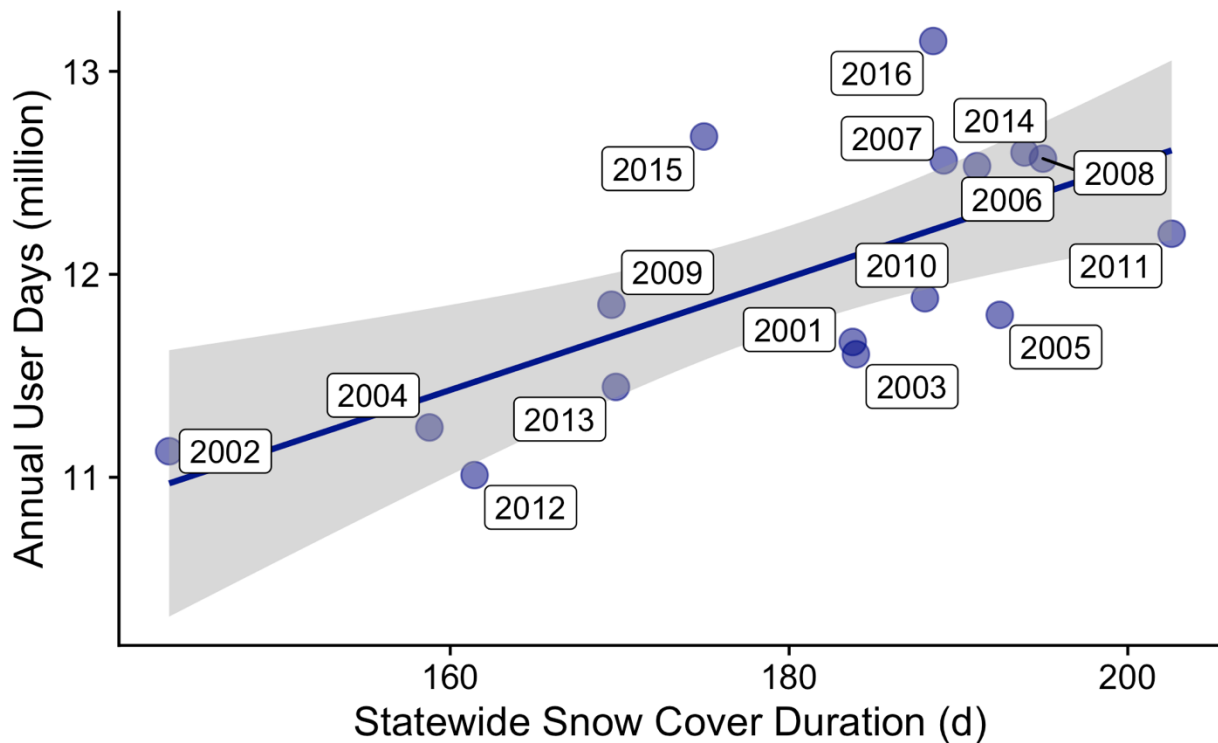


Figure 6-1. Annual user days predicted by MODIS-derived statewide average snow cover duration at Colorado ski resorts. The solid line is the line of best fit computed by ordinary least squares regression ($r^2 = 0.49$, p -value < 0.005) and the gray shading represents the uncertainty of the fit.

Based on this information, we used the MODIS data to determine the best threshold for the number of snowmaking days (defined to be days with mean air temperature $< 32^\circ\text{F}$) to determine season opening date. Here, we optimized our modeled season lengths aggregated to the state level to best match the MODIS-derived snow cover duration over the period of overlapping simulated and satellite data: 2001–2014. Based on this analysis, we used 29 d of air temperatures below freezing at the resort base to signify the season start date. We then used the Wobus et al. (2017) 100 mm summit SWE threshold to identify the end of the season. This combination produced a reasonable fit to the statewide MODIS data (Figure 6-2.).

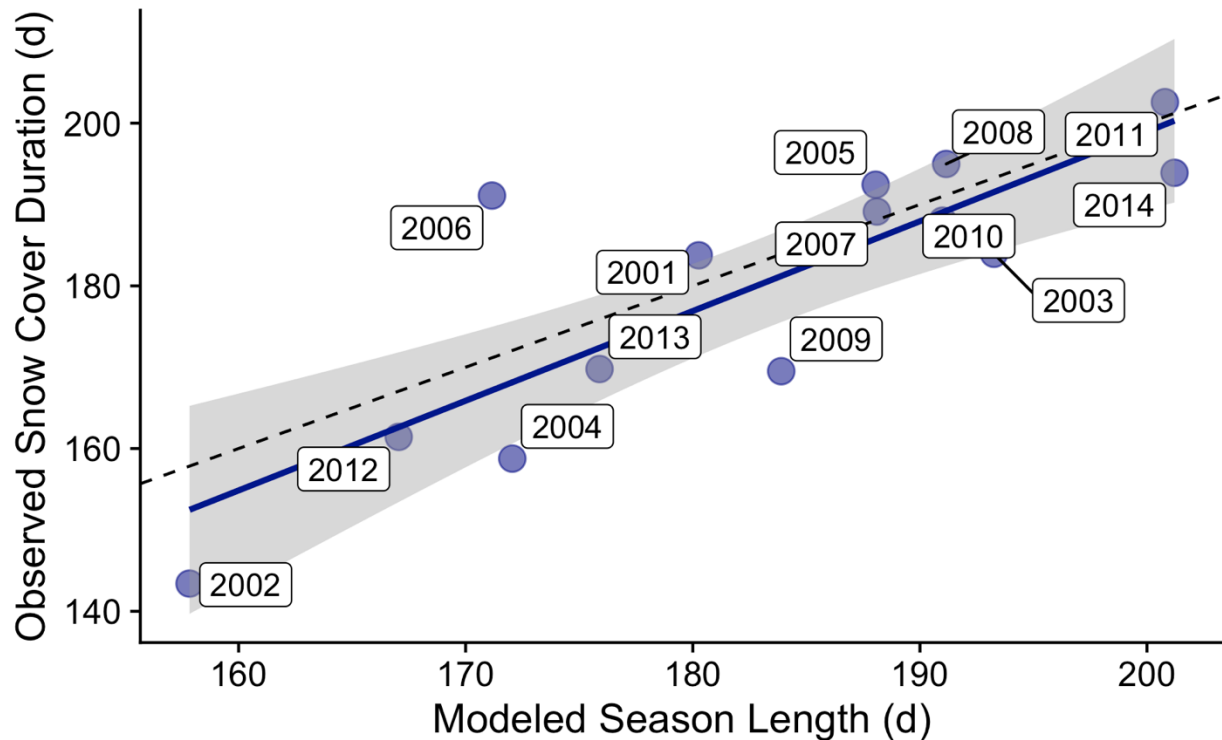


Figure 6-2. Observed MODIS-derived statewide average snow cover duration plotted against modeled statewide average season length. The solid line is the line of best fit computed by ordinary least squares regression ($r^2 = 0.70$, p -value < 0.0005) and the gray shading represents the uncertainty of the fit. The dashed line is the 1:1 line.

We next joined the optimized modeled season lengths to the observed user days from 2001–2014. Overall, this produced a similar relationship to the MODIS data, where user days decreased with shorter modeled season lengths (Figure 6-3.). We then performed a linear regression on the two variables so that we could estimate user days as a function of modeled season length for both historic and future climate scenarios:

$$UserDays_{est} = \beta + \alpha L_{SSN}$$

where $UserDays_{est}$ is estimated user days, β is the y-intercept, α is the slope of the relationship, and L_{SSN} is statewide average modeled season length (d). This relationship was slightly more sensitive than the MODIS-based relationship, with each lost snow cover day corresponding to a loss of 29,000 user days under current population conditions.

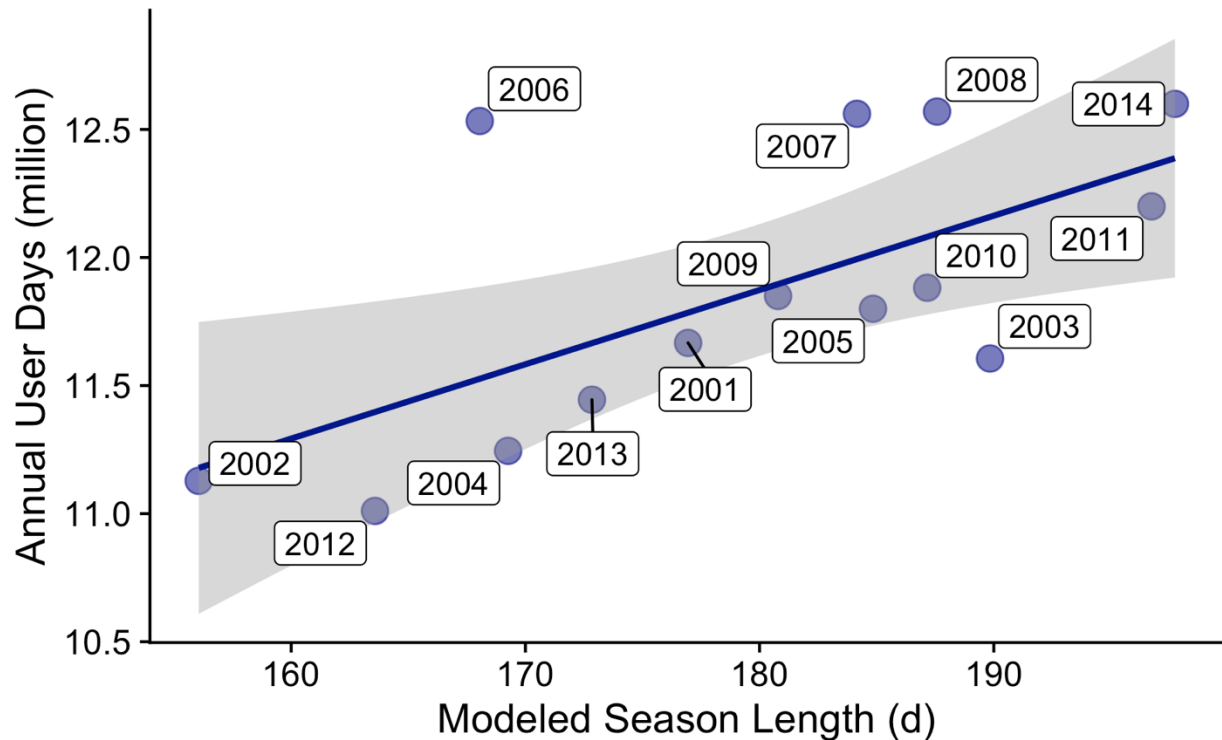


Figure 6-3. Observed annual user days plotted against modeled statewide average season length. The solid line is the line of best fit computed by ordinary least squares regression ($r^2 = 0.42$, p -value < 0.05) and the gray shading represents the uncertainty of the fit.

To note, we use season length as a proxy for snowiness. In some cases, the modeled season length is longer than the period for which the resort can operate due to lease terms with the US Forest Service. Our assumption is that as snowiness decreases in the future, skier user days will decline.

6.3.3.3 Estimating Baseline User Days and Revenue Anomalies

Once we had developed an optimized rule for season start date, we applied it to each of our resort base models. We then computed season length for each resort and year as the difference between the start and end dates, which was the date when summit SWE melted below 100 mm. We then computed a statewide average for each year to get an annual time series of season length. We next applied the linear regression model to these data to estimate annual user days as a function of statewide season length. In order to convert user days to revenue, we multiplied the estimated user days by the average daily expenditure of \$286.73 (Sect. 6.3.2.4). From this time series of revenue, we compute baseline revenue, \bar{R} , as the average annual revenue. We then calculated the annual revenue anomaly as the difference between \bar{R} and the R for each year. If the revenue anomaly were negative (i.e., R is less than the baseline), then we assumed this to be an economic damage due to below-normal snow conditions (i.e. drought).

6.3.3.4 Calculating Expected Annual Damages

We then used the time series of revenue losses to calculate an expected annual damage for drought years, which occur when modeled season length and user days are below average. Here, the expected annual damage is a function of the probability of a given revenue anomaly occurring and its magnitude in terms of lost revenue. The final expected annual damage is an integration of all such probabilities and magnitudes (Sect. 4.2).

6.3.3.5 Disaggregating to the County Level Using Lift Capacity

We then took the statewide expected annual damage value and disaggregated it to the county level based on published lift capacity. We assumed resorts with larger lift capacities would have greater annual user days, which was supported by the limited per-resort user day data from Shelesky (2016). For this step we summed the uphill lift capacity for all resorts in a given county. These values were then used to create a county-level weighting term and calculate county EAD:

$$EAD_{county} = \frac{LC_{county}}{\sum LC} EAD$$

where EAD_{county} is county-level EAD, LC_{county} is county total lift capacity, and $\sum LC$ is statewide total lift capacity.

6.3.3.6 Accounting for Climate and Population Change

After computing historic expected annual damages (i.e., current climate, current population), we followed the steps above taking both climate change and population growth into account. For climate change, we reran the base and summit resort models after adjusting the daily air temperature and precipitation by the scale factors for the Moderate and More Severe climate change scenarios. We next made new time series of $UserDays_{est}$ by plugging the Moderate and More Severe statewide modeled season lengths into the linear model created from the Baseline climate data. Once we had new $UserDays_{est}$ values, we followed the steps in Sects. 6.3.3.3–6.3.3.5 to get expected annual damages for the Moderate and More Severe scenarios. To note, \bar{R} stayed constant across the climate scenarios in order to compute the costs of climate change relative to historic conditions.

Finally, we adjusted the expected annual damages for the three future population scenarios: Low, Medium, and High Growth. We did this by updating annual user days based on the historic skiing rate of Coloradans and the number of new residents. According to Colorado Ski Country USA, 44.4% of annual resort user days are from Colorado residents (Colorado Ski Country USA, 2015). Given a lack of other data, we assumed the percentage of user days coming from Colorado residents stayed constant from year to year. This means for each ski season we can compute the rate of user days from Colorado residents per person. For example, if the estimated resident user days for a single year were equal to the baseline population, we would assume, on average, each Coloradan skis one time. We thus add to $UserDays_{est}$ a new number of skiers calculated from the skiing rate and population increase. To use the previous example,



if the rate were 1 user day per Colorado resident, we would add a number of user days equal to the projected population increase. From this new user day number, we then recompute annual revenue values. In this case, we calculate a new \bar{R} for each population scenario in order to isolate the effect of climate change on skiing revenue losses under different statewide populations. In general, this had the effect of making “good” years better and “bad” years worse relative to the recomputed baseline (i.e., total revenue goes up, but damages increase due to larger negative swings in drought years). We then rerun the steps in Sects. 6.3.3.4–6.3.3.5 to estimate EAD_{county} for the population scenarios.

6.3.4 Model Outputs

The ultimate product created by the steps outlined in this document is a per-county expected annual damage for each combination of the three climate and four population scenarios (i.e., each county has 12 unique expected annual damage values). These are the data that can be found in the interactive online visualization tool. In addition to this product is a series of intermediate model outputs listed below:

1. Spatially continuous raster maps of annual snow cover duration across Colorado (2001–2016)
2. Snow model output for all resort base and summit elevations for historic and future climatic conditions
3. Annual time series of resort and statewide season lengths (1949–2014) for historic and future climatic conditions
4. Annual time series of statewide user days (1949–2014) for historic and future climatic conditions
5. Annual time series of statewide revenue and revenue anomalies (1949–2014) for historic and future climatic conditions

6.3.5 Assumptions and Limitations

- We assume the SNOW-17 model can be used to represent future snow conditions.
- For all scenarios, we keep per-user-day expenditures constant, even though lift tickets are likely to become more expensive in the future. We also do not simulate the effects of supply and demand on future prices.
- We assume that Colorado’s transportation infrastructure and the ski resorts themselves will be able to handle population growth and increased ski visitation. This will likely require expansion on both accounts.
- We do not consider additional snow management techniques (e.g., snow harvesting) besides snowmaking. We also do not include any potential future improvements in snowmaking technology.



6.4 Drought Technical Approach: Rafting

6.4.1 Overview

Colorado's commercial rafting industry is critically dependent on river flows. During periods of hydrologic drought, below average flows truncate the rafting season, limiting visitation, and incurring economic impacts compared to higher or average flow years in the counties with access to popular river reaches. Although Colorado's commercial rafting industry is relatively small (~\$177 M statewide economic impact in 2018), it is a key part of Colorado's warm weather recreational portfolio, particularly in counties with popular river reaches (e.g. Chaffee County, home to popular stretches of the Upper Arkansas River). Moreover, the rafting industry is a quantifiable indicator of the greater private river recreation economy. For this section, our objective is to quantify the effect of drought on Colorado's commercial rafting industry.

6.4.2 Data and Inputs

Industry economic data are used to model the financial effects of historical droughts, state and federally curated streamflow data are used to assess boating conditions, and climate data are used to drive hydrologic models that predict natural flows. Below is a detailed description of the data and data products used in this study.

6.4.2.1 Industry Economic Data

Industry economic data were provided by The Colorado River Outfitters Association (CROA), who releases annual user day reports for major recreational rivers in Colorado (CROA, 2018). This dataset is assembled by documenting user day allocations from commercial outfitter permits issued by state and federal agencies. Additionally, CROA estimates statewide annual economic impact as the product of user days, user direct expenditures, and an economic multiplier accounting for secondary impacts. For example, the total number of user days reported in 2018 was 520,217 and the average user direct expenditure was \$132.65. Assuming a secondary impact multiplier of 2.56, CROA estimates the statewide economic impact of the commercial rafting industry in 2018 to be \$176.7 M (CROA, 2018). We rely on CROA data for user days and economic impact estimates.

6.4.2.2 American Whitewater Runnable Ranges

American Whitewater is a non-profit river conservation and boating advocacy organization. American Whitewater reports the range of runnable flows for many popular river segments in the US. The runnable flow range denotes the range of flows within which whitewater boating conditions are suitable. We collected data on the runnable ranges from American Whitewater's website for segments on rivers for which CROA collects and reports user day information (Appendix C—River Reach Info).

6.4.2.3 Streamflow Data

Streamflow data are used to assess historical whitewater rafting conditions. We identified all gauges in the state used by American Whitewater to assess flow conditions on the rivers for which industry economic data were available. In total, daily average streamflow archives were

obtained from 51 USGS and DWR gauges. Colorado Decision Support System's TSTool was used to access and process gauge data.

6.4.2.4 *Climate Data and Scenarios*

This analysis relies on the same Maurer et al. (2002) gridded climate data and future scalars as described in Sect. 6.1.2.1. and 2.2.2.

6.4.3 *Model Approach/Methods*

Our analytical approach is distilled into five steps. First, we analyze historical river flow and industry economic data to develop a linear model capable of estimating user days as a function of flow-based metrics. Second, we use a physically based hydrologic model to simulate historical natural flows. Third, the regression model (step 1) is used to estimate statewide user days and economic impact as a function of simulated natural flows. Here, annual damage is defined as negative economic impact anomalies relative to historical average conditions. Fourth, statewide damages are disaggregated to the county-scale using market share and river length as scaling variables. Finally, steps two through four are repeated under a variety of climate change and population growth scenarios.

6.4.3.1 *Streamflow-User Day Relationship*

We developed a linear regression model to represent the relationship between streamflow and user days. Specifically, our model computed statewide total annual user days as a function of statewide average annual boatable days. Annual boatable days is the number days in a year that flows are within American Whitewater's runnable range (Appendix C—River Reach Info). Annual boatable days were counted for every reach during all years between 1998–2018 and the statewide annual averages were calculated.

A strong relationship emerges between annual average boatable days and statewide total user days (Figure 6-4, $R^2 = 0.79$, $p\text{-value} < 0.05$). The data reveal a direct relationship, whereby user days increase with boatable days. The slope of the relationship is 2925 user days/boatable day, suggesting that the loss of a single boatable day results in a statewide loss of 2925 user days. During known drought years, such as 2012 and 2002, boatable days and user days were well below average. This relationship underpins the conceptual model of our technical approach, namely that drought years reduce the number boatable days, and thereby the number of user days.



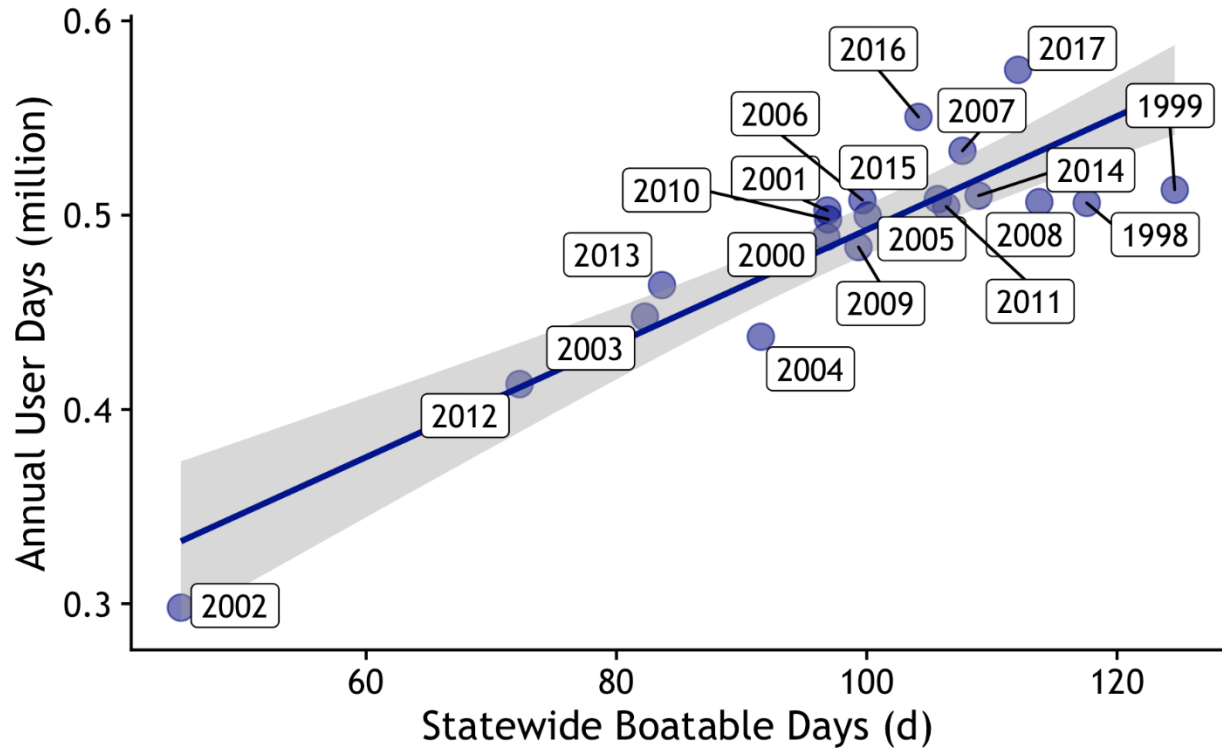


Figure 6-4. Positive linear relationship between boatable days and user days. This relationship provides insight into how drought affects the commercial rafting industry: During drought years boatable days and user days are lower than average (e.g. 2012, highlighted in red). $R^2 = 0.79$, $p\text{-value} < 0.05$

6.4.3.2 Simulating natural flows

A hydrological model simulated natural flows at each of the gauges listed in Appendix C—River Reach Info. This approach allowed us to 1) extend the duration of historical hydrologic records, and 2) project changes in streamflow timing and magnitude associated with various climate scenarios. We used the Variable Infiltration Capacity (VIC) model, which is a semi-distributed (gridded) regional-scale physical hydrology model (Liang et al., 1994). VIC is forced with a time series of meteorological variables and produces a time series of hydrologic output, including runoff, for each grid cell.

We took simulated runoff directly from the VIC models developed as parts of the CRWAS-II project (Harding, 2015). These models were developed to assess the sensitivity of natural flows to various climate scenarios. The temporal domain of the models extends from 1949 – 2014 with a daily timestep. The spatial domain of the model envelops the entire state with a $1/8^\circ$ spatial resolution.

Drawing from the CRWAS-II simulations, monthly runoff was estimated at gauges in Appendix C—River Reach Info by taking the area weighted sum of daily runoff over all model grid cells within the contributing area. To estimate daily flows, we converted monthly runoff to a volumetric flow rate and interpolated to a daily timestep. This abstraction bypasses the use of a routing model, though may obscure boatable day estimates by fewer than 10 days (the relatively short timescales of flood wave propagation).

6.4.3.3 Computing statewide expected annual damage

We estimated statewide annual average boatable days from VIC-simulated natural flows for 1949–2014, using American Whitewater runnable ranges. The regression model was used to estimate potential statewide total user days from simulated boatable days, yielding a 65-year time series of estimated user days. We transformed annual user days into annual economic impact, using CROA-reported 2018 per-user direct expenditures and secondary economic impact factor of 2.56 (Figure 6-5). It is important to note that the model is not necessarily estimating economic impact of the commercial rafting industry in historical years, such as 1949 when the industry was either very small or nonexistent. Rather, the model is estimating what the economic impact of the industry would be under today’s economic conditions, given historical flow conditions. See Section 4.4 for more discussion on this concept.

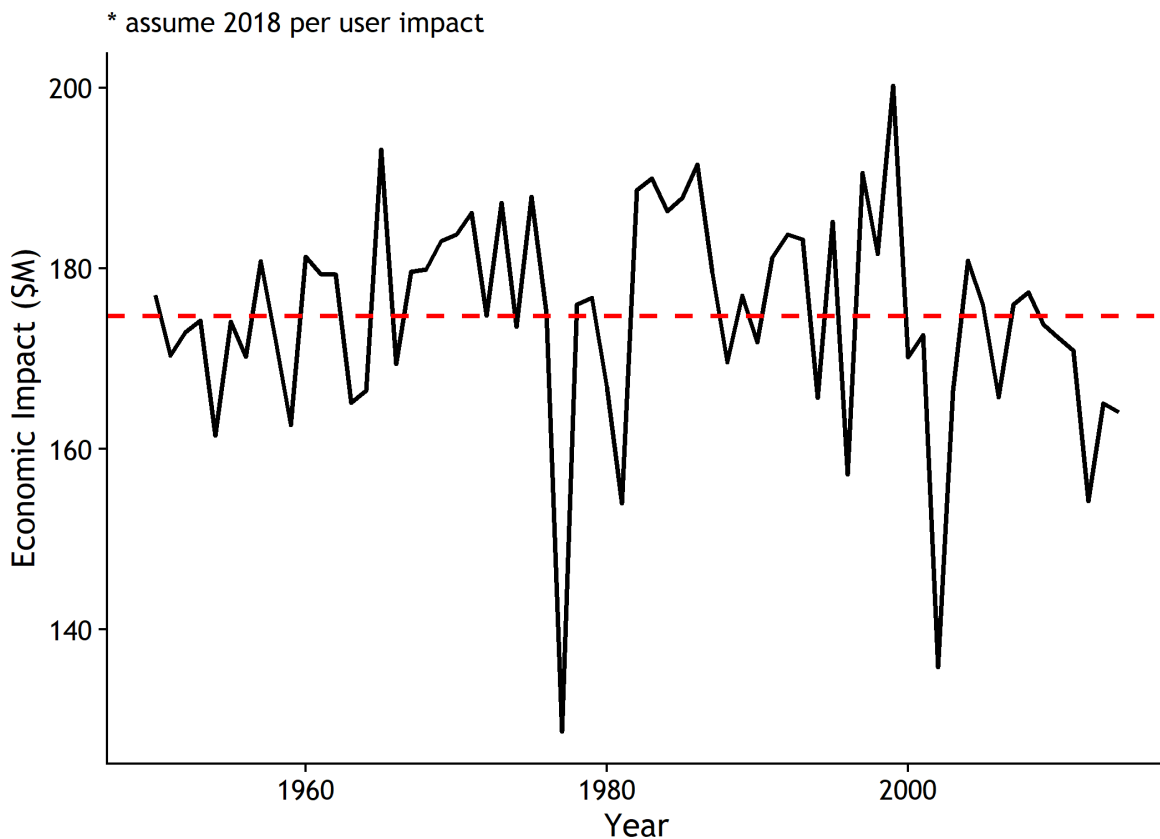


Figure 6-5. Economic impact is estimated over a 65-year period. The red dashed line indicates the 65-year average economic impact. Annual damages were quantified as negative economic impact anomalies relative to the average.

Finally, damages were quantified as negative economic impact anomalies relative to the average, similar to the method used in Sect. 6.3.3.4. In other words, years in which the black line drops below the red line in Figure 6-5 are years in which a drought-induced damage was incurred. The magnitude of the damage is equal to the difference between annual realized economic impact and the 65-year average economic impact.

Discrete annual damage estimates were synthesized in terms of expected annual damages, a function of the probability a drought occurring and its associated damage magnitude. In this context, large annual damages have a low probability of occurring and small annual damages have a higher probability of occurring. The expected annual damage is an integration of all such probabilities and magnitudes:

$$EAD_{state} = \int D dP$$

where EAD is the statewide expected annual damage, D is a vector of discrete annual damages, and P is the probability of annual damage occurrence.

6.4.3.4 *Disaggregating to the county scale*

We disaggregated statewide expected annual damages to the county level by using river market share and river length as scaling parameters:

$$EAD_{county}^j = \sum_{i=1}^n (EAD_{state} * S_i * L_i^j)$$

where EAD_{county}^j is the expected annual damage in county j , n is the number of commercial rafting rivers flowing through county j , EAD_{state} is the statewide expected annual damage, S_i is the 2018 market share of river i , and L_i is the length of river i in county j . We determined river market share, S_i , as the ratio user days for river i to statewide total user days reported by CROA (2018).

6.4.3.5 *Considering climate change and population growth scenarios.*

To account for the impact of climate change on commercial rafting risk, we repeated steps two through four above using climate adjusted meteorological data for the Moderate and More Severe 2050 climate scenarios. For population change, we applied the same approach as in the skiing analysis (Sect. 6.3.3.6) wherein we computed new user days and new baseline economic impacts for each scenario.

6.4.4 Model Outputs

The ultimate products generated by this workflow are county-level expected annual damage estimates for 12 permutations of climate and population scenarios. These results are presented in the interactive online visualization tool. In addition to this product is a series of intermediate model outputs listed below:

1. Historical annual boatable day series for all river segments listed in Appendix C—River Reach Info
2. A linear regression model relating statewide average boatable days to statewide total user days.



3. Monthly natural flow simulations (1949-2014) at all gauges listed in Table 1 for Baseline, Moderate, and More Severe climate scenarios.
4. Simulated statewide economic impact (1949 – 2014) for Baseline, Moderate, and More Severe climate scenarios.

6.4.5 Assumptions and Limitations

- We assume that the state’s commercial rafting outfitters can expand capacity to accommodate new users as the population grows.
- We did not use a hydraulic routing model to simulate the downstream propagation of simulated flows. This likely causes errors in annual boatable day estimates, though the errors should be small (fewer than 10 days), because the timescales of wave propagation are short, relative to the duration of the rafting season.
- River management is not accounted for when simulating future flows. Diversions and reservoir management can affect boating conditions for better or worse. On one hand, reservoir releases can prop up instream flows during dry years. On the other hand, reservoir management can lower instream flows.



7 Technical Approach: Wildfire

7.1 Wildfire Technical Approach: Buildings

7.1.1 Overview

The number of wildfires in Colorado more than doubled from 457 in the 1960s to 1,300 in the 1990s, doubling again from the 1990s to the 2000s (Morgan, 2019). Since 2000 Colorado has had 6 years with wildfire property damage greater than \$10 million and 3 years above \$100 million, with total statewide damages over \$1.5 billion (National Centers for Environmental Information, 2020). These tallies include insured losses from major fires, such as Missionary Ridge in 2002 (insured losses of \$17.7 million), Hayman in 2002 (\$39 million), Fourmile Canyon in 2010 (\$230 million), and Waldo Canyon in 2012 (\$460 million) (Denver Post, 2016). As a warming climate provides more favorable wildfire conditions, the wildfire season is projected to increase in duration (Abatzoglou & Williams, 2016), which may increase the risk of wildfire property damage and loss. Here we present the methods for quantifying current and future wildfire damages to buildings in Colorado using an advanced, high-resolution wildfire model.

7.1.2 Data and Inputs

Figure 7-1 shows the general workflow for this project. The first step was to retrieve all input data needed to perform the fire analysis, including digital elevation models, vegetation data (surface fuels and canopy characteristics), and historical climate data.

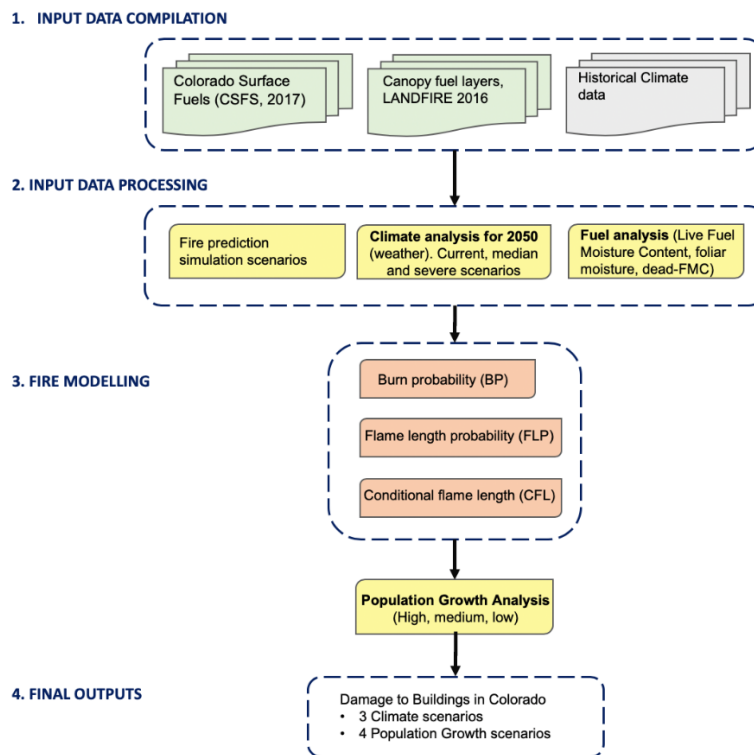


Figure 7-1: Conceptual wildfire modeling workflow.



7.1.2.1 Historical Climate Data

For the current climate scenario, we used the North American Regional Reanalysis (NARR) gridded climate product (Mesinger et al., 2006) for the period 1988–2017. NARR assimilates a wide range of observational data to produce a long-term gridded dataset of various meteorological variables. We downscaled air temperature (at 2 m), relative humidity (at 2 m), and wind speed and direction (at 10 m) from the native 32-km grid resolution to the 30 m grid resolution of the wildfire model. These data were then grouped into four categories by percentile: Extreme (97th), High (90th), Moderate (50th), and Low (25th). For more information on how weather percentiles are incorporated into the wildfire model, please see the 2017 Colorado Wildfire Risk Assessment (CO-WRA) Update for more information (Colorado State Forest Service, 2018).

7.1.2.2 Vegetation and Fuels Data

In addition to the climate data, key inputs for the wildfire model include vegetation and surface fuels datasets developed by the Colorado State Forest Service and Technosylva Inc. for the 2017 CO-WRA Update (Colorado State Forest Service, 2018). The vegetation dataset describes the land use type (developed, agriculture, shrubland, conifer, etc.), while the fuels dataset describes the characteristics of surface fuel (based on the Scott and Burgan (2005) fuel family) and canopy fuels (canopy cover, canopy height, canopy base height, and canopy bulk density).

7.1.2.3 Fuel Moisture

Fuel moisture describes the water content of vegetation as a percent of dry mass and it is seasonal in nature, increasing during the early growing season and then decreasing during late summer, fall, and winter. In this project, fuel moisture is broken out by fuel type: herbaceous, woody, and canopy foliar. Herbaceous fuels are annual or perennial and have soft, non-woody tissue (e.g., grasses). Woody fuels include deciduous trees and shrubs that annually shed their leaves as well as evergreens that maintain the majority of their foliage. Canopy foliar fuels moisture is specific to tree crowns. Fuel moisture content varies from as low as 30% to as high as 300%, where fuels that reach 30% are considered dead and have their own classification scheme (National Wildfire Coordinating Group, n.d.). To note, fuel moisture content can exceed 100% because it is the percent of water mass relative to dry mass (i.e., the mass of water can exceed dry mass during wet conditions). How fuel moisture content is related to fuel type and weather percentile is provided in Table 7-1 below.

Table 7-1. Fuel moisture content from the Colorado Wildfire Risk Assessment (Colorado State Forest Service, 2018).

Fuel Type	Fuel Moisture Content (%)			
	Extreme (97 th percentile)	High (90 th percentile)	Moderate (50 th percentile)	Low (25 th percentile)
Herbaceous	30	39	66	102
Woody	70	76	86	102
Foliar	90	90	100	110



7.1.3 Model Approach/Methods

Wildfire risk was calculated according to the methods outlined in *A Wildfire Risk Assessment Framework for Land and Resource Management* (J. H. Scott, Thompson, & Calkin, 2013), which also align with those methods used in the 2017 CO-WRA Update (Colorado State Forest Service, 2018). Fire simulations were performed with Technosylva's Wildfire Analyst™ software (WFA, Ramirez et al., 2011), which provides real-time analysis of wildfire behavior and simulates the spread of wildfires.

For the building sector, we computed wildfire risk as the product of hazard and vulnerability, where the hazard is the product of modeled burn probability and intensity, and vulnerability is determined by asset exposure and its susceptibility to fire. The burn probability and intensity (flame length) are direct outputs from the wildfire model. Asset exposure is determined using building replacement costs from the Hazus building stock inventory (Federal Emergency Management Agency, 2015), similar to our approach for flooding. The asset susceptibility was calculated using a predefined relationship between intensity (flame length) and building damage. Details on these processes are included in the sections below.

The practical implication of this wildfire risk framework is that counties with more buildings (more exposure) and a high wildfire hazard (higher probability of wildfire) will have the highest wildfire risk, as measured in dollars. Conversely, counties with fewer buildings (lower exposure) and a low wildfire hazard (lower probability of wildfire) will have lower wildfire risk in dollars. It should also be noted that counties with high wildfire hazard and lower exposure (e.g., Rio Blanco) may have similar risk (in dollars) to counties with low wildfire hazard and higher exposure (e.g., Adams).

7.1.3.1 Modeling Wildfire Hazard

To be consistent with the 2017 CO-WRA Update, we modeled wildfire hazard in WFA using meteorological, surface fuel, vegetation, land cover, and historical fire ignition datasets. One key model output is annual burn probability, calculated in WFA by performing 2.3 million Monte Carlo simulations of burn ignitions every 500 meters across Colorado, resulting in a mean ignition density of 8.68 fires/km². The final burn probability value is the number of times a grid cell ignited divided by the number of Monte Carlo simulations, weighted by the spatial distribution of historical fires in Colorado from 1992 to 2015 (Short, 2017). In this way, we take into account both the probability of ignition and potential spread of fires. Final output is a 30 m raster grid with values from 0 to 1 representing annual burn probabilities (Figure 7-2).



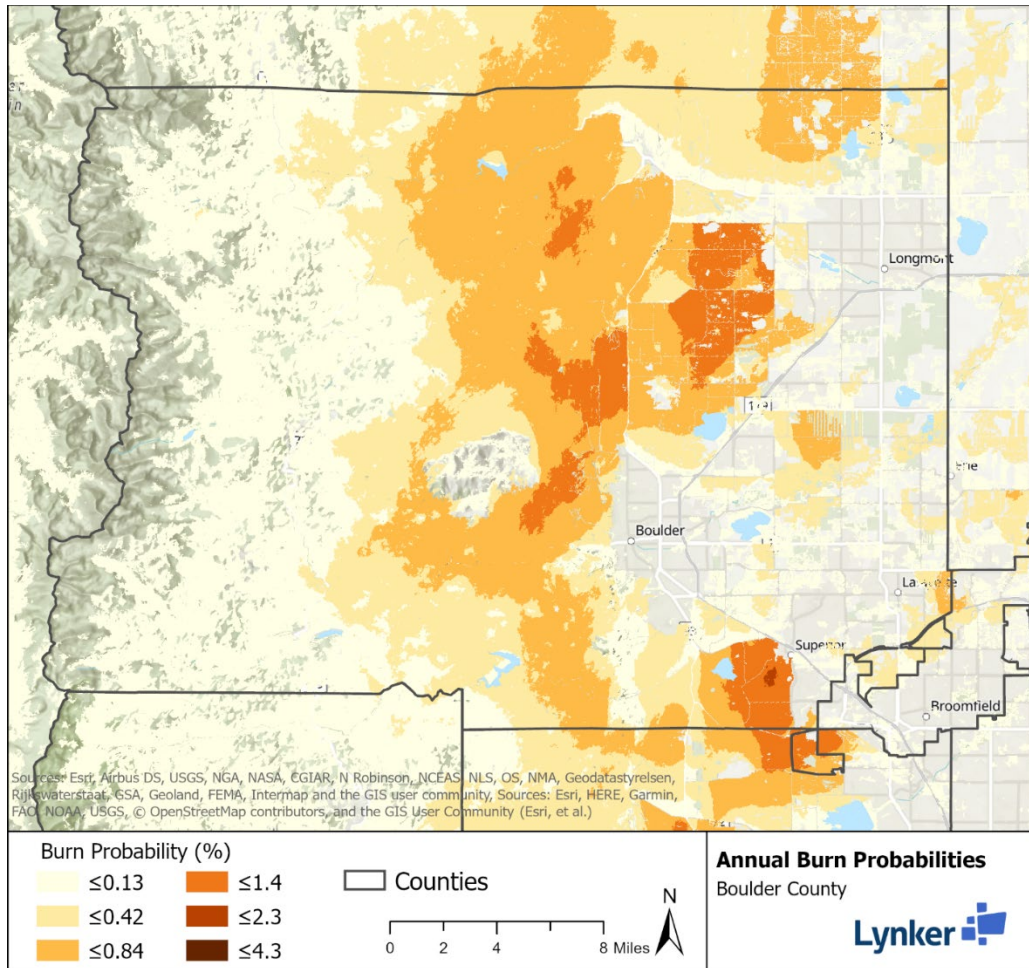


Figure 7-2. Burn probability map centered over Boulder County.

Another output from WFA is flame length, which represents wildfire intensity (severity) and is a function of fuels, weather and topography. The flame length model output is binned into six classes: 0-2 ft, 2-4 ft, 4-6 ft, 6-8 ft, 8-12 ft, and 12+ feet, each of which has its own raster. The flame length rasters express the probability of occurrence of a specific flame length class, all of which sum to 1 for each grid cell. The set of six flame length rasters for Boulder County are shown in Figure 7-3. Note that the lowest flame lengths (0-2 feet) are most probable, as represented by dark red colors, in the higher elevations below treeline and in the plains in the eastern part of the county. The highest flame lengths (12+ feet) are most probable in the montane zone, which has significant wildland urban interface development. Note that in the alpine zone (above 11,500 ft.) flame length data do not exist, indicating the model does not simulate fires in this region due to its vegetation and meteorological conditions.

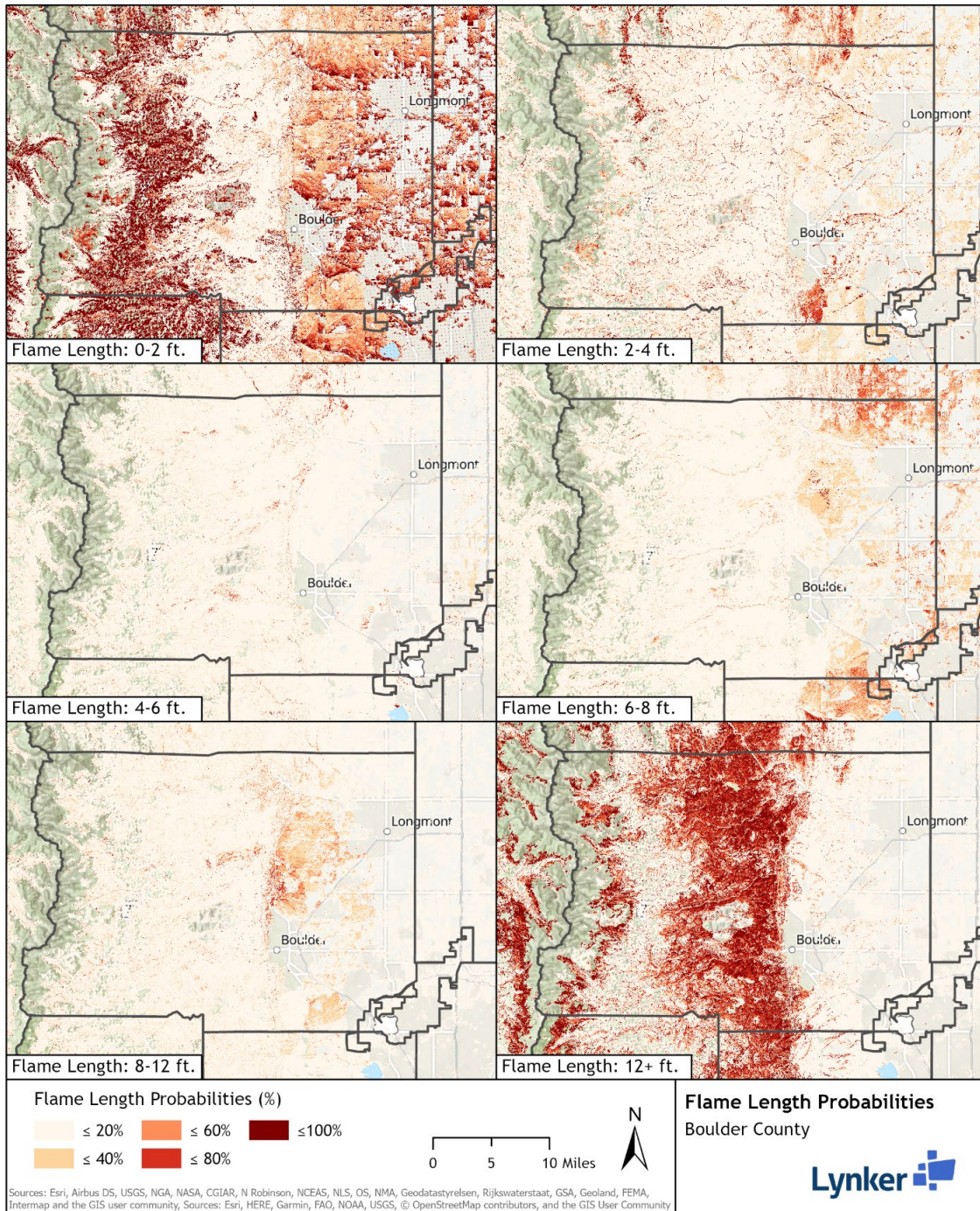


Figure 7-3. Flame length rasters for Boulder County. Flame lengths are binned into six groups (0-2 ft., 2-4 ft., 4-6 ft., 6-8 ft., 8-12 ft., 12+ ft.) and a flame length probability is assigned to each group, such that the total probability sums to 1 for every grid cell.

7.1.3.2 Computing Wildfire Vulnerability

In this project, we determined wildfire vulnerability as a function of building replacement cost and a damage response function that relates conditional flame length to a percent damage level. For building replacement cost we used the same Hazus (Federal Emergency Management Agency, 2015) and ICLUS (U.S. Environmental Protection Agency, 2017) datasets as in the

buildings sector for flooding Sect. 5.1.3.3. Example building replacement costs are displayed in Figure 7-4 below.

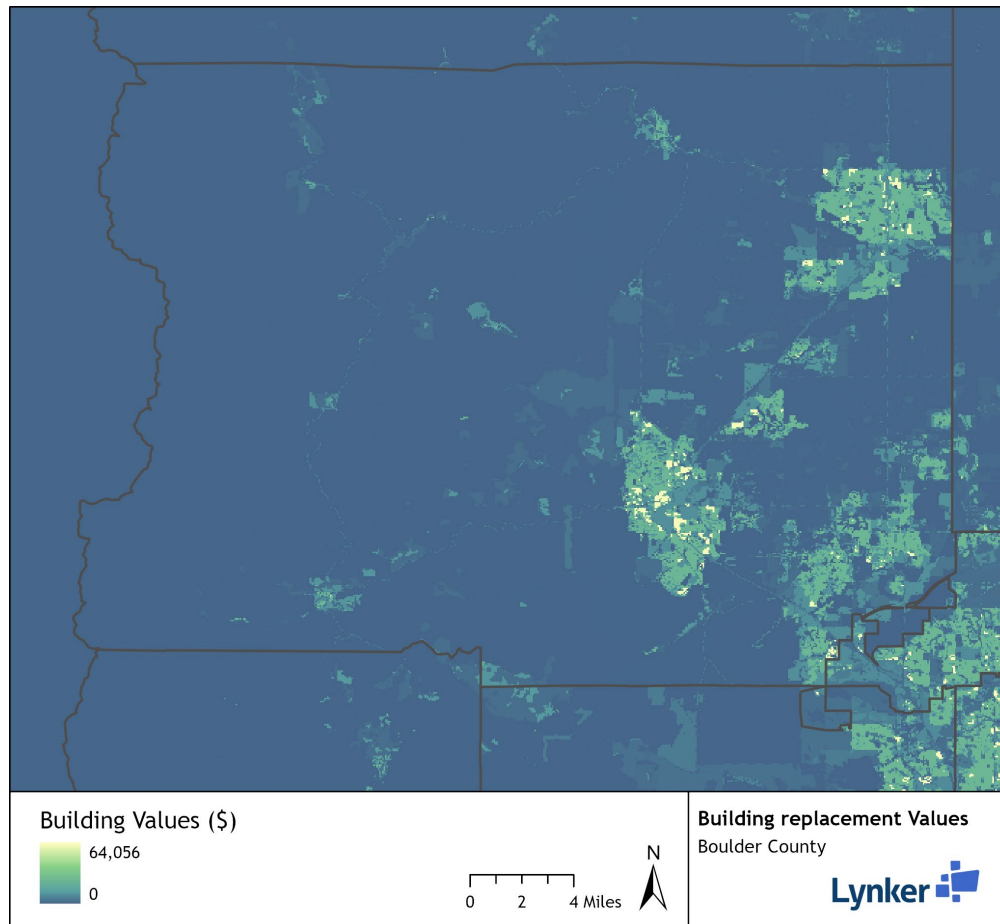


Figure 7-4: Building replacement values for Boulder County.

Our damage response function relates each flame length bin to a building damage level. Unlike the flood hazard, where there are numerous sources of depth-damage functions relating building damage to depth of flooding, there are few published wildfire damage response functions. As a result, we based our function on previous work from Alcasena et al. (2017), Scott et al. (2013), and expert opinions from multiple wildfire agencies including the Colorado State Forest Service, the Colorado Division of Fire Prevention and Control, the Colorado Springs Fire Department, Durango Fire Protection District, and Anchor Point Group, among others. The wildfire damage response function for this project is provided below in Table 7-2.

Table 7-2. Flame length damage response function. Building damage percentages correspond to the percent of the building replacement costs incurred per flame length bin, where 0% equals no cost and 100% equals total replacement cost.

Flame Length Bin	Flame Length Building Damage
0-2 ft	0%
2-4 ft	25%
4-6 ft	50%

6-8 ft	75%
8-12 ft	100%
12+ ft	100%

7.1.3.3 Calculating Wildfire Damages

Wildfire damages are conceptually represented as the intersection of wildfire hazard (burn probability and intensity) and asset vulnerability (building replacement costs) as shown in Figure 7-5, where darker orange and red colors represent greater damages. While most of the building value is in the urban core of the city (see lighter green and yellow colors in Figure 7-4), these developed areas lack the fuels necessary for wildfire, thus their hazard is zero (see gaps in the orange-shaded burn probabilities depicted in Figure 7-2). The coincidence of wildfire hazard and asset vulnerability is typically the wildland-urban interface, commonly referred to as the WUI.

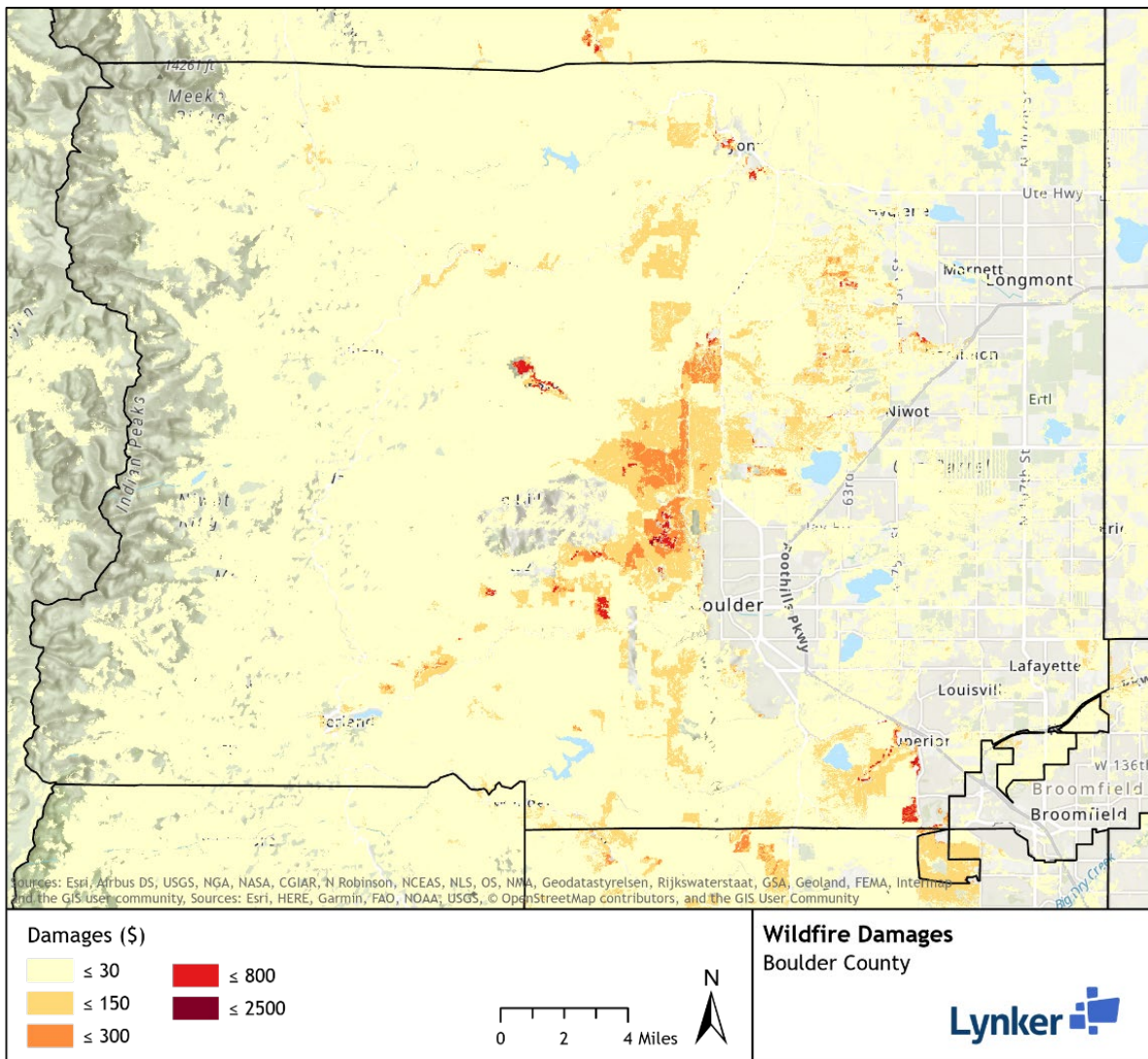


Figure 7-5. Wildfire damages for Boulder County.

For this project, we calculated wildfire damages at each grid cell as the product of wildfire hazard and vulnerability:

$$Damage = Cost * BP * \sum_{i=1}^6 FLP_i * FLBD_i$$

where *Cost* is the building replacement cost for a given grid cell, *BP* is the annual burn probability for a given grid cell, *FLP* is the flame length probability for a given grid cell (Figure 7-3) and flame length bin *i*, and *FLBD* is the flame length building damage percent (Table 7-2), per flame length bin *i*. We then aggregated the grid cell damages to the county level.

7.1.3.4 Bias-Correcting Wildfire Building Damages

To ensure our modeled damages were commensurate with observed values, we bias-corrected county-level damages. To do this, we first summed the modeled county values to the state level and compared this to the average of observed insured property losses from 2010–2019 (National Centers for Environmental Information, 2020):

$$Cost_{corr} = \frac{\overline{Cost_{obs}}}{Cost_{mod}}$$

where *Cost_{corr}* is the statewide bias-correction factor, $\overline{Cost_{obs}}$ is the 10-year average annual observed statewide building damage and *Cost_{mod}* is the annual modeled statewide building damage. We then multiplied each county’s modeled damage by *Cost_{corr}* to get a final, bias-corrected damage value.

7.1.3.5 Applying Climate Change Scenarios

To estimate future wildfire risk due to climate change, we adjusted air temperature and live fuel moisture content (LFMC) in WFA based on output from the previously developed Moderate and More Severe climate scenarios (2.2.2). Further details on the changes made to both variables are described below.

First, we developed monthly air temperature offsets, which we calculated as the difference between future projections (2035–2064) and simulated historical conditions (1988–2017). One key difference between wildfire and drought in this project and between wildfire and the CRWAS-II project is the historical period of record. Drought and CRWAS-II used a 30-year window from 1970–1999, while the wildfire model used a 30-year window from 1988–2017. The air temperature offsets for the two climate change scenarios are provided below in Table 7-3.

Table 7-3 Monthly air temperature offsets used in the wildfire future climate scenarios.

Month	Air Temperature Offset (°C)	
	Moderate	More Severe
January	0.90	1.34



February	1.08	1.42
March	1.23	1.49
April	1.26	1.53
May	1.59	1.96
June	1.54	1.92
July	1.47	2.00
August	1.91	2.04
September	1.72	1.93
October	1.85	1.61
November	1.46	1.48
December	1.42	1.17

Next, we adjusted future LFMC values by developing a relationship between the Standardized Precipitation Evapotranspiration Index (SPEI) and observed LFMC. SPEI, a drought indicator that combines air temperature, precipitation, and evapotranspiration, was computed using the “SPEI” R Package (Beguería & Vicente-Serrano, 2017). We calculated SPEI from 1949–2014 at a 1/8° spatial resolution for the entire state of Colorado using the Maurer et al. (2002) dataset we used in the drought sectors. To get monthly evapotranspiration estimates, we ran the Variable Infiltration Capacity (VIC) macroscale hydrologic model (Liang et al., 1994) with the Maurer et al. (2002) data. Monthly potential evapotranspiration was calculated with the Penman-Monteith routine embedded in the VIC model. Because SPEI is a relative index describing departures in the water balance from “normal” conditions, a 65-year spin up period was used to orient the algorithm to “normal” conditions.

Once we had a historic time series of SPEI, we related the drought indicator to measurements of LFMC taken across the state. Here, we used a 12-month SPEI smoothing window, which we found to correlate well with woody and canopy foliar LFMC measurements from the National Fuel Moisture Database. We took this relationship and applied it to the climate change scenarios in order to perturb future LFMC values as described in the next paragraph.

For this, we first computed SPEI for the two climate change scenarios by rerunning the SPEI algorithm with updated air temperature and precipitation from the Maurer et al. (2002) dataset and evapotranspiration from VIC. We then used the new SPEI time series to estimate future LFMC. We found an average decrease in LFMC by 12.4% for the Moderate climate scenario and 21% for the More Severe scenario. We then reran WFA using the modified air temperature and adjusted LFMC.

7.1.3.6 Applying Population Change Scenarios

We used ICLUS (Sects. 3.3.1 and 3.3.4) in two ways to evaluate the effect of population growth on wildfire risk. First, we masked out new areas of land that changed from undeveloped (grassland, for instance) to developed. This was consistent with the methods used in CO-WRA, where the developed urban core of cities and towns was excluded from the risk analysis because annual burn probabilities in these areas were set to 0. Second, we used ICLUS to project future building replacement costs in 2050 by applying the approach outlined in 3.3.1.

Additionally, the fuels dataset was not explicitly modeled to project the progression of fuels for 2050 conditions (e.g., a possible future transition from grass to shrub).

7.1.4 Model Outputs

The model outputs created by the wildfire buildings damage analysis are as follows for each current and future climate and population scenario:

1. 1 burn probability raster
2. 1 set of 6 flame length probability rasters
3. 1 wildfire hazard raster
4. 1 wildfire building damage raster in dollars

7.1.5 Assumptions and Limitations

- We have assumed a damage response function relating flame length to building damage using professional judgement from Colorado wildfire experts.
- We have assumed significant change under future climate change through air temperature and LFMC. There is high certainty in the scientific community regarding future increases in air temperature. Future changes in LFMC is less studied as it is a derivative data product; however fuel moisture content is expected to decrease due to future climate change (Liu, 2017). Other researchers note that adjusting fuel drying is likely the best way to forecast future climate change effects on wildfire (Macias Fauria, Michaletz, & Johnson, 2011).
- Building replacement values are based on the Hazus 2.2 dataset, which uses 2010 census data. This dataset has been attributed to a 10-meter gridded data product for this project; however, its native resolution is the census block.
- The damages for future population scenarios are dependent upon the underlying modeling decisions made in the development of the EPA ICLUS dataset.
- This method assumes that all buildings (all building values) are impacted equally within the 10-meter grid (i.e., a 2-4 ft flame length damages all buildings within the cell by 25%).



7.2 Wildfire Technical Approach: Suppression Costs

7.2.1 Overview

In addition to exacting a large toll on buildings and livelihoods in the wildland urban interface, wildfires require significant financial resources to suppress. At the federal level, recent years have seen total suppression costs balloon over \$2 billion (National Interagency Fire Center, 2019) as wildfires increase in frequency and severity (Abatzoglou & Williams, 2016). In Colorado, state suppression costs have exceeded \$40 million during the worst fire years of the past decade (Colorado Division of Fire Prevention and Control, 2018). Previous research indicates that suppression costs scale with fire size as well as the number of buildings within and near the fire perimeter (Gude, Jones, Rasker, & Greenwood, 2013). Therefore, future wildfire suppression costs may rise in Colorado as the climate warms and the wildland urban interface expands. In this document we describe how we used observed and modeled data to quantify the cost of wildfire suppression under historic and future climatic conditions.

7.2.2 Data and Inputs

7.2.2.1 *Observed Wildfire Perimeters*

The Geospatial Multi-Agency Coordination (GeoMAC) program produces maps of wildfire burn perimeters from 2000–present (GeoMAC, 2019). The perimeter shapefile includes such information as wildfire name, unique ID, year, burn area, and other parameters.

7.2.2.2 *Wildfire Suppression Costs*

We accessed Colorado wildfire suppression costs from a variety of sources. These are detailed in Appendix D—Historic Colorado Wildfire Suppression Costs. Additionally, the Colorado Division of Fire Prevention and Control has published the state’s total direct wildfire suppression costs from 2010–2018 (Colorado Division of Fire Prevention and Control, 2018).

7.2.2.3 *Wildfire Burn Probability Maps*

We used the Technosylva burn probability maps for historic and future climate as detailed in Sect. 7.1.3.1.

7.2.2.4 *Building Footprints and Land Use*

We converted the Microsoft building footprint database (Sect. 5.1.2.3) to points to tally the number of buildings within and near wildfire perimeters. In order to estimate future changes to the number of buildings in Colorado, we used the ICLUS dataset described in Sect. 5.1.2.5.

7.2.2.5 *Climate Data and Scenarios*

This section uses the same climate data and scenarios as described in Sects. 2.2.2 and 7.1.3.5).

7.2.3 Model Approach/Methods



7.2.3.1 Relating Historic Fire Size and Building Counts to Total Suppression Cost

We associated each wildfire in our suppression cost database (Appendix D—Historic Colorado Wildfire Suppression Costs) to a matching GeoMAC wildfire perimeter based on the fire name, year, and location. We then created a 6 mi. buffer around each fire and computed the number of buildings within the original fire perimeter and the buffer zone. Next, we created a multiple linear regression model to estimate suppression cost as a function of wildfire size and number of buildings within the buffered perimeter:

$$Cost_{est} = \alpha_1 A_{fire} + \alpha_2 n_{buildings}$$

where $Cost_{est}$ is the estimated suppression cost, α_1 and α_2 are the regression slopes, A_{fire} is the area of the fire, and $n_{buildings}$ is the number of buildings within the buffered perimeter. The regression y-intercept was forced to 0. This model explained 69% of the variance in suppression costs, with a p-value < 0.0005. The model estimated an increase of \$87,000 in suppression costs for every extra 1 km² burned and \$110 for every extra building within the buffered perimeter (Figure 7-6.).

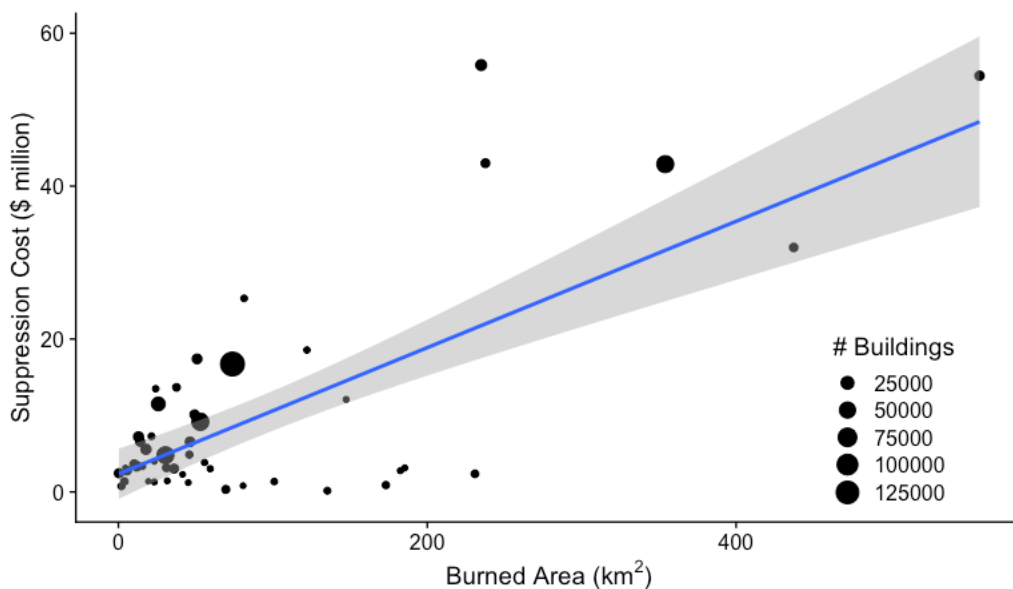


Figure 7-6. Suppression cost (in millions of dollars) plotted against burned area for major Colorado wildfires. Point size represents the number of buildings within the buffered perimeter and the blue line is a linear regression fit to the data.

7.2.3.2 Computing Suppression Costs

We then computed suppression costs using the Technosylva baseline burn probability raster (Sect. 7.1.3.1), building footprint data, and the multiple linear regression model described in Sect. 7.2.3.1 above. We first aggregated the burn probability data from its native 98.4 ft. (30 m) grid spacing to 6 mi. (9.7 km) to match the resolution of the buffer to assess threatened buildings. Next, we calculated the area burned per grid cell as the burn probability times grid cell area. We then ran the multiple linear regression model using the area burned and building

count within the grid cell for all those with a baseline burn probability greater than 0.2%, which was done to eliminate urban and alpine areas with negligible burn probabilities.

7.2.3.3 *Bias-Correcting and Aggregating Suppression Costs to the County Level*

We next aggregated all grid cell values to the county level to get an annual estimated suppression cost for each county in Colorado. However, the multiple linear regression model was built with suppression costs figures that included both state and federal responsibility. This meant modeled suppression costs were higher than what the state costs would be in an average year, which necessitated a bias-correction protocol. To do this, we multiplied each county-level estimated suppression cost value by a bias-correction term computed from observed statewide suppression costs and statewide total modeled costs:

$$Cost_{corr} = Cost_{est} \frac{\overline{Cost_{obs}}}{\sum Cost_{est}}$$

where $Cost_{corr}$ is the bias-corrected county-level suppression cost, $Cost_{est}$ is the county-level estimated suppression cost, $\overline{Cost_{obs}}$ is the average annual observed statewide suppression cost and $\sum Cost_{est}$ is the sum of all county-level estimated suppression costs.

7.2.3.4 *Accounting for Climate and Population Change*

To account for the effect of increasing wildfire frequency due to climate change, we used the approach outlined in Sect. 7.1.3.5 for the Moderate and More Severe climate scenarios. In this case, we used the burn probability rasters for the two new climate scenarios and repeated the steps in Sects. 7.2.3.2 and 7.2.3.3. The only modification is we used the same bias-correction term as computed in the baseline.

For the population scenarios, we modified the number of buildings per aggregated burn probability grid cell by tracking the change in ICLUS-reported land use. For each ICLUS category, we computed the average number of buildings per grid cell type from the baseline ICLUS raster and the building footprint dataset. We then tracked the change in each cell from the baseline to the new population scenario and added buildings where necessary as development continued in the wildland urban interface. We then reran the steps in Sects. 7.2.3.2 and 7.2.3.3 with Baseline, Moderate, and More Severe burn probability rasters for each population scenario. As stated in the paragraph above, we did not change the bias-correction term.

7.2.4 *Model Outputs*

The ultimate product created by the steps outlined in this document is a per-county wildfire suppression cost for each combination of the three climate and four population scenarios (i.e., each county has 12 unique values). These are the data that can be found in the interactive online visualization tool. In addition to this product is a series of intermediate model outputs listed below:



1. Table of historic total suppression costs and related GeoMAC data for major wildfires from 2000–2018
2. Gridded maps of annual suppression costs for each combination of the climate and population scenarios

7.2.5 Assumptions and Limitations

- The modeled burn probability and observed suppression costs cover two different time periods. We use the latter to bias-correct suppression costs estimated from the former.
- ICLUS-derived changes in the number of buildings per county may not represent the proper locations and intensity of future development due to population growth. We additionally do not account for any adaptation measures that can improve the fire safety of buildings and development.



8 References

- Abatzoglou, J. T., & Williams, A. P. (2016). Impact of anthropogenic climate change on wildfire across western US forests. *Proceedings of the National Academy of Sciences of the United States of America*, 113(42), 11770–11775. <https://doi.org/10.1073/pnas.1607171113>
- Alcasena, F. J., Salis, M., Ager, A. A., Castell, R., & Vega-García, C. (2017). Assessing wildland fire risk transmission to communities in northern Spain. *Forests*, 8(2), 30. <https://doi.org/10.3390/f8020030>
- Anderson, E. (2006). *Snow Accumulation and Ablation Model - SNOW-17*.
- Awuku-Budu, C., & Franks, C. (2019). *Outdoor Recreation Satellite Account, U.S. and Prototype for States, 2017*. Retrieved from https://www.bea.gov/system/files/2019-09/orsa0919_1.pdf
- Beguéría, S., & Vicente-Serrano, S. M. (2017). SPEI: Calculation of the Standardised Precipitation-Evapotranspiration Index. R package version 1.7. Retrieved from <https://cran.r-project.org/package=SPEI>
- BLS. (2020). *Historical Consumer Price Index for All Urban Consumers (CPI-U): U.S. city average, all items, by month*. Washington, D.C.
- Brown, J., & Blevins, J. (2018). Wildfires in Colorado cost \$130 million in 2018. Here are the details, down to the \$40 daily rate on portable toilets. – The Colorado Sun. Retrieved March 31, 2020, from The Colorado Sun website: <https://coloradosun.com/2018/11/01/wildfire-costs-colorado-2018/>
- Burakowski, E., & Magnusson, M. (2012). *Climate impacts on the winter tourism economy in the United States*. Retrieved from <https://scholars.unh.edu/cgi/viewcontent.cgi?article=1020&context=sustainability>
- Bureau of Reclamation. (2013). *Downscaled CMIP3 and CMIP5 Climate Projections, Release of Downscaled CMIP5 Climate Projections, Comparison with Preceding Information, and Summary of User Needs*. Denver, CO.
- Colorado Department of Transportation. (2019). *2013 Bridge Costs*.
- Colorado Division of Fire Prevention and Control. (2013). *Preliminary Report on the 2012 Wildfire Season*. Lakewood, CO.
- Colorado Division of Fire Prevention and Control. (2018). *Strategic Plan for Supporting Colorado's Fire Agencies*. Lakewood, CO.
- Colorado Parks and Wildlife. (2018). *2019 Statewide Comprehensive Outdoor Recreation Plan*.
- Colorado Ski Country USA. (2015). Economic Study Reveals Ski Industry's \$4.8 Billion Annual Impact to Colorado - Colorado Ski Country USA. Retrieved November 11, 2019, from https://www.coloradoski.com/media_manager/mm_collections/view/183
- Colorado State Forest Service. (2018). *2017 Colorado Wildfire Risk Assessment Update*. La Jolla, CA.
- Countryman, A. M., Paarlberg, P. L., & Lee, J. G. (2016). Dynamic effects of drought on the U.S. beef supply chain. *Agricultural and Resource Economics Review*, 45(3), 459–484. <https://doi.org/10.1017/age.2016.4>
- CROA. (2018). *Commercial River Use in the State of Colorado: 1988 - 2018*.
- Crout, Y., & Millo, G. (2008). Panel data econometrics in R: The plm package. *Journal of Statistical Software*, 27(2), 1–43. <https://doi.org/10.18637/jss.v027.i02>



- CWCB. (2013). *Flood Hazard Mitigation Plan for Colorado*.
- CWCB. (2019a). Current and 2050 Planning Scenario Agricultural Diversion Demand. In *Analysis and Technical Update to the Colorado Water Plan*. Denver, Colorado.
- CWCB. (2019b). Temperature Offsets and Precipitation Change Factors Implicit in the CRWAS-II Planning Scenarios. *Analysis and Technical Update to the Colorado Water Plan*, 2(14), 1–10.
- CWCB. (2019c). Updated Population Projections for Water Plan Scenarios. *Analysis and Technical Update to the Colorado Water Plan*, 2(2), 1–15.
- Denver Post. (2016). Colorado's largest wildfires (burn area). Retrieved March 31, 2020, from The Denver Post website: <https://www.denverpost.com/2012/06/25/colorados-largest-wildfires-burn-area/>
- Duan, Y. (1993). *Shuffled Complex Evolution Approach for Effective and Efficient Global Minimization*. 76(3).
- Etchevers, P., Martin, E., Brown, R., Fierz, C., Lejeune, Y., Bazile, E., ... Yang, Z. L. (2004). Validation of the energy budget of an alpine snowpack simulated by several snow models (SnowMIP project). *Annals of Glaciology*, 38, 150–158. <https://doi.org/10.3189/172756404781814825>
- Federal Emergency Management Agency. (2015). *Hazus 2.2*. Retrieved from <https://www.fema.gov/hazus>
- Federal Highway Administration. (2019). National Bridge Inventory.
- GeoMAC. (2019). *Historic Wildland Fire Perimeters - 2000-2019*. Denver, CO.
- Gochis, D., Schumacher, R., Friedrich, K., Doesken, N., Kelsch, M., Sun, J., ... Brown, B. (2015). The Great Colorado Flood of September 2013. *Bulletin of the American Meteorological Society*, 96(9), 1461–1487. <https://doi.org/10.1175/BAMS-D-13-00241.1>
- Gonzalez, P., Garfin, G. M., Breshears, D. D., Brooks, K. M., Brown, H. E., Elias, E. H., ... Udal, B. H. (2018). Fourth National Climate Assessment: Southwest. In *Impacts, Risks, and Adaptation in the United States: Fourth National Climate Assessment*. <https://doi.org/10.7930/NCA4.2018.CH25>
- Gorelick, N., Hancher, M., Dixon, M., Ilyushchenko, S., Thau, D., & Moore, R. (2017). Google Earth Engine: Planetary-scale geospatial analysis for everyone. *Remote Sensing of Environment*, 202, 18–27. <https://doi.org/10.1016/j.rse.2017.06.031>
- Gude, P. H., Jones, K., Rasker, R., & Greenwood, M. C. (2013). Evidence for the effect of homes on wildfire suppression costs. *International Journal of Wildland Fire*, 22(4), 537. <https://doi.org/10.1071/WF11095>
- Hagenstad, M., Burakowski, E., & Hill, R. (2018). *Economic Contributions of Winter Sports in a Changing Climate*. Retrieved from <https://scholars.unh.edu/ersc/191>
- Hall, J., Seay, W., & Baker, S. (2009). *Nutrition and Feeding of the Cow-Calf Herd: Essential Nutrients, Feed Classification, and Nutrient Content of Feeds*. Blacksburg, VA.
- Harding, B. (2015). *Technical Memorandum: CRWAS Phas II Climate, Task 1, Approach for constructing climate scenarios*. Boulder, Colorado USA.
- Hock, R. (2003). *Temperature index melt modelling in mountain areas*. 282, 104–115. [https://doi.org/10.1016/S0022-1694\(03\)00257-9](https://doi.org/10.1016/S0022-1694(03)00257-9)
- Jeavons, D., & Verdone, M. (2019). *Analysis and Technical Update to the Colorado Water Plan: Updated Population Projections for Water Plan Scenarios*. Denver, Colorado.



- Liang, X., Lettenmaier, D. P., Wood, E. F., & Burges, S. J. (1994). A simple hydrologically based model of land surface water and energy fluxes for general circulation models. *Journal of Geophysical Research*, 99(D7), 14415. <https://doi.org/10.1029/94JD00483>
- Liu, Y. (2017). Responses of dead forest fuel moisture to climate change. *Ecohydrology*, 10(2), 1–10. <https://doi.org/10.1002/eco.1760>
- Longwoods International. (2019). *Colorado Travel Year 2018 Final Report*. Retrieved from https://industry.colorado.com/sites/default/files/Colorado2018finalreport_online.pdf
- Macias Fauria, M., Michaletz, S. T., & Johnson, E. A. (2011). Predicting climate change effects on wildfires requires linking processes across scales. *Wiley Interdisciplinary Reviews: Climate Change*, 2(1), 99–112. <https://doi.org/10.1002/wcc.92>
- Mahoney, K., Lukas, J., & Mueller, M. (2018). *Colorado-New Mexico Regional Extreme Precipitation Study, volume VI Considering Climate Change in the Estimation of Extreme Precipitation for Dam Safety*. Denver, CO.
- Maurer, E. P., Wood, A. W., Adam, J. C., Lettenmaier, D. P., & Nijssen, B. (2002). A Long-Term Hydrologically Based Dataset of Land Surface Fluxes and States for the Conterminous United States*. *Journal of Climate*, 15(22), 3237–3251. [https://doi.org/10.1175/1520-0442\(2002\)015<3237:ALTHBD>2.0.CO;2](https://doi.org/10.1175/1520-0442(2002)015<3237:ALTHBD>2.0.CO;2)
- Meehl, G. A., Covey, C., Delworth, T., Latif, M., McAvaney, B., Mitchell, J. F. B., ... Taylor, K. E. (2007). THE WCRP CMIP3 Multimodel Dataset: A New Era in Climate Change Research. *Bulletin of the American Meteorological Society*, 88(9), 1383–1394. <https://doi.org/10.1175/BAMS-88-9-1383>
- Mesinger, F., DiMego, G., Kalnay, E., Mitchell, K., Shafran, P. C., Ebisuzaki, W., ... Shi, W. (2006). North American regional reanalysis. *Bulletin of the American Meteorological Society*, 87(3), 343–360. <https://doi.org/10.1175/BAMS-87-3-343>
- Microsoft. (2018). *US Building Footprints*. Retrieved from <https://github.com/Microsoft/USBuildingFootprints>
- Mitchell, K. (2018). Updated for 2018: 20 largest wildfires in Colorado history by acreage burned – The Denver Post. Retrieved March 31, 2020, from The Denver Post website: <https://www.denverpost.com/2018/07/04/20-largest-wildfires-in-colorado-history-in-acreage-burned/>
- Morgan, M. (2019). *Memorandum on 2019 Wildfire Preparedness Plan*.
- National Interagency Fire Center. (2019). *Federal Firefighting Costs (Suppression Only)*.
- National Park Service. (2013). *Fern Lake Fire*. Estes Park, CO.
- National Wildfire Coordinating Group. (n.d.). Live Fuel Moisture Content. Retrieved April 17, 2020, from <https://www.nwccg.gov/publications/pms437/fuel-moisture/live-fuel-moisture-content>
- NOAA National Centers for Environmental Information. (2020). Storm Events Database - Wildfire in Colorado. Retrieved April 15, 2020, from https://www.ncdc.noaa.gov/stormevents/listevents.jsp?eventType=%2828%29+Wildfire&beginDate_mm=01&beginDate_dd=01&beginDate_yyyy=2000&endDate_mm=10&endDate_dd=31&endDate_yyyy=2019&county=ALL&hailfilter=0.00&tornfilter=0&windfilter=000&sort=DT&submitButton=S
- OpenStreetMap Contributors. (2019). OpenStreetMap.
- Outdoor Industry Association. (2017). *The Economic Contributions of Outdoor Recreation*:



- Technical Report on Study Scope, Methods, and Procedures*. Retrieved from <http://oia.outdoorindustry.org/oretech>
- R Core Team. (2019). *R: A Language and Environment for Statistical Computing*. Vienna, Austria.
- Ramirez, J., Monedero, S., & Buckley, D. (2011). New approaches in fire simulations analysis with Wildfire Analyst. *The 5th International Wildland Fire Conference*. Sun City, South Africa.
- Reclamation. (2014). *Downscaled CMIP3 and CMIP5 Climate and Hydrology Projections: Release of Hydrology Projections, Comparison with preceding Information, and Summary of User Needs*. Denver, CO.
- Rojas-Downing, M. M., Nejadhashemi, A. P., Harrigan, T., & Woznicki, S. A. (2017). Climate change and livestock: Impacts, adaptation, and mitigation. *Climate Risk Management*, Vol. 16, pp. 145–163. <https://doi.org/10.1016/j.crm.2017.02.001>
- Romeo, J. (2019). Federal government sues Durango train for starting 416 Fire. Retrieved March 31, 2020, from The Durango Herald website: <https://durangoherald.com/articles/283967>
- Rutter, N., Essery, R., Pomeroy, J., Altimir, N., Andreadis, K., Baker, I., ... Yamazaki, T. (2009). Evaluation of forest snow processes models (SnowMIP2). *Journal of Geophysical Research Atmospheres*, 114(6). <https://doi.org/10.1029/2008JD011063>
- Scott, D., & McBoyle, G. (2007). Climate change adaptation in the ski industry. *Mitigation and Adaptation Strategies for Global Change*, 12(8), 1411–1431. <https://doi.org/10.1007/s11027-006-9071-4>
- Scott, D., McBoyle, G., Minogue, A., & Mills, B. (2006). Climate change and the sustainability of ski-based tourism in eastern North America: A reassessment. *Journal of Sustainable Tourism*, 14(4), 376–398. <https://doi.org/10.2167/jost550.0>
- Scott, J. H., & Burgan, R. E. (2005). *Standard Fire Behavior Fuel Models: A Comprehensive Set for Use with Rothermel's Surface Fire Spread Model*. Retrieved from <http://www.fs.fed.us/rm/publications>
- Scott, J. H., Thompson, M. P., & Calkin, D. E. (2013). *A Wildfire Risk Assessment Framework for Land and Resource Management*. Retrieved from <http://www.fs.fed.us/rmrs>
- Shelesky, S. (2016). *Examining the Economic Impacts of Climate Change on Colorado Ski Communities Through 2050*. Retrieved from https://scholar.colorado.edu/honr_theses/1103/
- Short, K. C. (2017). *Spatial wildfire occurrence data for the United States, 1992-2015 [FPA_FOD_20170508]. 4th Edition*. <https://doi.org/10.2737/RDS-2013-0009.4>
- Sproles, E. A., Crumley, R. L., Nolin, A. W., Mar, E., & Moreno, J. I. L. (2018). SnowCloudHydro—A New Framework for Forecasting Streamflow in Snowy, Data-Scarce Regions. *Remote Sensing*, 10(8), 1276. <https://doi.org/10.3390/rs10081276>
- Steiger, R., Scott, D., Abegg, B., Pons, M., & Aall, C. (2019). A critical review of climate change risk for ski tourism. *Current Issues in Tourism*, 22(11), 1343–1379. <https://doi.org/10.1080/13683500.2017.1410110>
- Taylor, K. E., Stouffer, R. J., & Meehl, G. A. (2012). An Overview of CMIP5 and the Experiment Design. *Bulletin of the American Meteorological Society*, 93(4), 485–498. <https://doi.org/10.1175/BAMS-D-11-00094.1>
- Thoma, D. P., Bailey, D. W., Long, D. S., Nielsen, G. A., Henry, M. P., Breneman, M. C., & Montagne, C. (2002). Short-term monitoring of rangeland forage conditions with AVHRR



- imagery. *Journal of Range Management*, 55(4), 383–389.
<https://doi.org/10.2307/4003475>
- U.S. Department of Agriculture. (2019). *U.S. and State-Level Farm Income and Wealth Statistics*.
- U.S. Department of Agriculture. (2020). *National Agricultural Statistics Service*. Retrieved from <https://www.nass.usda.gov/>
- U.S. Environmental Protection Agency. (2017). *Updates to the Demographic and Spatial Allocation Models to Produce Integrated Climate and Land Use Scenarios (ICLUS) Version 2*. Washington, DC.
- United States Geological Survey. (2019). National Hydrography Dataset. Retrieved December 15, 2019, from <https://www.usgs.gov/core-science-systems/ngp/national-hydrography/access-national-hydrography-products>
- US Forest Service. (2009). Colorado Ski Permitted and Allocated Area Boundaries. Retrieved October 29, 2019, from https://fs.usda.gov/Internet/FSE_DOCUMENTS/stelprdb5145323.zip
- Wehner, M. F., Arnold, J. R., Knutson, T., Kunkel, K. E., & LeGrande, A. N. (2017). Ch. 8: Droughts, Floods, and Wildfires. Climate Science Special Report: Fourth National Climate Assessment, Volume I. *Climate Science Special Report: Fourth National Climate Assessment, Volume I*, 231–256. <https://doi.org/10.7930/JOCJ8BNN>
- Wells, N., Goddard, S., & Hayes, M. J. (2004). A Self-Calibrating Palmer Drought Severity Index. *Journal of Climate*, 17(12), 2335–2351. [https://doi.org/10.1175/1520-0442\(2004\)017<2335:ASPDSI>2.0.CO;2](https://doi.org/10.1175/1520-0442(2004)017<2335:ASPDSI>2.0.CO;2)
- Wilson Water Group. (2019). Current and 2050 Planning Scenario Agricultural Diversion Demand. In *Analysis and Technical Update to the Colorado Water Plan*. Denver, Colorado.
- Wobus, C., Zheng, P., Stein, J., Lay, C., Mahoney, H., Lorie, M., ... Martinich, J. (2019). Projecting Changes in Expected Annual Damages From Riverine Flooding in the United States. *Earth's Future*, 7(5), 2018EF001119. <https://doi.org/10.1029/2018EF001119>
- Wobus, Cameron, Gutmann, E., Jones, R., Rissing, M., Mizukami, N., Lorie, M., ... Martinich, J. (2017). Climate change impacts on flood risk and asset damages within mapped 100-year floodplains of the contiguous United States. *Natural Hazards and Earth System Sciences*, 17(12), 2199–2211. <https://doi.org/10.5194/nhess-17-2199-2017>
- Wobus, Cameron, Small, E. E., Hosterman, H., Mills, D., Stein, J., Rissing, M., ... Martinich, J. (2017). Projected climate change impacts on skiing and snowmobiling: A case study of the United States. *Global Environmental Change*, 45, 1–14. <https://doi.org/10.1016/j.gloenvcha.2017.04.006>
- Yang, L., Jin, S., Danielson, P., Homer, C., Gass, L., Bender, S. M., ... Xian, G. (2018). A new generation of the United States National Land Cover Database: Requirements, research priorities, design, and implementation strategies. *ISPRS Journal of Photogrammetry and Remote Sensing*, 146, 108–123. <https://doi.org/10.1016/J.ISPRSJPRS.2018.09.006>
- Zhong, R., Chen, X., Wang, Z., & Lai, C. (2018). *scPDSI: Calculation of the Conventional and Self-Calibrating Palmer Drought Severity Index*. R package.
- Zipper, S. C., Qiu, J., & Kucharik, C. J. (2016). Drought effects on US maize and soybean production: Spatiotemporal patterns and historical changes. *Environmental Research Letters*, 11(9). <https://doi.org/10.1088/1748-9326/11/9/094021>





9 Appendix A—Climate Scenario Tables

Table 9-1. Descriptions of Current Climate, Moderate Future Climate, and More Severe Future Climate scenarios for the three natural hazards.

	Current Climate 	Moderate Future Climate 	More Severe Future Climate 
 Flood	Calculate current magnitudes of 10-year through 200-year flood events from downscaled hydrology (Reclamation, 2013), and assign these flood magnitudes to state-wide floodplain maps. Time period = 2009-2028 (20-year window centered on 2019)	Calculate changes in frequency of current flood events from downscaled hydrology using 10-model ensemble representing 2 °C summertime warming at 2050. Time period = 2040-2059 (20-year window centered on 2050)	Calculate changes in frequency of current flood events assuming 3 °C summertime warming in 2050, and 7% per °C increase in extreme flood events
 Drought	Gridded historical temperature and precipitation (Maurer et al., 2002). Time period = 1949-2014	Adjusted temperature and precipitation, using a model ensemble consistent with the Colorado River Water Availability Study Phase II (CRWAS II) "Center" scenario (Harding et al., 2015). This corresponds to an average annual air temperature increase of 2.1 °C and a 5% gain in annual precipitation. Time period = 2035-2064 (30-year window centered on 2050)	Adjusted temperature and precipitation, using a model ensemble consistent with CRWAS II "7525" scenario (Harding et al., 2015). This corresponds to an average annual air temperature increase of 2.3 °C and a 1% loss in annual precipitation. Time period = 2035-2064 (30-year window centered on 2050).
 Wildfire	Gridded historical climate (air temperature, relative humidity, wind) using National Centers for Environmental Prediction (NCEP) gridded reanalysis data (North American Regional Reanalysis (NARR)). Time period = 1988-2017.	Adjusted air temperature using monthly anomalies from CRWAS II "Center" scenario ensemble. Adjusted live fuel moisture content (LFMC) using the standardized precipitation evapotranspiration index (SPEI), which is adjusted with future precipitation and evaporation. Time period = 2035-2064 (30-year window centered on 2050)	Adjusted air temperature using monthly anomalies from CRWAS II "7525" scenario ensemble. Adjusted LFMC using SPEI drought index, which is adjusted with precipitation and evaporation. Time period = 2035-2064 (30-year window centered on 2050).

Table 9-2. Variables and outputs used in generating and applying the climate scenarios to the different sectors.

	Climate Model Variables	Derived Variables	Model Outputs
 Flood	Precipitation, Temperature	Modeled streamflow, extreme precipitation	Changes in frequency of historical flood events
 Drought	Agriculture: Precipitation, Temperature	Agriculture: Evapotranspiration (plant consumptive irrigation requirement, or CIR); Palmer drought severity index (PDSI); satellite-derived vegetation greenness	Agriculture: Changes in crop yields; changes in feed costs
	Skiing: Precipitation, Temperature	Skiing: Winter snowpack	Skiing: Changes in snow season length
	Rafting: Precipitation, Temperature	Rafting: Monthly river runoff	Rafting: Changes in boatable days
 Wildfire	Precipitation, Temperature	Standardized Precipitation Evapotranspiration Index (SPEI), Live Fuel Moisture Content (LFMC)	Changes in burn probability and flame length probability distributions

10 Appendix B—Population Scenario Table

Table 10-1. Descriptions of the population growth scenarios along with how they affect various relevant variables for the different hazards and sectors.

	Current Population 	Low Growth Future 	Medium Growth Future 	High Growth Future 
Hazus Datasets	Building replacement values from the Hazus (v2.2) 2010 dataset at the census block level. Valuations were provided in 2014 dollars and adjusted to 2019 dollars using the consumer price index (CPI). Building categories include residential, commercial, industrial, and other (religious, government, education) buildings. Future projections of replacement cost are based on spatial buildout distribution from the Integrated Climate and Land Use Scenarios (ICLUS v2).			
 Flood	<u>Statewide Totals</u> 2015 Population: 5.45M Hazus Building Inventory Replacement Value: \$574B	<u>2050 Statewide Totals</u> Population: 7.68M Hazus Building Inventory Replacement Value: \$871B	<u>2050 Statewide Totals</u> Population: 8.46M Hazus Building Inventory Replacement Value: \$962B	<u>2050 Statewide Totals</u> Population: 9.31M Hazus Building Inventory Replacement Value: \$1062B
 Drought	<u>Statewide Totals</u> Acres of Irrigated Cropland: 2.70M Acres of Pasture/Grassland: 20.0M Baseline Annual Ski User Days: 11.5M Baseline Annual Rafting User Days: 515k	<u>2050 Statewide Totals</u> Acres of Irrigated Cropland: 2.45M Acres of Pasture/Grassland: 19.7M Baseline Annual Ski User Days: 13.8M Baseline Annual Rafting User Days: 739k	<u>2050 Statewide Totals</u> Acres of Irrigated Cropland: 2.45M Acres of Pasture/Grassland: 19.5M Baseline Annual Ski User Days: 14.5M Baseline Annual Rafting User Days: 814k	<u>2050 Statewide Totals</u> Acres of Irrigated Cropland: 2.34M Acres of Pasture/Grassland: 19.4M Baseline Annual Ski User Days: 15.3M Baseline Annual Rafting User Days: 895k
 Wildfire	<u>Statewide Totals</u> 2015 Population: 5.45M Building Inventory: # of Structures: 2.1M Hazus Replacement Value: \$574B	<u>2050 Statewide Totals</u> Population: 7.68M Building Inventory: # of Structures: 3.2M Hazus Replacement Value: \$871B	<u>2050 Statewide Totals</u> Population: 8.46M Building Inventory: # of Structures: 3.4M Hazus Replacement Value: \$962B	<u>2050 Statewide Totals</u> Population: 9.31M Building Inventory: # of Structures: 3.7M Hazus Replacement Value: \$1062B

11 Appendix C—River Reach Info

Table 11-1. Reference gauges and runnable ranges for American Whitewater segments comprising CROA-reported rivers.

River for which CROA reports user days	American Whitewater segment name	Reference streamflow gauge used to assess segment boating conditions	Runnable range (lower) cfs	Runnable range (upper) cfs
Animas – Upper	Silverton to Tacoma	USGS 09359020 ANIMAS RIVER BELOW SILVERTON, CO	300	2000
Animas - Upper	Tacoma to Rockwood Rail Yard	USGS 09359500 ANIMAS RIVER AT TALL TIMBER RESORT ABOVE TACOMA, CO	300	3000
Animas - Upper	Bakers Bridge to Trimble Lane	USGS 09361500 ANIMAS RIVER AT DURANGO, CO	500	4000
Animas - Upper	Trimble Lake to 32nd Street Park	USGS 09361500 ANIMAS RIVER AT DURANGO, CO	500	4000
Animas	32nd Street Park to Purple Cliffs	USGS 09361500 ANIMAS RIVER AT DURANGO, CO	1000	6000
Animas	Purple Cliffs to State Line	USGS 09361500 ANIMAS RIVER AT DURANGO, CO	500	6000
Arkansas	The Numbers	DWR (ARKGRNCO)	200	5000
Arkansas	Railroad Bridge Launch to Buena Vista	DWR (ARKGRNCO)	200	5000
Arkansas	Buena Vista to Fisherman's Bridge	USGS 07091200 ARKANSAS RIVER NEAR NATHROP, CO	300	5000
Arkansas	Fisherman's Bridge to Stone Bridge Access	USGS 07091200 ARKANSAS RIVER NEAR NATHROP, CO	300	5000
Arkansas	Stone Bridge to Salida	USGS 07091200 ARKANSAS RIVER NEAR NATHROP, CO	300	5000
Arkansas	Salida to Rincon	USGS 07091200 ARKANSAS RIVER NEAR NATHROP, CO	300	5000
Arkansas	Rincon to Pinnacle Rock	USGS 07094500 ARKANSAS RIVER AT PARKDALE, CO	300	5000
Arkansas	Pinnacle Rock to Parkdale Launch	USGS 07094500 ARKANSAS RIVER AT PARKDALE, CO	300	5000
Arkansas	Pinnacle Rock to Canon City (Royal Gorge)	DWR (ARKWELCO)	150	7000
Blue	Blue River Campground to Columbine Landing	USGS 09050700 BLUE RIVER BELOW DILLON, CO	200	2000
Clear Creek	Kermit's to Green Bay Rock	USGS 06716500 CLEAR CREEK NEAR LAWSON, CO	199	1000
Colorado - Glenwood	Glenwood	USGS 09070500 COLORADO RIVER NEAR DOTSERO, CO	900	5000
Colorado - Upper	Gore Canyon	USGS 09058000 COLORADO RIVER NEAR KREMMLING, CO	700	2500
Colorado - Horsethief - Ruby	Ruby Horsethief	USGS 09163500 COLORADO RIVER NEAR COLORADO-UTAH STATE LINE	2500	50000
Colorado - Westwater	Westwater	USGS 09163500 COLORADO RIVER NEAR COLORADO-UTAH STATE LINE	2000	30000
Dolores	Rico to Big Rock	USGS 09166500 DOLORES RIVER AT DOLORES, CO	200	3000
Dolores	West Fork to McPhee Res	USGS 09165000 DOLORES RIVER BELOW RICO, CO	400	3000
Dolores	McPhee to Dove Creek Pump Station	DOLORES RIVER BELOW MCPHEE RESERVOIR (DOLBMCCO)	700	5000
Dolores	Slickrock to Bedrock	USGS 09168730 DOLORES RIVER NEAR SLICK ROCK, CO	800	5000
Dolores	Bedrock to Gateway	USGS 09171100 DOLORES RIVER NEAR BEDROCK, CO	800	5000
Dolores	Gateway to Colorado River	USGS 09180000 DOLORES RIVER NEAR CISCO, UT	800	5000
Eagle - Upper	Camp Hale to Red Cliff	USGS 09063000 EAGLE RIVER AT RED CLIFF, CO	200	1000
Eagle - Upper	Gilman Gorge	USGS 09064600 EAGLE RIVER NEAR MINTURN, CO	275	2000



Eagle - Upper	Minturn Town Run	USGS 09064600 EAGLE RIVER NEAR MINTURN, CO	100	2000
Eagle - Upper	Dowd Chute	USGS 09064600 EAGLE RIVER NEAR MINTURN, CO	250	4000
Eagle - Lower	River Run to Edwards	USGS 394220106431500 EAGLE RIVER BELOW MILK CREEK NEAR WOLCOTT, CO	1000	3000
Eagle - Lower	Edwards to Eagle	USGS 394220106431500 EAGLE RIVER BELOW MILK CREEK NEAR WOLCOTT, CO	700	5000
Eagle - Lower	Eagle to Gypsum	USGS 394220106431500 EAGLE RIVER BELOW MILK CREEK NEAR WOLCOTT, CO	200	7000
Eagle - Lower	Gypsum to Dotsoro	USGS 09070000 EAGLE RIVER BELOW GYPSUM, CO	100	8000
Gore Creek - Vail	East Vail Exit to Vail	USGS 09066325 GORE CREEK ABV RED SANDSTONE CREEK AT VAIL, CO	300	2000
Gore Creek - Vail	Vail to Eagle River	USGS 09066510 GORE CREEK AT MOUTH NEAR MINTURN, CO	150	500
Green/Yampa	Flaming Gorge to Lodore	USGS 09234500 GREEN RIVER NEAR GREENDALE, UT	200	5000
Green/Yampa	Lodore to Echo Park	USGS 09234500 GREEN RIVER NEAR GREENDALE, UT	1100	20000
Green/Yampa	Echo Park to Split Mountain	USGS 09261000 GREEN RIVER NEAR JENSEN, UT	200	20000
Green/Yampa	River Park to Transit Center	USGS 09239500 YAMPA RIVER AT STEAMBOAT SPRINGS, CO	700	5000
Green/Yampa	Transit Center to Pump Station	USGS 09244490 YAMPA RIVER ABOVE ELKHEAD CREEK NEAR HAYDEN, CO	500	5000
Green/Yampa	Little Yampa Canyon	USGS 09247600 YAMPA RIVER BELOW CRAIG, CO	1100	10000
Green/Yampa	85 Rd to Deer Lodge Park Rd	USGS 09251000 YAMPA RIVER NEAR MAYBELL, CO	700	5000
Green/Yampa	Deerlodge Park to Echo Park	USGS 09260050 YAMPA RIVER AT DEERLODGE PARK, CO	1300	25000
Gunnison - Upper (Town Run)	Almont to Blue Mesa	USGS 09114500 GUNNISON RIVER NEAR GUNNISON, CO	500	3000
Gunnison Gorge	Chrystal Dam to Chukar Trail	USGS 09128000 GUNNISON RIVER BELOW GUNNISON TUNNEL, CO	600	3000
Gunnison Gorge	Chukar to N. Fork	USGS 09128000 GUNNISON RIVER BELOW GUNNISON TUNNEL, CO	280	15000
Gunnison - Escelante	Delta to Whitewater	USGS 09144250 GUNNISON RIVER AT DELTA, CO	800	20000
Gunnison - Forks to Austin	Forks to Austin	USGS 09144250 GUNNISON RIVER AT DELTA, CO	800	20000
Gunnison Lake Fork	Lake City Town Run	USGS 09124500 LAKE FORK AT GATEVIEW, CO	300	2000
North Platte	State Line to French Creek	USGS 06620000 NORTH PLATTE RIVER NEAR NORTHGATE, CO	400	3000
Piedra	Upper Piedra CG to 1st Fork Bridge	USGS 09349800 PIEDRA RIVER NEAR ARBOLES, CO	550	4000
Piedra	1st Fork Bridge to Lower Piedre CG	USGS 09349800 PIEDRA RIVER NEAR ARBOLES, CO	400	3500
Piedra	Lower Piedre CG to Navajo Reservoir	USGS 09349800 PIEDRA RIVER NEAR ARBOLES, CO	400	4000
Poudre	Big South Campground to Tunnel Picnic Ground	DWR CACHE LA POUDE AT CANYON MOUTH NEAR FORT COLLINS (CLAFTCCO)	300	900
Poudre	Home Moraine to Indian Meadows Bridge	DWR CACHE LA POUDE AT CANYON MOUTH NEAR FORT COLLINS (CLAFTCCO)	600	3000
Poudre	Indian Meadows Bridge to Narrows Picnic Ground	DWR CACHE LA POUDE AT CANYON MOUTH NEAR FORT COLLINS (CLAFTCCO)	650	3000
Poudre	Narrows Picnic Ground to Steven's Gulch Access	DWR CACHE LA POUDE AT CANYON MOUTH NEAR FORT COLLINS (CLAFTCCO)	150	1300



Poudre	Stevens Gulch to Mishawaka	DWR CACHE LA POUFRE AT CANYON MOUTH NEAR FORT COLLINS (CLAFTCCO)	300	3000
Poudre	Mishawaka to Poudre Park	DWR CACHE LA POUFRE AT CANYON MOUTH NEAR FORT COLLINS (CLAFTCCO)	250	3000
Poudre	Poudre Park Picnic Ground to below Pine View Falls	DWR CACHE LA POUFRE AT CANYON MOUTH NEAR FORT COLLINS (CLAFTCCO)	250	2500
Poudre	Pineview Falls to Bridges Take-out	DWR CACHE LA POUFRE AT CANYON MOUTH NEAR FORT COLLINS (CLAFTCCO)	250	3000
Poudre	Below Filter Plant to Picnic Rock Access	DWR CACHE LA POUFRE AT CANYON MOUTH NEAR FORT COLLINS (CLAFTCCO)	300	2500
Rio Grande	Wagon Wheel Gap to South Fork	DWR (RIOWAGCO)	100	5500
Rio Grande	South Fork to Del Norte	DWR (RIODELCO)	100	9000
Rio Grande	Alamosa to Lasauses	DWR (RIOALACO)	100	4500
Roaring Fork - Above Basalt	Weller Lake to Difficult CG	USGS 09073300 ROARING FORK RIVER AB DIFFICULT C NR ASPEN, CO	100	1000
Roaring Fork - Above Basalt	Slaughterhouse	USGS 09076300 ROARING FORK RIVER BLW MAROON CREEK NR ASPEN, CO	635	2700
Roaring Fork - Above Basalt	Upper Woody Creek Bridge to Lower Woods Creek Bridge	USGS 09076300 ROARING FORK RIVER BLW MAROON CREEK NR ASPEN, CO	200	1400
Roaring Fork - Above Basalt	Lower Woody Creek Bridge to rte. 82 Bridge	USGS 09076300 ROARING FORK RIVER BLW MAROON CREEK NR ASPEN, CO	200	1400
Roaring Fork - Below Basalt	Basalt to Carbondale	USGS 09081000 ROARING FORK RIVER NEAR EMMA, CO	200	1500
Roaring Fork - Below Basalt	Black Bridge to Veltus Park	USGS 09085000 ROARING FORK RIVER AT GLENWOOD SPRINGS, CO	200	10000
San Juan - Pagosa	Riverside Campground to Yamaguchi Park	USGS 09342500 SAN JUAN RIVER AT PAGOSA SPRINGS, CO	200	2000
San Juan - Pagosa	Pagosa Springs to Trujillo Rd	USGS 09342500 SAN JUAN RIVER AT PAGOSA SPRINGS, CO	400	2500
San Miguel	Bilk Creek to Down Valley Park	USGS 09172500 SAN MIGUEL RIVER NEAR PLACERVILLE, CO	500	5000
San Miguel	Down Valley Park to Specie Creek	USGS 09172500 SAN MIGUEL RIVER NEAR PLACERVILLE, CO	500	5000
San Miguel	Specie Creek to Beaver Creek	USGS 09172500 SAN MIGUEL RIVER NEAR PLACERVILLE, CO	500	5000
San Miguel	Beaver Creek to Pinon Bridge	USGS 09174600 SAN MIGUEL RIVER AT BROOKS BRIDGE NEAR NUCLA CO	600	5000
San Miguel	Pinon Bridge to Naturita	USGS 09174600 SAN MIGUEL RIVER AT BROOKS BRIDGE NEAR NUCLA CO	600	5000
San Miguel	Naturita to Dolores confluence	USGS 09177000 SAN MIGUEL RIVER AT URAVAN, CO	600	5000
Taylor	Bridge to Pieplant Ranch	USGS 09107000 TAYLOR RIVER AT TAYLOR PARK, CO	500	1000
Taylor	Taylor Park Reservoir to Almont	USGS 09110000 TAYLOR RIVER AT ALMONT, CO	400	3000



12 Appendix D—Historic Colorado Wildfire Suppression Costs

Table 12-1. Historic Colorado wildfire suppression costs used to optimize the model in Sect. 7.2.3.1. Entries in the table below are ordered by fire size and are derived from multiple sources as noted (Brown & Blevins, 2018; Colorado Division of Fire Prevention and Control, 2013; Denver Post, 2016; Mitchell, 2018; National Park Service, 2013; Romeo, 2019). Suppression costs are given in nominal dollars for the year in which the fire took place.

Year	Fire Name	Size (acres)	Suppression Cost (\$ million)	Source
2002	Hayman Fire	137760	39	Colorado Division of Fire Prevention and Control (2013)
2013	West Fork Complex fire	109049	2.2	Denver Post (2016)
2018	Spring Creek	108045	31.98	Brown and Blevins (2018)
2012	High Park Fire	87250	39.2	Colorado Division of Fire Prevention and Control (2013)
2002	Missionary Ridge	71739	40	Colorado Division of Fire Prevention and Control (2013)
2018	“416” and Burro Fire Complex	57000	40	Romeo (2019)
2018	Badger Hole	50671	0.166	Brown and Blevins (2018)
2008	Bridger Fire	45800	2.7	Colorado Division of Fire Prevention and Control (2013)
2011	Bear Springs/Callie Marie Fires	44662	2.5	Colorado Division of Fire Prevention and Control (2013)
2018	MM 117	42795	0.9	Brown and Blevins (2018)
2018	Bull Draw	36549	12.1	Brown and Blevins (2018)
2002	Trinidad Complex	33000	2.18	Colorado Division of Fire Prevention and Control (2013)
2002	Mount Zirkel Complex	31016	13.3	Colorado Division of Fire Prevention and Control (2013)
2018	Stateline	28105	2.3	Brown and Blevins (2018)
2012	Little Sand	24900	1.25	Colorado Division of Fire Prevention and Control (2013)
2000	Bircher	23607	5	Colorado Division of Fire Prevention and Control (2013)
2018	Silver Creek	20120	25.32	Brown and Blevins (2018)
2018	Divide	19955	0.82	Brown and Blevins (2018)
2012	Waldo Canyon	18247	15.3	Colorado Division of Fire Prevention and Control (2013)
2013	Black Forest	14280	8.5	Mitchell (2018)
2011	Ft. Lyons Fires	14000	0.302	Colorado Division of Fire Prevention and Control (2013)
2006	Mato Vega Fire	13820	3.1	Colorado Division of Fire Prevention and Control (2013)
2011	Shell Complex	13312	1.1	Colorado Division of Fire Prevention and Control (2013)
2018	Weston Pass	13023	9.65	Brown and Blevins (2018)



2018	Lake Christine	12588	17.4	Brown and Blevins (2018)
2002	Coal Seam	12200	7.25	Colorado Division of Fire Prevention and Control (2013)
2005	Mason Fire	11357	3.8	Colorado Division of Fire Prevention and Control (2013)
2002	Spring Creek	11000	7	Colorado Division of Fire Prevention and Control (2013)
2000	Hi Meadow	10800	4.5	Colorado Division of Fire Prevention and Control (2013)
2000	Bobcat Fire	10559	3.3	Colorado Division of Fire Prevention and Control (2013)
2002	Million	9346	9.8	Colorado Division of Fire Prevention and Control (2013)
2004	Picnic Rock Fire	8908	2.3	Colorado Division of Fire Prevention and Control (2013)
2004	Greasewood	7815	1.093	Colorado Division of Fire Prevention and Control (2013)
2012	Hewlett	7685	2.9	Colorado Division of Fire Prevention and Control (2013)
2010	Fourmile Canyon	6388	10	Denver Post (2016)
2012	Sunrise Mine	6017	1.2	Denver Post (2016)
2018	Cabin Lake	5975	13.15	Brown and Blevins (2018)
2018	Red Canyon	5722	3.98	Brown and Blevins (2018)
2002	Bear	4800	1	Denver Post (2016)
2012	Lower North Fork	4500	6.6	Colorado Division of Fire Prevention and Control (2013)
2002	Big Elk	4413	4	Mitchell (2018)
2002	Schoonover	3860	2.4	Denver Post (2016)
2012	Fern Lake	3500	6	National Park Service (2013)
2011	Crystal	3000	3	Mitchell (2018)
2002	Snaking	2590	2.6	Denver Post (2016)
2018	2018 RBC Complex	1438	3.16	Brown and Blevins (2018)
2018	Chateau	1423	2.78	Brown and Blevins (2018)
2018	Sulphur	977	1.39	Brown and Blevins (2018)
2018	Skunk Creek	620	0.8	Brown and Blevins (2018)
2018	Upper Mailbox	474	0.75	Brown and Blevins (2018)
2018	Buffalo Mountain	91	2.45	Brown and Blevins (2018)

